Applying wire-based directed energy deposition for in-space manufacturing of solar array structures

Niels van Staaveren

Master's thesis

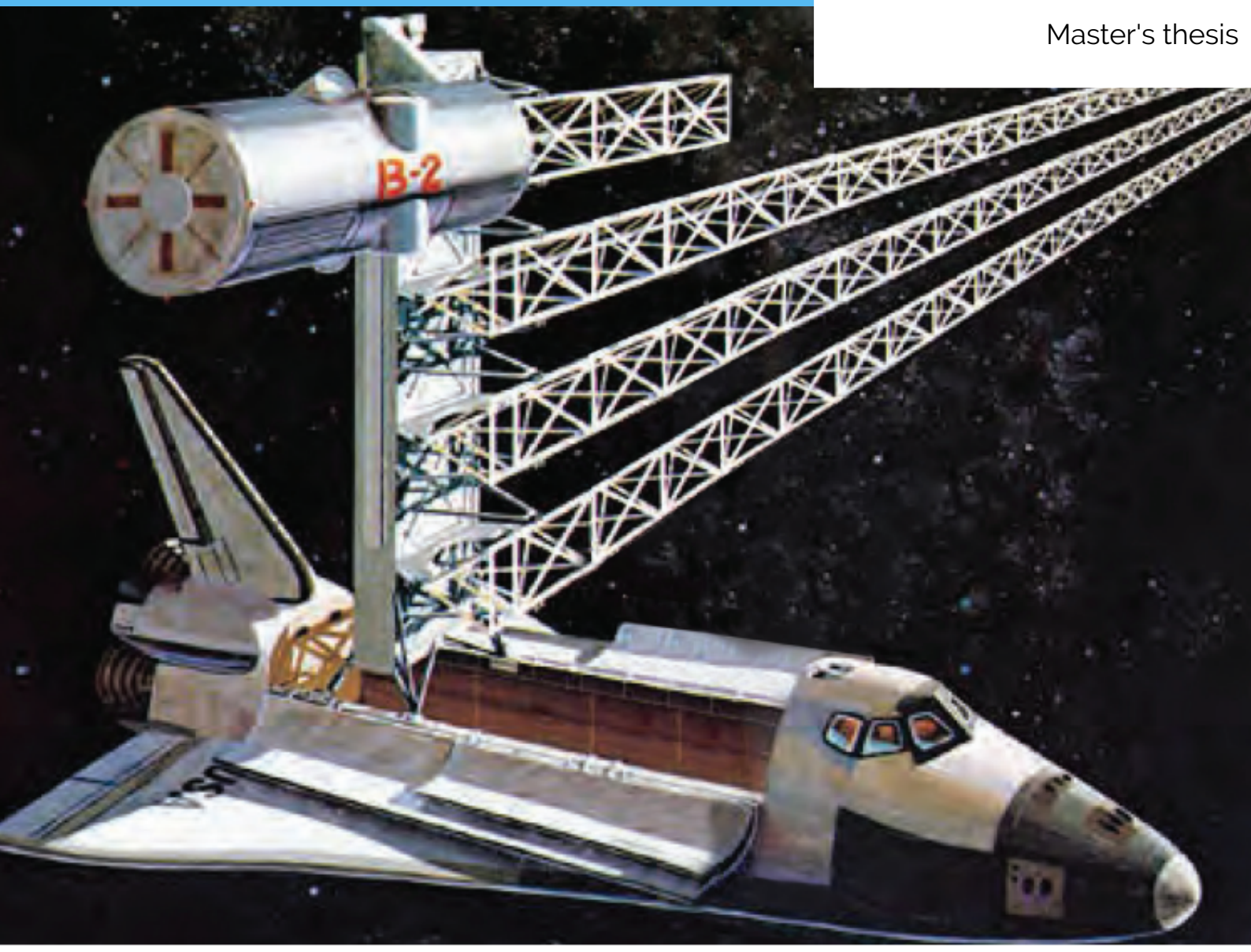

TU Delft

Applying wire-based directed energy deposition for in-space manufacturing of solar array structures

By

N. M. van Staaveren

in partial fulfilment of the requirements for the degree of

Master of Science
in Aerospace Engineering

at the Delft University of Technology,
to be defended publicly on Wednesday September 28, 2022 at 11:00 AM.

Student number :	4474422	
Supervisors:	Dr. A. Cervone,	TU Delft
	Ir. N.O. Bernving,	NLR
	Ir. S.S. Lie	NLR
Thesis committee:	Dr. A. Cervone,	TU Delft
	Dr. B. Giovanardi,	TU Delft
	M.Ş. Uludağ,	TU Delft

TU Delft

Preface

This Master's thesis was the final assignment to be done to complete my Master's Aerospace engineering with a specialization in Space Engineering. Finalizing my Master's thesis marks the end of my study career and the beginning of a new phase. This is by far the biggest university project I have done and all by myself. The literature study, research methodology course and thesis itself combined took almost 11 months (including holidays) to complete. I am proud of what I have achieved and I have learned many new things and skills along the way. Additive manufacturing has always been interesting to me and through this thesis I was able to learn a great deal more about it. Hopefully I will be able to put the knowledge gained in this research to practical use in my professional career.

I would like to thank NLR for providing the possibility for me to do this research. It was funny how this thesis came into being. When I was first informed Arnaud van Kleef about NLR's ambitions in in-space manufacturing, I was immediately interested. The topic additive manufacturing in space stood out to me above all other thesis topics. But, we met at the wrong time. Due to decisions made by the department, the option to do a thesis in this topic was put off and simultaneously I had postponed my thesis to do Delft Hyperloop. Exactly one year later, Arnaud and I spoke again and both the thesis position and I were available again. It worked out after all.
Thanks to Niels Bernving for supervising me throughout this graduation project and thanks to Sonny Lie for being my substitute supervisor. Also, thanks to the people in the ASIS department and everyone from NLR that helped me in my thesis.

I would like to express my gratitude to Dr. Angelo Cervone for being my TU Delft supervisor. One thing in our collaboration stood out to me, for which I am extremely grateful. If there was a prize for the professor that is quickest to reply to his emails and provide feedback, I am certain you would win it! Being able to get answers to my questions the same day, usually within an hour, was amazing.

Lastly, I would like to thank the people around me in my personal life for their support. My family and partner in particular. Although your knowledge in this subject was (very) limited, your out-of-the-box ideas were extremely helpful for me to find interesting thoughts and get me into new directions. The way you motivate me is always greatly appreciated.

To all readers: enjoy reading and I hope you learn something new!

Niels van Staaveren
10-09-2022, Delft

Abstract

In-space manufacturing (ISM) is an upcoming technology in the space industry. Unprecedented applications can be achieved by producing objects in space, as opposed to bringing objects to space that were produced on Earth. For solar arrays, this means that extremely large array sizes can be achieved, because with ISM the array size is not limited by the maximum payload volume of the launch vehicle. Additionally, the array can be lighter, because the structure does not need to withstand the harsh launch conditions.

Additive manufacturing, wire-based directed energy deposition in particular, was identified as the best in-space manufacturing method for solar array structures. This thesis aims to find the best system to achieve this and investigate the limitations and challenges to applying metal additive manufacturing in space. A top-level system design is proposed and thermal, power and mechanical limitations are explored. This technology is still at a low TRL level and a lot of development is needed. Therefore, the most important points for future research are provided.

Contents

Abbreviations

ACRONYM	DESCRIPTION
ADCS	Attitude determination & control system
AM	Additive manufacturing
ASTM	American Society for Testing and Materials
AU	Astronomical unit
BOL	Beginning-of-life
CDH	Command & data handling
CMT	Cold metal transfer
COPUOS	Committee on the Peaceful Uses of Outer Space
DED	Directed energy deposition
EBW	Electron beam welding
ERA	European Robotic Arm
FEA	Finite element analysis
FEM	Finite element method
FFF	Fused filament fabrication
FRUSA	Flexible Roll-Up Solar Array
GEO	Geostationary orbit
GMA	Gas metal arc
GMAW	Gas metal arc welding
GNC	Guidance, navigation & control
GTAW	Gas tungsten arc welding
GUI	Graphical user interface
HST	Hubble Space Telescope
IADC	Inter-Agency Space Debris Coordination Committee
ISM	In-space manufacturing
ISO	International Organization for Standardization
ISRU	In-situ resource utilization
ITSAT	Inflatable Torus Solar Array Technology
JWST	James Webb Space Telescope
LEO	Low Earth orbit
MELD	Mobile End-effector Laser Device
MIG	Metal inert gas
NASA	National Aeronautics & Space Association
NLR	Royal NLR - Netherlands Aerospace Centre
PAW	Plasma arc welding
PBF	Powder bed fusion

ACRONYM	DESCRIPTION
ROSA	Roll-Out Solar Array
SAFE	Solar Array Flight Experiment
SAW	Solar array wing
STEM	Storable Tubular Extendible Member
TRL	Technology readiness level
UV	Ultraviolet
VWAT	Volume weighted average temperature
WAAM	Wire and arc additive manufacturing
WEAM	Wire and electron beam additive manufacturing
WLAM	Wire and laser additive manufacturing

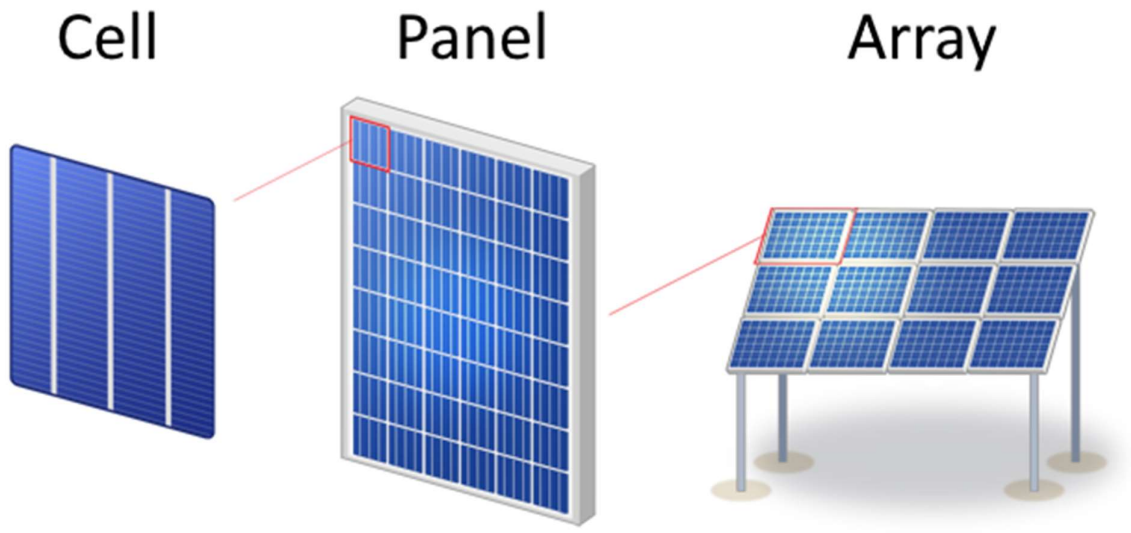

Figure 1: Solar power components nomenclature

Symbols

SYMBOL	MEANING
δ	Deflection
ε	Emissivity
κ	Thermal conductivity
ρ	Density
σ	Stefan-Boltzmann constant
σ_f	Flexural strength
τ	Time
Φ	Spacecraft orbit angle
A	Surface area
a	Albedo
C	Case specific constant
c_p	Specific heat capacity
E	Young's modulus
F_f	Failure force
F_{SC-P}	View factor between surface and planet
G_s	Solar constant
I	Second moment of inertia
L	Length
L_f	Specific latent heat of fusion
M	Mass
N	Material index
P	Power
p	Perimeter
Q	Heat
Q_{con}	Heat dissipation through conduction
Q_L	Latent heat
Q_{melt}	Heat required to melt material
Q_{rad}	Heat dissipation through radiation
q_{alb}	Albedo radiation
q_{sun}	Solar radiation
q_{Earth}	Earth radiation
r	Radius
r_f	Failure force critical radius
r_i	Inner radius
r_o	Outer radius

SYMBOL	MEANING
r_s	Stiffness critical radius
S	Stiffness
ΔT	Temperature difference
T	Temperature
T_m	Melting temperature
$T_{o,max}$	Maximum operating temperature
$T_{o,min}$	Minimum operating temperature
t	Thickness
V	Volume
y_m	Maximum distance in y-direction
Z	Moment of inertia in Z-direction

List of figures

List of tables

Executive summary

In-space manufacturing is an upcoming technology that will enable new opportunities in space. The development of in-space manufacturing is still in an early stage. A lot of research is to be done before in-space manufacturing methods will be seen in space missions on a large scale. This report makes an effort in the taking the first steps in this direction. This project was started by the Netherlands Aerospace Centre (NLR) in collaboration with Maana Electric.

Additive manufacturing (AM) has been identified as the most interesting manufacturing method for space applications, because as opposed to subtractive methods, little waste is produced. This is highly beneficial since the cost to launch mass into space is substantial. In preparation of this thesis, a literature study was performed on in-space manufacturing, focused on additive manufacturing. It was found that directed energy deposition (DED) is the additive manufacturing method that is most suitable for producing large objects in space. It is the only AM category that is not limited by a build volume and does not require post-processing procedures for metals. In this thesis, the implementation of this manufacturing method is researched for the production in space of structures for solar arrays. The combination of additive manufacturing in space and solar arrays allows for unprecedented array sizes. This research focusses on a stand-alone manufacturing platform that is capable of donating manufactured solar arrays to other satellites and restocking of raw materials. Potential limitations to the manufacturing platform are identified. DED has not been performed in space to this date, so this causes uncertainty. The main concerns are heat dissipation, power consumption and the behaviour of DED in space.

There are three major benefits of applying additive manufacturing for solar arrays in space. Firstly, the maximum array size that can be produced is theoretically unlimited. Conventional (deployable) solar arrays are produced on Earth and placed in a rocket in a stowed configuration. Even if the solar arrays are folded, there is a limited to the size that can be placed in the payload area of a rocket. Therefore, the solar array size is limited. Since the proposed application manufactures the solar arrays in space, it is not limited by the launch vehicle. The array size is only limited by the quantity of raw materials, which can be restocked through supply missions. So, ISM solar arrays can be enormous. This will allow spacecrafts to use an amount of power that was previously unachievable.
Secondly, ISM solar arrays can achieve a higher power to mass ratio. Conventional arrays launched from Earth need to withstand the heavy loads during launch. The solar array structures are designed for these loads. The experienced loads in space are significantly smaller, so the structural mass can be lower. Additionally, AM allows for complex shapes, so geometry optimization can be used.
Lastly, manufacturing in space allows for more flexibility. Deployable alternatives have predetermined shapes and cannot change this at a later stage. Using ISM, the structure geometry can be changed any time and the length of the solar array can be chosen.

DED can be divided into two types based on feedstock: powder and wire. In powder-based DED, particles of around $100\ \mu m$ are blasted onto the subject using high-pressured gas. A heat source, such as a laser creates a melt pool and melts the particles and subject together. Powder-based DED has a capture efficiency between 20% and 90%. According to the Liability Convention (1972), space debris must be limited. It cannot be guaranteed that the non-captured particles drift into space. Protective solutions will be complex and heavy. Therefore, wire-based DED is the best option. It has a capture efficiency of nearly 100%. Also, it does not require a consumable gas. Various heat sources are possible for DED. Wire and arc additive manufacturing (gas metal arc welding) was found to be the best option for this application. Its benefits are that it uses cheap, simple equipment and has high energy efficiency. Its negative traits are spattering, arc instability and higher internal stresses. However, for slightly different mission characteristics, other heat sources can be a better option.

For the type of solar panel on the manufactured array, it was found that a flexible deployable type is best. The panel from ROSA is assumed to be used, because this is the state of the art for deployable panels. This stowed panel is rolled up in a drum and has the highest power capacity to volume ratio among its kind. The solar array structure that is produced by AM should be optimized in future research, but in this report a hollow tube on either side of the panel is assumed. The manufacturing platform is equipped with two DED printers attached to a robotic arm, one for each tube, and an assembly robotic arm to install the manufactured array on other spacecrafts and swap out material drums.

In a power analysis information on DED equipment and robotic arms was investigated. It was calculated that during printing operation the manufacturing system consumes on average $2385\ W$ of power. Based on an estimation equation for communication satellites, because no manufacturing platforms exist yet, the total power consumption of the spacecraft was estimated to be $3043\ W$. For a spacecraft, this is high but not unfeasible. Two ways can be used to achieve this. The spacecraft can initially be equipped with solar arrays capable of this power demand, or the spacecraft can initially be equipped with smaller panels and produces its own large solar arrays. The manufacturing process is able to pause for periods where the spacecraft's batteries are recharged, produces until the batteries are drained and repeats this cycle.

A material selection has been performed for the structure. The manufacturing process, performance, environment and non-technical aspects all have an influence on what the ideal material is.
The manufacturing process mostly requires good thermal properties. High emissivity and thermal conductivity, and low melting temperature, specific heat capacity and specific latent heat of fusion. DED also requires the material to be able to be produced in filament form. The space environment requires the material to be able to withstand both high and low temperatures. The minimum operating window that is set is $-120℃$ to $120℃$. Regarding non-technical parameters, ideally, the material is cheap and easily available.
The material selection process uses material indices to assess all options. An index is created for stiffness per mass and strength per mass. These are combined into a single index: $N_{12} = \frac{\sqrt[3]{E}*\sqrt{\sigma_f}}{\rho^2}$. To assess the thermal performance, an index is based on the melting energy and thermal conductivity: $N_{34} = \frac{\kappa}{C_{p}*\rho*(T_m-T_0)+L_f*\rho}{}_P$.
Using the software package GRANTA EduPack it was found that beryllium, magnesium and aluminium are the best performing materials. Out of these three, magnesium has worse specific strength and stiffness. Beryllium shows slightly better performance than aluminium, but the cost per kilogram is around 80x higher. Therefore, aluminium is the best material for this application. Specifically, aluminium 6005A T5.

In comparison to other manufacturing methods, DED has terrible performance for geometrical accuracy. A surface roughness in the order of $1\ mm$ can be expected, which is caused by the layering effect. Depending on system specifics, part accuracy can be off by centimetres in the worst cases. Process monitoring can greatly improve part accuracy and will be required for applying DED in space. The solar array structure does not require high accuracy geometry, with the exception of the connection points. Therefore, DED is suitable for the application. For critical points alternative solutions can be used, such as the proposed premanufactured print base structure.

The process will behave differently in space than on Earth. The most critical environmental differences are microgravity, vacuum and thermal fluctuations. Buoyancy and fluid convection in the liquid metal in the weld, caused by locally different densities, are diminished in space. Surface tension becomes the most important factor in fluid behaviour. The functionality of 3D printers in space has been proven by the 3D Printing in Zero-G Technology Demonstration, as well as tests on Earth. Future research needs to thoroughly investigate DED behaviour in microgravity in simulations and practical tests.

Vacuum in space removes the convection component in heat dissipation. To investigate the consequences, as thermal model was made. Vacuum also creates benefits. GMAW WAAM is normally combined with an inert shielding gas to remove oxygen and contaminating particles from the weld pool. This is not need in space. The effects of vacuum on the material properties need to be further investigated in future research.
Thermal fluctuations have an impact on both the 3D print and the equipment. Firstly, all materials need to be able to withstand both high and low temperatures. Secondly, the system needs to be operational despite the thermal expansion and shrinkage. These effects can be diminished be implementing a sunshield.

Through simulations the thermal behaviour of DED in space can be better understood. Abaqus combined with an additive manufacturing plug-in were used to make these simulations. Typical parameters for wire-based DED are used, as well as the material properties for aluminium 6005A T5. By changing thermal properties, the importance of these parameters was found. This was used to get a better understanding of the impact of thermal properties in the material selection.
A model was created in which a worst case scenario for irradiation was simulated. This is when the irradiation from the Sun and Earth on the tube are largest. The results of the simulation showed that the irradiation components do not significantly impact the tube temperature during the printing process.
Interpass temperature is an important parameter in additive manufacturing. This is the temperature right in front of the location were printing takes place, in the previous layer. When the interpass temperature is too high, the print can fail due to deformations or thermal stresses. It was found that under regular operating parameters, the interpass temperature was around 350℃. In the literature 150℃ was commonly set as the maximum for interpass temperature. Higher temperatures negatively affect the microstructure of aluminium, thus material properties. Idle time in between layers is required to not exceed the maximum interpass temperature. In the model, print speed was reduced from 10 mm/s to 5 mm/s and an idle time of 120 s was added to achieve this. This means that in the proposed concept for manufacturing of solar arrays in space, the manufacturing rate is heat limited.

Modelling is critical for the success of additive manufacturing in space. High predictability must be achieved. There are many improvements to be made to the model created in this thesis, for which recommendations have been provided. In general, the behaviour of the DED process in space needs to be better understood. This can be done through research and experiments. When more information and understanding is gained, the design choices need to be iterated upon. The feasibility and critical aspects of applying directed energy deposition for in-space manufacturing of solar arrays have been demonstrated.

1 Introduction

The goal of this research is to learn about the limitations and system needs of applying wire-based directed energy deposition for in-space manufacturing of solar array structures. This is done by analysing the behaviour of directed energy deposition in a space environment, determining the material and design limitations of the structures and investigating the platform architecture and its limitations. This report proposes a design for an in-space manufacturing platform for solar arrays. This is the first step taken in the direction of realising such a system.

This thesis is a collaboration between Delft University of Technology, Netherlands Aerospace Centre (NLR) and Maana Electric. NLR and Maana Electric have the desire to do a project on in-space manufacturing (ISM). Both companies have not performed research on this specific topic yet and this thesis is the starting point for their project. There are multiple desires for the aim of the research. NLR would like to see an in-orbit structure builder, preferably using in-house additive manufacturing (AM) technologies. Maana Electric would like to see a system that makes use of their filtering system, which is capable of producing pure materials, like silicon and aluminium. Also, they have experience with autonomous solar panel manufacturing on Earth.
Research is done in exploring the challenges and limitations to make the additive manufacturing process work in space. In-space manufacturing (ISM) has some great benefits for solar arrays: larger and lighter arrays can be achieved. Though, ISM is a complex task, as there are many things that can go wrong. There are many parameters that influence the process, which cause uncertainty and inconsistent prints. The manufacturing process that has been chosen is wire-based directed energy deposition (DED). The literature study on in-space manufacturing [1], conducted prior to this thesis research, has concluded that DED is the best additive manufacturing method for solar array structures.

Since this is a new project, there are many directions this project can go. Along the way of exploring different aspects of this manufacturing platform, choices and assumptions were made. Decisions were made and researched to be able to go in depth. If the decisions made turn out to be unfeasible, it is still possible to take a step back and make changes. Iterations in future research will be required to make improvements on this proposal. There is a lot of work to be done to further develop this concept, for which recommendations are provided. This thesis project is the first step in finding the best way to approach this application.

The research has been divided into three phases, which each consist of a number of tasks. See Figure 2 for the break-down of the report structure in a block diagram. The first phase is called: *system architecture*. This phase explores what a spacecraft would look like that is capable of manufacturing solar arrays using DED. Necessary subsystems and functionalities are identified. A concept of what such a manufacturing system could look like is presented. More information is given about how directed energy deposition works. Certain choices, such as the type of solar panel, are made. Based on the found subsystems, an analysis of the required spacecraft power is made.
The second phase is: *material and design*. A methodical material selection method is applied for the solar array structure. Important material properties are discussed to figure out what is important and not. These parameters are based on environment, manufacturing method, performance and more.
Phase three: *DED in space* mainly revolves around the thermal behaviour of 3D printing in space. A thermal model is made to predict this. Problems in heat dissipation can be expected due to the lack of convection in space. Therefore, an analysis is made to see if alterations need to be made compared to normal DED operation on Earth. Additionally, other impactful factors that pertain to the space environment are discussed.

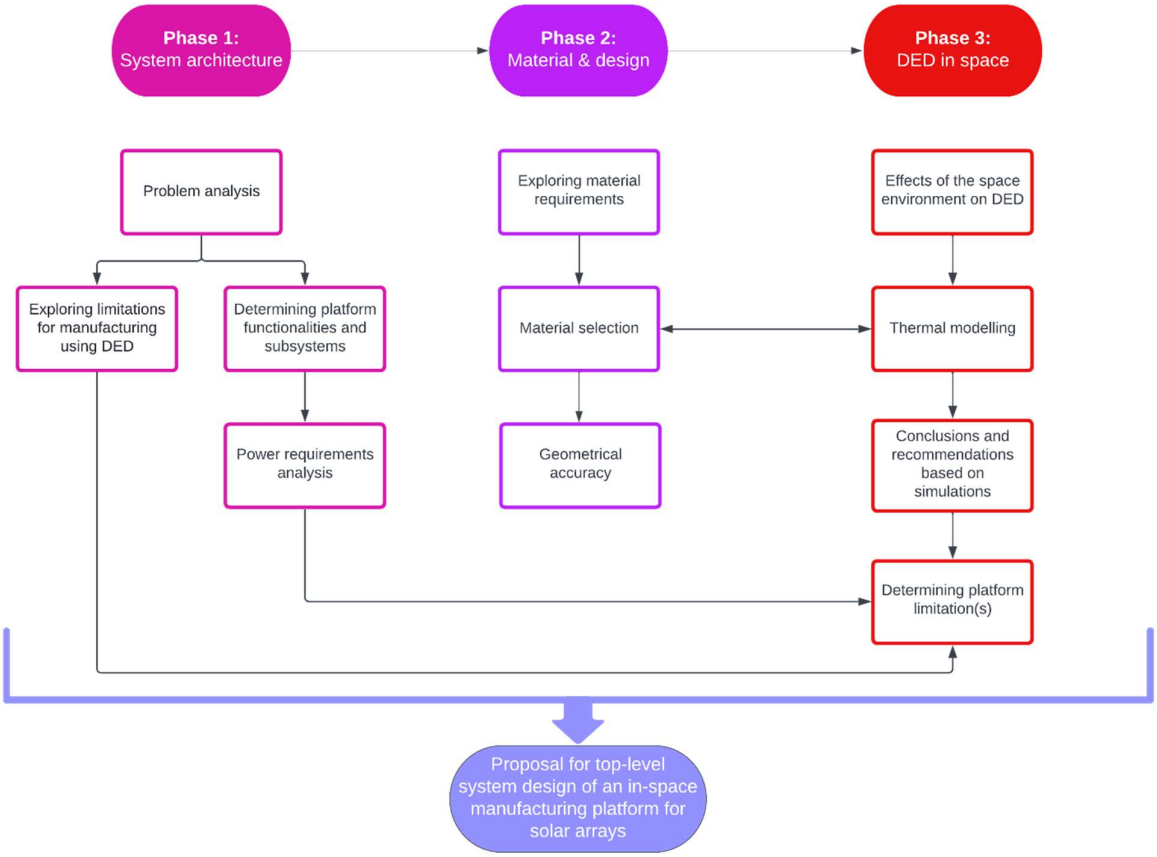

Figure 2: Block diagram explaining the layout of the research

Research questions have been formulated to set a goal for this thesis research. The comprehensive main research question has been divided into three sub-questions, each with their own components.

Main research question:
How can metal wire-based directed energy deposition be applied to in-orbit manufacturing of solar array structures?

Sub-questions:

1. What does the system architecture of the in-space manufacturing platform look like?
    a. Which functionalities and subsystems are required on the platform?
    b. What are the power system requirements for the manufacturing platform?
    c. What is the limiting factor in manufacturing rate for DED in space?
2. What are material and design possibilities for the solar array structures?
    a. What environment will the solar array structure endure?
    b. What is the optimal feedstock material?
    c. What are the geometrical limitations of the manufacturing process?
3. How will wire-based directed energy deposition handle the space environment?
    a. What are the influences of performing DED in space and how will this impact the manufacturing process?
    b. What does the thermal behaviour of the additive manufacturing process look like in space?

2 System architecture

This chapter looks into different top-level aspects for manufacturing spacecraft as a whole. Many routes can be taken to reach the goal of in-space manufacturing a certain component, so the possible routes are identified and based on current knowledge, the best option is selected. First, the problem and selected manufacturing technique are explained. Analyses are made of the options that are possible in the following fields:

- Directed energy deposition
- Solar arrays
- Use cases

Characteristics of the options are weighed-off and the best option is selected. A clearer image of what the spacecraft can look like and comprise of is created. This includes a simplified schematic overview of the systems on the envisioned spacecraft. The rest of the report is based on the choices made in this chapter. Without this basic system architecture, it is not possible to learn about the details of the system and obtain accurate findings on the feasibility of the system. Additionally, the power needs for the manufacturing platform are examined. Power is one of the factors that can possibly be the limiting factor to additive manufacturing in space. The power requirements for the manufacturing system are determined to calculate the total power requirement using estimation equations. The feasibility of the power estimation is discussed.

2.1 Why additive manufacturing of solar arrays in space

Operating a manufacturing and assembly system in space is an extremely difficult assignment, which is the biggest reason why many people disregard this opportunity immediately. A great deal of complexity is introduced by launching manufacturing machinery into space. However, there are good reasons that justify this. Fabricating solar arrays in space, instead of on Earth, will enable new missions and radically new approaches to satellite manufacturing. The most valuable reason why in-space solar array manufacturing is so useful, is because array sizes can be achieved that are way larger than what the current state of the art is capable of. Semi-finished products and raw material can be stored more efficiently than stowed solar arrays. The second reason is that in-space manufactured arrays can be much lower mass per panel surface area than their launched and deployed counterpart. The arrays do not have to withstand the launch loads if they are manufactured in space. The third benefit is that complex geometries can easily be created using additive manufacturing, that cannot or are difficult to create using conventional methods.

Solar panels are the most used source of energy for satellites. They are generally applied in two ways: stationary panels or deployable panels. Both use prefabricated arrays that have been built on Earth. The size that these panels can have is limited by the payload volume of the launcher. The envelope assigned by the launch service cannot be exceeded, so even in the stowed configuration, the solar array can never be bigger than a certain size. In contrast, in-space manufactured arrays are only limited by raw material supply. Solar cells and DED feedstock material can be stored in an extremely compact package. Additionally, if the raw materials are depleted, it is still possible to refill the manufacturing spacecraft's stock through supply missions.
An argument can be made that pre-built deployable solar arrays can be supplied to a single spacecraft through supply missions. The International Space Station (ISS) is a good example. The ISS has the largest surface area of solar arrays of any spacecraft. Initially, it was installed with eight solar array wings (SAW), each $35\ m$ x $12\ m$ in deployed state and capable of generating $31\ kW$ [2]. These are the largest solar arrays ever deployed in space. NASA will increase the total power generated on the ISS by adding three Roll Out Solar Arrays [3]. All of these panels have gradually been added

through different missions, generally one or two panels at a time. However, all these deployable panels total to a massive amount of mass. Each of the SAW panels has a mass of nearly $1100\ kg$. This is where another advantage of in-space manufacturing of solar arrays shines: mass-saving.

A lot of time and resources are spent on the development of solar cells, to keep increasing their efficiency. The goal is to obtain the maximum amount of power in space in the smallest package. These high efficiency solar cells are much more expensive than the standard household solar cells. This is necessary to keep the mass of the solar arrays as low as possible. However, the cost of satellite solar arrays is not solely determined by the cost of the solar cells themselves. The solar panels that are used for current satellites are designed for sufficient strength at a low mass. Low mass is always a key driver to the design of components that are launched into space, because the cost per kilogram is extremely high for the payload in launch vehicles. See the literature study on in-space manufacturing [1] for examples of launch costs. It is possible in some cases that the cost of the solar cells and electronics is lower than the cost of launching the mass of the solar array [4]. Therefore, it is crucial to keep the structural mass low, considering that it is difficult and costly to lower the mass of the solar cells and electronics even further. Solar array structure means in this case the parts in the array assembly that support the solar cells; material that is used to maintain the desired panel shape and achieve the required structural strength.
The required strength of the panel structure is predominantly determined by the loads that will be experienced during launch. The launch environment is extremely harsh. Strong vibrations and large accelerations can be expected. The environment in orbit is less demanding for strength requirements of passive structures, because of the microgravity experienced in space and the small movements the solar panels will endure compared to launching. Manufacturing the structure in space means that the strength required for launch conditions is not needed. Because less strength is required in orbit, the solar panel structure design can be made thinner. Therefore, less structural mass is needed, which lowers launch cost. Though, mass is added by the equipment that is required for manufacturing. At a certain solar array size, manufacturing in orbit will be cheaper. This is at the point where the mass and cost saved by not using a deployable structure is higher than the mass and cost added by the manufacturing facility.
At this stage, cost is difficult to quantify for in-space manufacturing. As opposed to deployable solar arrays, ISM technology for solar arrays is at a low technology readiness level (TRL) and no flight-proven system is ready to implement on a mission. Additionally, the structural shape must be investigated first to find a meaningful answer for the expected structural mass, which is not part of the scope of this thesis. There are currently too many unknowns to determine the minimum solar array size where in-space manufacturing is a better option than deployable arrays.

Figure 3: Example of generative design, an optimized robotic arm 3D printed using DED (WAAM) [5]

The third benefit relates specifically to using additive manufacturing as the ISM method. AM has the benefit over other methods to produce complex geometry for the solar array structure. For example, geometry optimization can be applied to the design of the structure. Geometry optimization is a method that perfects a design through computer software. The program reduces the mass as much as possible based on the expected forces. It does this by repeatedly trying different permutations of the same design. Shaving or adding material and running finite element method (FEM) analyses. Through each iteration the program learns more about what the best possible design is. This commonly results in odd shapes with lots of curves and changing thicknesses. Connecting rods can be slender in the middle and thicker at the ends where stress concentrations are expected. Figure 3 shows and example where a traditional part has been optimized, resulting in natural, flowing shapes.

Other manufacturing methods are unable to create such complex shapes or the increased shape complexity creates more difficulty in the manufacturing process. Milling, casting or welding prefabricated beams all have significant limitations and cannot achieve the level of weight saving that AM can. The opportunities for designs are nearly unlimited using AM, without adding much build time or risk. This applied to DED in particular, since it is not limited to a build volume the way powder bed fusion (PBF) methods are and it uses a robotic arm to be able to reach everywhere.

It is important to note that this research does not develop or choose a certain structure shape. Instead, the top-level aspects that influence the specific design are researched. Opportunities and limitations are discussed. Determining the ideal structural design is a research topic by itself, in which a lot of time need to be invested. Findings in this report can help with creating a specific structural design by providing conclusions, advice or findings in the literature. Research on the structural design of in-space manufactured solar arrays is a great follow-up study to this research.

2.2 Problem analysis

The goal for this thesis research is to investigate the top-level design and feasibility of an in-orbit solar array manufacturing platform. To do that, first the outline of the project and the choices that have been made leading up to the current plan are explained. Manufacturing of the structures for solar arrays by a manufacturing platform in space is the topic that NLR chosen to research. This will be done using additive manufacturing. Prior to this thesis research, a literature study was done on in-space manufacturing with a focus on additive manufacturing [1]. The goal for this study was to understand the current state of the art, which ISM projects have been flight-demonstrated and what knowledge is available/missing in the literature.
Additive manufacturing is particularly interesting for in-space manufacturing. Because of its nature, it produces less waste than most conventual manufacturing techniques. The field of additive manufacturing is space is new, but strongly in development by many different companies. NASA has handed out a lot of funding to various companies for ISM projects. In the literature study on ISM it was found that the best AM method for the production of large (metres scale) objects is directed energy deposition. Powder bed techniques will not work in a microgravity environment in the way it is used on Earth. Most other AM techniques require more complex, bulky equipment or additional post-processing procedures. Directed energy deposition has the benefit that it has a great amount of design freedom when combined with a robotic arm, as is often done. The process and equipment are relatively simple, which is preferred for space applications. DED can achieve the highest production rates among AM methods.

In Section 2.3 the DED process is explained so readers will have a basic understanding of the process, as well as the components that are needed on the spacecraft and what aspects require consideration in the process of applying DED in space.

2.2.1 Need statement

The need statement is a short description that explains the operational need of the system. It provides a concise, clear explanation of the goal is for the complete system. For this research it helps to keep the focus in the right direction. Topics in this report can get extremely detailed, which makes it easy to get on a tangent and get distracted from the important parts. Coming back to this need statement will quickly help with getting back on track. Here is the general need statement for this project:

“A manufacturing spacecraft will be proposed that is capable of fabricating solar arrays using directed energy deposition for additive manufacturing of the solar panel’s structures while orbiting Earth.”

2.2.2 Stakeholders and their needs

At this state of technology and in the frame of this project, the only stakeholders are the project owners NLR and Maana Electric, as well as TU Delft to a small degree. The project is still at a low TRL and in development. There is no client currently. Though, these companies have certain desires for the goals of this in-space manufacturing platform.

NLR mainly steers the top-level aspects of this project, such as a preference for additive manufacturing for in-space manufacturing. There are no desires for the system specifics. Their wish is to find the most feasible system. For the mission, some parameters are provided by NLR. The goal is to design a system with a lifetime of 10 to 15 years. The

spacecraft will orbit Earth, however the specific orbit remains unspecified. A height of $500 - 1000\ km$ can be taken as an estimation of the height of the orbit, but this is just for calculation purposes and certainly not definitive. For the real platform, the orbit will be greatly influenced by the customers. There have to be plenty of spacecrafts near this orbit that need large solar arrays to make this manufacturing platform feasible. Low Earth orbit (LEO) contains the most spacecrafts and it is the cheapest to launch to. Alternatively, geostationary Earth orbit (GEO) would be interesting for the platform, since most power-demanding communication satellites are in that orbit.

Maana Electric is a company that works on technology that is capable of filtering input material into the pure form of one of its contents and supplying this in some shape that is required by the manufacturing method, such as beads or powder. Currently, this is being used for automated, local manufacturing of solar arrays in deserts areas on Earth. This system uses sand as an input material and can purify the silicon content for the use in the production of solar panels. Maana Electric's vision is set beyond Earth. Their aim is the realisation of in-situ resource utilization (ISRU) that can be used anywhere, including space.
The involvement of Maana Electric for this project comes from their interest in the supply of feedstock material. How this will be done exactly is to be determined in a later stage of the project. This can, for example, be done through the recycling of space debris, which is sorted, purified and processed into feedstock material for the DED process. Another source of raw material is regolith. Lunar or Martian soil contains usable materials for building structures, which can be purified using Maana Electric's systems.
Maana Electric's processes are able to provide different types of feedstock. Wire has been chosen for the additive manufacturing process, but beads and powder are also available types of feedstock for different types of systems. For the materials, silicon and aluminium have their preference. Alloys of these elements are also possible. If the results for the material selection show that other metals perform better than silicon and aluminium, it is possible for Maana Electric to investigate the options of supplying that material.

TU Delft's only involvement is in guiding the research process of this thesis. Advice and feedback are given on the structure, planning and contents of this report. No preferences for the direction of this project can be given by TU Delft, as the university does not collaborate with NLR on this project.

2.3 Directed energy deposition

AM is well suited for manufacturing in space. Since the process is additive instead of subtractive, like milling for example, there is little waste. Waste is highly undesirable for space, because the cost to launch material mass into space is high. Solutions for waste in the form of recycling systems have been proposed and are even being developed currently. Though, this adds mass and complexity to the already complex manufacturing platform, so AM is preferred considering waste. Recycling and AM can be combined as well, but, as opposed to subtractive processes, this is not essential to make it feasible. So, this can be investigated in a later stage of development.
Additive manufacturing also allows for great design freedom. There are few limitations to the shapes that are possible and complex shapes do not add difficulty to the manufacturing process. This means that optimized, complex shapes can be generated, which lower the structural mass compared to designs for conventional manufacturing methods.

Different additive manufacturing technologies have been researched in the literature study on in-space manufacturing [1]. It was concluded that directed energy deposition (DED) is the best method for in-space manufacturing of solar array structures. As opposed to many other methods, DED allows for large component sizes, while not requiring complex post-processing procedures. The only other AM methods that are not bound by a build volume are material extrusion and material jetting. However, products resulting from both of these methods must undergo debinding and sintering processes. Separate facilities are required to do this, while DED does not need additional post-processing procedures. Although DED also has some limitations, such as to the geometrical detail, this is deemed the best method for in-orbit applications. See the literature study on in-space manufacturing for a more elaborate explanation on why DED is the best method for this application [1]. Additionally, the topic geometrical accuracy of DED is covered in Section 3.3.
DED 3D printing requires an inert environment with low oxygen and moisture levels to prevent oxidation on the part at the high temperatures that are experienced during the process. Therefore, facilities on Earth either purge the machine environment with an inert gas, jet the inert gas around the nozzle or pull a near-vacuum to protect the melt pool. The space environment is ideal to perform DED in. The ultra-high vacuum in space will prevent oxidation on the part. Also, space is a clean environment, so contaminations that can be embedded in part during the manufacturing process are not expected.

2.3.1 Space debris particles and legislation

DED can be performed using two types of feedstock: wire and powder. The use of powder in space is accompanied by restrictions, complications and uncertainty. It cannot be guaranteed that all particles stick to the build plate or object, thus some powder will inevitably drift into space. Although the particles are small, introducing new waste in space is highly undesirable, especially if powder-based DED would be applied in space on a large scale. Even small particles can do serious damage when equipped with the extremely high relative speeds that can be achieved in space. Currently, there are already various sources that introduce space debris particles, such as aluminium oxide particles from rocket boosters, aluminium fragments caused by small impacts, paint flakes and more. These exist besides larger pieces of space debris, like malfunctioning or end-of-life objects, collision debris and jettisoned parts as according to normal launch operations.
Convention on International Liability for Damages Caused by Space Objects (Liability Convention, 1972) [6] has set up a list of rules and procedures to guide situations in space where damage is inflicted involving multiple states, which is ratified by 98 states. This treaty contains procedures on how to act after damage has occurred. There are no specific rules related to creating space debris, merely what to do if one state's space debris causes damage on another state's

property or people. Article IX expresses the responsibility to conduct exploration to avoid harmful contamination. Nevertheless, there are no legal obligations created by this treaty.
Other organisations have created guidelines to expand on the Liability Convection by providing technical recommendations on how to avoid the introduction of unnecessary space debris. *Space Debris Mitigation Guidelines* was first published by IADC in 2002. Similar to these recommendations, COPUOS created *Space Debris Mitigation Guidelines of the Committee on the Peaceful Uses of Outer Space* in 2007. International Organization for Standardization (ISO) has created guidelines for mitigation of debris in space: *ISO 24113:2019*. This is the third edition of this document and updated its guidelines over the years. Low Earth orbit (LEO) and geostationary Earth orbit (GEO) are protected regions. Special guidelines are set for these areas to ensure safe long-term use. *ISO 24113:2019* states: "Spacecraft shall be designed so as not to release space debris into Earth orbit during normal operations, other than space debris from pyrotechnics and solid rocket motors." (Art. 6.1.1.1). Pyrotechnics and solid rocket motors are not allowed to release particles larger than $1\ mm$ (Art. 6.1.2.1 & 6.1.2.2).
Although none of these norms for the mitigation of space debris are binding, many countries have already implemented similar rules into their national legislation [7]. Still, several states disregard these guidelines as they keep creating new space debris, though fortunately at a declining rate. This is caused in particular due to the lack of legal repercussions for these actions.
The prime focus of these debris mitigation guidelines is large objects. It was found that large objects are also the main cause of creating smaller particles, because of collisions. No specific attention is given to objects smaller than $1\ mm$, besides the general statement of "limit debris released during normal operations". Also, during the inspection of the above-mentioned documents, zero rules or guidelines were found specifically relating to in-space manufacturing.

Wire-based DED has a nearly 100% capture efficiency of the feedstock (the amount of material binding to the subject), whereas capture efficiency for powder-based DED is at maximum 90%, but can be as low as 20% [8] [9]. Figure 4 clearly demonstrates that not all material adheres to the subject and particles are spread into the environment. This information is for operation on Earth, as there is no information available in the literature on DED in space. However, it is expected that this is not significantly different in space.
A solution to particles drifting away is to perform powder-based DED in an enclosed area. However, this will introduce more complexity and mass to the system, since dedicated enclosure parts need to be equipped for this. Choosing wire-based DED of powder-based is a simpler solution.
The guidelines or rules for releasing small particles ($< 1\ mm$) into space are limited. The wire thickness for DED is typically in the order of millimetres. It is not expected that DED creates free flying particles larger than $1\ mm$. Although it would not be illegal to apply powder-based DED in space, it is undesirable and must be avoided at high cost. One could make a case that wire-based should not be applied in space either, because still some small particles will drift into space, as the capture efficiency is not exactly 100%. However, based on current (international) legislation, guidelines and impact, the benefits outweigh the risks. Guidelines say debris must be limited, not zero, which is done by choosing wire-based DED over powder-based. The total impact is low at this stage of technology for DED in space. This would increase when more DED equipment will be used in space. In future work, an in-depth analysis should be made to find the impact of uncaptured particles created by the DED process. And interestingly, the number of particles created by in-space manufacturing equipment for solar arrays should be compared to the number of particles released by rocket motors used for the launch of spacecrafts with traditional solar arrays.

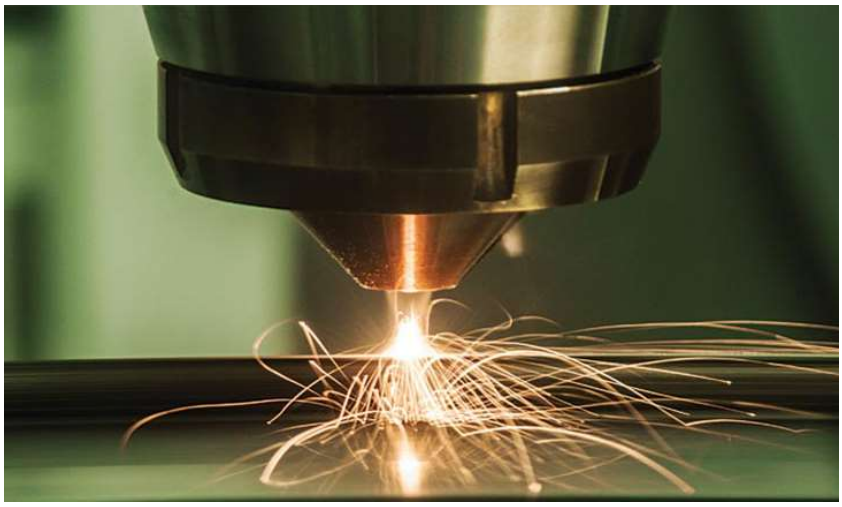

Figure 4: Powder-based DED scattering of particles [10]

2.3.2 Types of wire-based DED

Figure 5 shows a schematic representation of the working principles of wire-based DED. A material filament on a spool is fed into the nozzle which directs the wire onto the substrate. The wire used typically ranges from $1 - 3\ mm$ in diameter [9]. A thermal energy source is used to melt the wire as it touches the substrate. Different types of energy sources can be used to melt the material in DED. The melted feedstock wire is deposited onto the build object. This process is comparable to welding. Since welding has already been used in space for a long time, the knowledge gained in research on welding in space can for some cases be used to make predictions for DED behaviour in space. The fact that welding is a well-researched, flight-proven tool adds to the confidence for DED to be a viable method. Directing the deposition of material can happen in multiple ways. A robotic arm for the weld tool, a moving base plate or a combination of the two are most often used.

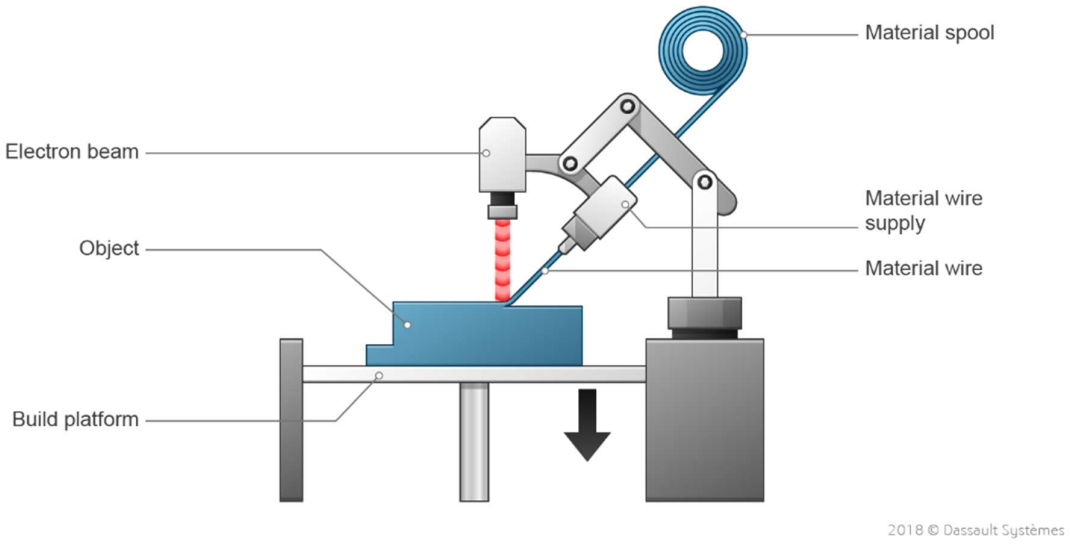

Figure 5: Schematic representation of the working principles of directed energy deposition, in this example of WEAM [11]

The various types of wire-based DED that exist have been summarized in an overview, see Table 1. In this table advantages and disadvantages have been listed to use for the selection procedure of the best method for this research's application. Figure 7 shows the different heat sources in action. Standards are available for DED processes. *ASTM F3187-16 Standard Guide for Directed Energy Deposition of Metals* [12] provides definitions, descriptions, process environment, post-processing, safety and much more regarding various DED processes. This document states that it is possible to use wire-based DED in a microgravity environment. Besides the ASTM guide, the papers *Directed Energy Deposition (DED) Process: State of the Art* by Ahn [8], *Directed energy deposition (DED) additive manufacturing: Physical characteristics, defects, challenges and applications* by Svetlizky et al. [9] and *Wire-feed additive manufacturing of metal components: technologies, developments and future interests* by Ding et al. [13] are used to obtain advantages and disadvantages for each type. These documents each combine the findings of multiple sources, so their results combined provides a thorough analysis of the different manufacturing processes.

The three optional heat sources for wire-based DED are arc, laser and electron beam. Wire and arc additive manufacturing (WAAM) can be subdivided into three processes, which have the same working principle as welding processes. Therefore, they are named after the respective welding processes: gas metal arc welding (GMAW), gas tungsten arc welding (GTAW) and plasma arc welding (PAW). Figure 6 shows the working principle of each process. In GMAW the wire that is used to add material to the subject is also the electrode. An arc forms between the consumable wire and the subject, creating a weld pool into which wire material is deposited. GTAW and PAW use an electrode, often tungsten, that is separate from the wire and is non-consumable. From a feeder nozzle, wire is inserted into the weld pool, melting it and depositing material. The difference between GTAW and PAW is the control of the created arc. In GTAW the electrode is visible from the outside and the arc is free, besides normally being surrounded by a shielding gas. In PAW the electrode is inside of the welding nozzle and not visible. The plasma arc is constricted by the inner copper nozzle and an inert shielding gas. The smaller welding zone for PAW creates a smaller weld.
GMAW and GTAW normally use a shielding gas to create a local inert environment. This is not required in the vacuum of space. PAW may not be suitable for use in vacuum, because it requires a gas to constrict and direct the plasma arc. Ejection of gas in a vacuum has a lot of uncertainties that need to be researched thoroughly before application. Boeing has researched GTAW in vacuum where argon gas was supplied through the hollow electrode [14]. They created a successful system which was able to consistently produce quality welds. Still, this is not ideal for the scope of this project, which is already very complex as it is, so uncertainties must be avoided. Additionally, gas is a consumable that needs to be resupplied over time, which is undesirable in space.

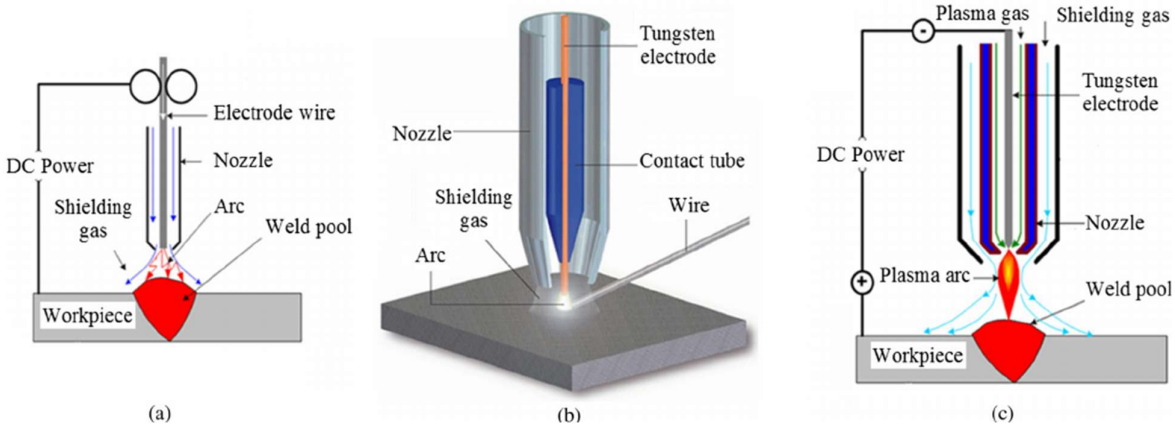

Figure 6: Working principles of different wire and arc processes: (a) GMAW, (b) GTAW and (c) PAW [13]

Welding using an arc in a vacuum is an interesting topic as there are uncertainties for how the arc behaves. Instinctively, it may not seem possible, because an arc requires an ionized gas for conduction. However, tests showed that arc welding in vacuum is possible [15] [16]. Enough electrons are emitted from the surface and vaporized metal particles are released to allow for a sustained arc. The behaviour of the arc in vacuum must be well understood to realize the application of an arc welding method in space.

A modified GMAW process has been developed to mitigate the undesirable traits of GMAW. This method is called cold metal transfer (CMT). It is based on controlled dip transfer. The current and wire insertion are controlled during the welding process as the metal droplets touch the surface. Without control, more fluctuations in current and voltage cycle is experienced, which has undesirable effects. Additionally, using CMT the arc length can be controlled. The benefits of the CMT process are lower spattering, less heat input in the part and higher quality welds.

Electron beam wire-based DED principles are shown in Figure 5. Wire and electron beam additive manufacturing (WEAM) uses an electron beam as the heat source to melt the substrate surface and wire. This beam consists of accelerated electrons, which are accelerated by an electrostatic field. The kinetic energy of the electrons is converted into heat upon impact with the materials. The wire can be fed from the centre of the nozzle and the electron beam is concentrically focussed on the wire tip. Whereas all metal wire AM processes require a protective environment, WEAM specifically requires a vacuum environment. This process is well suited for high deposition rates. High power is required to do this ($5 - 42\ kW$), so it must be investigated if the spacecraft has the energy capabilities to utilize this advantage. An energy analysis is done in Section 2.7. The hot or cold cathodes that are used for the electron beam gun have a limited service life. Depending on the type of cathode that is used, the cathode needs replacement after several tens to thousands of hours of operating time.

The principle of wire and laser additive manufacturing (WLAM) mostly works the same as for WEAM, but with the electron beam emitter replaced with a laser. WLAM uses a high-power laser to melt the wire and subject to create a weld pool. This is a relatively simple setup with the laser positioned directly above the subject and a nozzle besides it which feeds the wire at an angle into the weld pool. It is not able to position the wire and laser coaxially, like WEAM. That means that the wire feeder needs to rotate to make sure the wire is consistently inserted from the same direction. Otherwise the weld properties would be inconsistent. This results in a more complex path. As opposed to WAAM, WLAM causes the top layer to have a hardness gradient, which is the result of the rapid heating and cooling cycle. This causes the part to have a higher strength in the deposition direction than in the building direction.

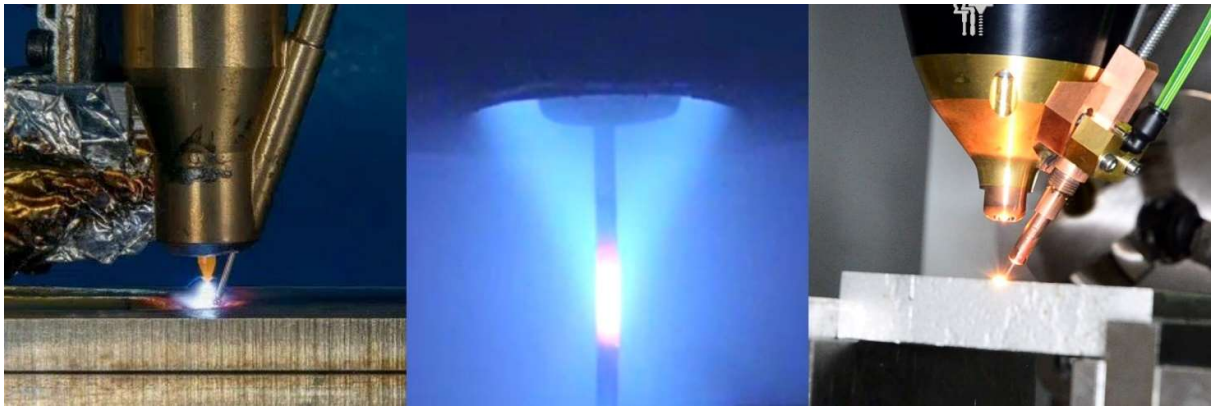

Figure 7: The three different types of heat sources for wire-based DED: WAAM-GTAW (left), WEAM (centre) and WLAM (right) [17] [18] [19]

Welding is a manufacturing method that has been used in space for decades and has been researched a lot, although mainly for use in a pressurized environment. Precedence and being flight-proven are valued greatly in spaceflight. Since wire-based DED has a lot is similarities with welding, it is examined which welding methods have been used for space applications already. To summarize *A review of Welding in Space and Related Technologies* by NASA from 2020 [20], electron beam welding is the most used method for space and has historically produced the highest quality welds. Arc welding techniques have also been researched, especially by the Soviet Union in the early years of spaceflight. Not many laser-based welding devices have been developed for space. Although they are functional, a reason for the lack of development interest is the problem of reflection that arises when using lasers. Materials with high reflection are difficult to weld or cannot be welded. Aluminium, the most common structural material for space, is one of those materials that has reflection issues.

Electron beam welding (EBW) is a method that has been proven to suit the space environment well [21]. In 2018, a new weld gun design for space was created and published, and again EBW was chosen. This was chosen over a laser-based gun, because of issues with reflection on materials, as well as the fact that EBW has created the highest quality weld in the past.

The Mobile End-effector Laser Device (MELD) is a project in development by Made In Space and funded by NASA. This project was investigated in the literature study on ISM [1]. MELD is a robot with the goal of repairing spacecraft structures damaged by micrometeorites or debris. To do this it is equipped with a robotic arm and weld gun. Laser is being used as the welding method. Another welding robot mentioned in the ISM literature study is by Busek Co. Inc. [20] [22]. It has a similar purpose as MELD, with the difference that it is attached to a mothership through an umbilical cord for power and data transmission. During Phase 1 of this project, one of the goals was to select a welding technology. The funding contract abstract states that its principal options are laser, EBW, arc-based techniques and spot welding. Unfortunately, no follow-up has been published on this development.

It is interesting that there is no one welding method that is universally used. The application affects the choice. Although EBW seems to be the favourite space welding method on historical use, it is important to note that welding in space has been used mostly, if not all, for human operation. Robotic, (semi-)autonomous welding in space has different requirements. Perhaps most notably in servicing. It challenging to create a system that is capable of replacing a consumable or worn part, so this must be avoided if possible to lower complexity and risk of failure. It is not explained why a laser is used in MELD, but maintenance expected be a big part of the reason.

Table 1: Wire-based DED processes and their advantages and disadvantages

Abbreviation	Name	Heat source	Comments
WAAM (GMAW)	Wire and arc additive manufacturing (gas metal arc welding)	Arc	• GMAW equipment is cheaper and less complex than GTAW and PAW. • Higher residual stresses and distortions than the other WAAM processes, induced by an excessive heat input • Simpler deposition path due to co-axial wire feed • Low arc stability • Spattering
WAAM (GTAW)	Wire and arc additive manufacturing (gas tungsten arc welding)	Arc	• GTAW equipment is cheaper and less complex than PAW • Relatively smooth surface and high strength • Greatly reduce porosity compared to GMAW • More stable and reliable process than the GMAW • Higher residual stresses and distortions than WLAM and WEAM • Off axis wire feeding, so more complicated deposition path
WAAM (PAW)	Wire and arc additive manufacturing (plasma arc welding)	Arc	• PAW can create relatively narrower deposition bead, causing less weld distortion • More stable and reliable process than GMAW • Off axis wire feeding, so more complicated deposition path • Higher residual stresses and distortions than WLAM and WEAM • Requires consumable gas
WLAM	Wire and laser additive manufacturing	Laser	• No porosity • Hardness gradient in top region • Does not work well with reflective materials • Off axis wire feeding, so more complicated deposition path
WEAM	Wire and electron beam additive manufacturing	Electron beam	• High deposition rates • Limited lifetime of cathode

Table 2: Typical parameters for DED techniques, powder-based is also included for reference

Process	Typical layer thickness (µm)	Minimum feature size (µm)	Density of heat flux (W/mm^2)	Energy efficiency (%)	Deposition rate (g/min)	Capture efficiency of feedstock (%)
WAAM (GMAW)	1000 - 2000	1000 - 2000	~10^4	<90	33.3 - 66.7	~100
WAAM (GTAW)	1000 - 2000	1000 - 2000	~10^4	<90	16.7 - 33.3	~100
WAAM (PAW)	1000 - 2000	1000 - 2000	~10^4	<90	33.3 - 66.7	~100
WLAM	>1000	5 - 15x wire diameter	~10^6	2 - 5	1.5 - 48.0	~100
WEAM	<3000	<1600	~10^8	15 - 20	<330	~100
Powder-based DED	200 - 500	380 - 1000	~10^6	<40	<8.3	<90

2.3.3 Wire-based DED heat source trade-off

A trade-off diagram is made to combine the many different parameters into a single performance value. This can be found in Table 3. Table 2 contains an overview of typical parameters for different types of DED [8]. These values are used as inputs to assess the types' performances in this trade-off.
The categories that are assessed are: detail, print quality/strength, deposition rate, durability, complexity, energy efficiency, system mass, system cost and application in space. A score is given per heat source category from a scale from one to fine, higher meaning better. Each of these categories is assigned a certain weight, which values the importance relative to the other categories. This is done on a scale from one to five, higher meaning more important. The most important categories are deposition rate, durability, complexity, energy efficiency and application in space. These all either relate to critical factors to placing the DED type in a space environment or to the performance of the manufacturing platform. At this stage it is still unknown what the limiting factor is, so it is hard to weigh out efficiency versus deposition rate for example. It is expected that power is limiting, so this is weighed the highest. To improve upon this trade-off, iterations of this process should be done using the results from this report.

Deposition rate and **energy efficiency** are directly rated based on the values from Table 2.
Detail is the combination of typical layer height and minimal feature size in Table 2 and this resembles how accurate the manufacturing method is able to create the geometry design. The performance is very similar for all, expect for WLAM. For WLAM the minimum feature size depends on the wire diameter, which is undesirable as this creates a trade-off between detail and deposition speed.
Durability says something about the service life of the tools, how often it needs maintenance or repair and how easy this is to perform. WEAM requires replacement of its cathode each couple of months at best. For the arc methods with a non-consumable electrode (GTAW and PAW) it is possible that the electrode gets damaged or contaminated. This requires repair of the electrode, though this only happens in improper operation or accidental contamination.
Print quality/strength evaluates to what degree internal stresses, porosity and distortions are experienced. These are all undesirable as they lower the strength and accuracy of the part, which lowers the performance of the structure. GMAW shows worse performance than other WAAM processes. WLAM has difficulty with reflective materials.
Complexity has been mentioned multiple times in this report, because it is undesirable for space applications. Complexity creates risk, because there will be more points in the system that can fail. In space there is almost never the option to service the spacecraft is something goes wrong, so risk of failure must be minimized. All of these methods require power electronics. GMAW is the simplest way of performing wire and arc welding, GTAW has more parts and PAW even more. The laser equipment may be hard to manufacture, but not much can go wrong during operation. The equipment needed to produce the electron beam is even more complicated.
Mass and **cost** are the least important parameters. That is also because the DED types do not differ greatly, relative to the mass and cost of the complete manufacturing spacecraft. Generally, they scale with the complexity. Though, the laser is expensive, yet not so complex. PAW requires a gas tank, which increase mass and cost.
Application in space is not a quantitative parameter, but it is there to represent the advantages and disadvantages that are specific to a DED type. GMAW has a higher degree of spattering, which is bad. Spattering is a cause of particles drifting into space. GTAW, PAW and WLAM all required off-axis wire feeding. This makes the deposition path more challenging as the angle of the wire to the weld direction needs to remain constant. The print head needs to be able to rotate to achieve this while printing a round tube. PAW requires a consumable gas, which is undesirable. The arc used in WAAM methods can cause some uncertainty in a vacuum environment. This must be further researched, whereas laser and electron beam are already well understood in vacuum.

Table 3: Wire-based DED heat source trade-off diagram

Category\Type	**Weight**	WAAM (GMAW)	WAAM (GTAW)	WAAM (PAW)	WLAM	WEAM
Detail	2	5	5	5	3	5
Print quality/strength	2	3	4	5	3	5
Deposition rate	4	3	2	3	2	5
Durability	4	5	3	2	5	1
Complexity	4	5	4	2	5	3
Energy efficiency	5	5	5	5	1	2
Mass	1	5	4	2	4	3
Cost	1	5	4	3	3	2
Application in space	4	3	3	2	4	5
Weighted sum	27	115	99	86	88	91

The results turned out to be very close. This confirms the impression that was obtained from the advantages and disadvantages overview in Table 1. Each method has distinct characteristics and no one method has all benefits for space application without any significant disadvantages. GMAW WAAM is chosen as the DED type to move forward with in this project. It has the highest total score, as is highlighted in green in Table 3. Top reasons for this conclusion are the energy efficiency and simplicity of the system that required little maintenance. Significant downsides for this method are the use of an uncontrolled arc in a vacuum and spattering. More research needs to be done to better understand the behaviour of the GMAW arc in space vacuum. A limited amount of information is currently available on this topic. Furthermore, behaviour of the arc in an additive manufacturing application in vacuum is even more unknown.

Spattering causes particles to escape the subject and float away in space. Creating space debris must be avoided, but in this case the advantages outweigh the disadvantages. Section 2.3.1 concluded that there is currently no legislation for space debris caused by in-space manufacturing. It can be expected that in the future rules will be created say something in the lines of "An in-space manufacturing platform may produce no bigger space debris particles larger than $1\ mm$ and no more than 0.01% of the deposited additive manufacturing material". It cannot be said at this point if that will be a problem for using GMAW WAAM. More research needs to be done to find out much spattering can be expected and how to amount of space debris can be minimized. CMT has already been identified as a method to reduce spattering and improve GMAW performance.

2.4 Solar panels

This research is focussed on the manufacturing aspect of the array as a whole. Therefore, a choice is made for the type of solar panel will be worked with. This will impact that way they need to be installed. A suitable panel type needs to be chosen that can be easily installed, which is a crucial requirement considering the large scale the array will be. Which type of photovoltaic cells are used on the panel type is not important for the manufacturing process of the solar array structure.

The most important parameter for in-space manufactured solar arrays is that the solar panels need to have the lowest volume in stowed configuration per power generation capacity. Size in deployed state is not a limitation in this case. A bigger panel does not add much to the complexity of the systems as a whole, as opposed to conventional solar power systems where each node or hinge adds significant complexity. These are vulnerable points where something might go wrong. Size in stowed configuration, however, is limited by the launch vehicle envelope. In the simplest application case the launch vehicle envelope is the limiting factor to how big the manufactured array can be. Restocking missions can be used to increase the maximum array size or number of arrays that can be manufactured. New filament spools and new solar panels will allow the manufacturing station to extend its operation.
The assumption that size is the limiting factor is under the condition that maximum payload mass is not exceeded. Since raw materials are launched instead of final products, the payload is more densely packed. Feedstock for the additive manufacturing system will have a higher density than a deployable structure, because it is a more compact package. Therefore, there is a possibility that mass limits are exceeded. To find what is actually the best factor to determine the best solar panel, mass or size, a case specific analysis needs to be made which calculates the required structural mass based on the structure geometry and panel mass. Also, the payload volume of the chosen launch vehicle must be compared to the platform's and its components' sizes. This will determine the driving factor. In conclusion, it will be assumed that the best solar panel is the one with the highest power generation capacity per unit of volume in stowed configuration.

Structural platforms for solar arrays can be divided into three different categories: rigid, flexible and concentrator systems [23]. These can be deployable or non-deployable systems, meaning that the array requires some type of unfolding or positioning action, or that it is ready for use in its launched state, respectively.
A non-deployable panel type could be combined with in-space additive manufacturing by placing complete solar cell modules onto the printed structure. This could be done in a way where solar panel sections or cell modules are picked up from its stored location by a robotic arm. The arm then mounts the section to the 3D printed structure. Although it is possible to mount individual modules onto an AM structure using a robotized system, it is a difficult task to do accurately by an automated system. In space, more actions means more risk. These movements done by a robot can be simplified by using a passive, deployable solar panel type. Although deployable systems still induce risk, such systems are generally simpler. An additional downside for this method is the power consumption of a robotic system required for assembling non-deployable solar panels. The AM facility already uses a considerable amount mass, as well as power, for which possible power generation limitations need to be investigated. Adding another power consuming system is undesirable. For these reasons, deployable flexible solar panels make the most sense to use in combination with in-orbit manufacturing.
Regarding the first mentioned three categories, rigid panels do not benefit from manufacturing in orbit. Honeycomb structures and composite plates are most often used for structural strength for solar panels in space. If they already contain a supporting structure than there would be no use to creating a new structure to place them on. This would unnecessarily increase the mass. The rigid solar panels would also still have to be strong enough to handle the launch environment as they a breakable. This excludes them for a big part from the benefit of weight saving by manufacturing in space. This does mean that the panels are strong enough on their own in orbit. A related application could be a

mission where rigid panels are connected using an assembly robot to create large solar arrays, similar to the idea of SpiderFab [24] [25]. For this, no AM facility is required. Though, the mass of the structure will be higher than an in-orbit manufactured structure, because it needs to handle the launch loads.
Concentrator solar panels use techniques to focus the light onto a smaller area. This is done using lenses or mirrors. The benefit of this is that less solar cells are required, which results into the possibility to use better performing, more expensive cells. Although this may lower the price of solar arrays, it adds complexity to the design of the manufacturing system and is uncommon practice for satellite solar power. Furthermore, improving solar cell efficiency or lowering solar panel cost is not the aim for this research. At this early stage the main priority is to design a well-functioning system. As the technology matures, cost will go down eventually as confidence grows in applying more complex techniques.

Deployable flexible solar panels are the best option for this in-space additive manufacturing application. Existing technologies in this category are looked at to see what is currently capable. There are a few options in this category that have successfully been used in space. ROSA and FRUSA are two systems that use roll-out solar arrays, SAFE is a pleated Z-fold array and lastly, UltraFlex and MegaFlex are circularly deployed arrays [26] [27].
Roll-Out Solar Array (ROSA) is the type that has been installed on the ISS as an upgrade to its current solar arrays. The technology was tested in space in 2017 [3]. See Figure 8 to see what this looks like. The design contains a flexible blanket solar array and deployment happens through two elastic tubular composite booms, which also create structural strength to the system in the deployed state. Although these Storable Tubular Extendible Members (STEM) are innovative and crucial to the ROSA system, it is the rolled up solar panel that is of interest to this research. The solar panel is stored in a compact cylinder in its rolled-up form, allowing large surface areas to be launched extremely efficiently. The solar cells are integrated in a flexible blanket, which is much thinner and lighter than its counterparts with stiff structures. The panel of $5.4\ m$ x $1.7\ m$ is capable of generating $3\ kW$ at beginning-of-life (BOL) and contains SolAero ZTJ, Spectrolab XTJ, and Northrop Grumman ZTJM triple junction solar cells.

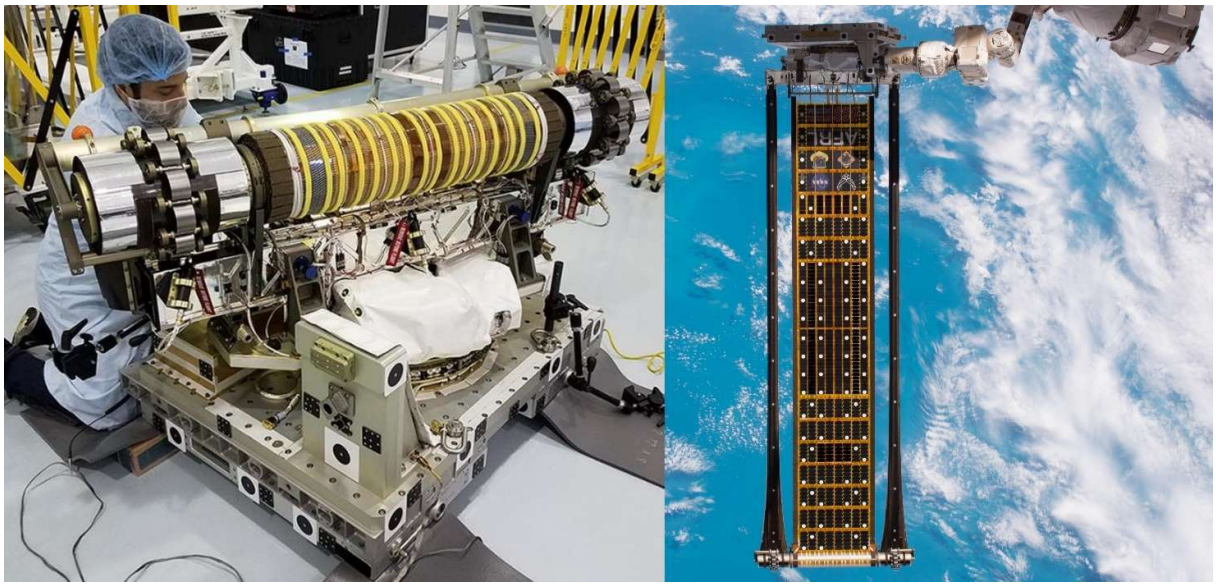

Figure 8: ROSA flight experiment in stowed state (left) and ROSA deployed (5.4m long x 1.7m wide solar panel), connected to the Canadarm2 on the ISS (right) [27]

The Flexible Roll-Up Solar Array (FRUSA) type panels were notably used on the Hubble Space Telescope (HST), see Figure 9. Small silicon cells were used ($2\ cm$ x $4\ cm$) to be able to wind the flexible panel and its cells around a small drum diameter. Thin stainless steel Bi-STEM booms were used for the deployment mechanism. FRUSA is the ancestor to ROSA in a way. ROSA achieves improvements by using bigger cells, which is made possible by including a foam backing layer to aid bending. Interestingly, thermal distortions were experienced in FRUSA, caused by thermal cycling, which hurt the telescope performance. The FRUSA panels were replaced by rigid panels in the 2nd HST servicing mission. ROSA made sure to do extensive research in simulating the panel behaviour to avoid these undesired distortions. During the ROSA flight experiment the panel behaviour was confirmed to be as expected in the simulations.

The Solar Array Flight Experiment (SAFE) type panels are used to generate the majority of power for the ISS. These are to date still the largest flow solar panels in space. Cells are placed on a flexible blanket, which folds similar to an accordion. The pleated Z-folding design allows the panel to be stowed without bending of the cells. Figure 9 shows a picture of the SAFE array on the ISS in its folded state, which was taken by a crewmember during the extravehicular spacewalk to install the array.

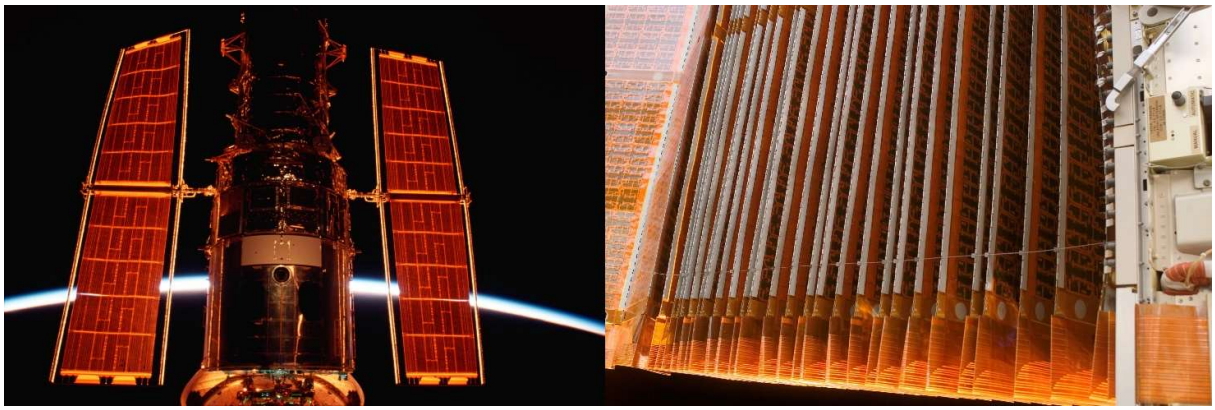

Figure 9: Deployed FRUSA solar panels on the HST (left) and folded SAFE panels on the ISS (right) [28] [29]

The UltraFlex and MegaFlex style solar arrays [30] deploy in a circular manner, as opposed to a linear motion for the previously mentioned types. The UltraFlex solar array is used on the InSight Mars lander for example. Triangular flexible panel sections are Z-folded in stowed position. The sections are connected to a number of spars, which are used in the same fashion as a fan. The solar cells are attached to woven mesh blankets. This way of deploying a solar array is not suited for the proposed concept in this research, because the circular method causes a limitation to the panel size that can be achieved, whereas a major benefit of the proposed concept is to be able to achieve extremely large panel sizes.

Figure 10: UltraFlex solar array by NASA and ATK during deployment (left) and fully deployed (right) [31]

The ROSA style solar array will be used for the purpose of this research. It is a flexible panel that is stowed in a roll in a cylindrical cartridge. The ROSA panel is state of the art technology, which is proven by the fact that this type was chosen to be installed as the new power source on the ISS. This type of solar panel offers the best combination of power to mass ratio, compact form factor and simplicity in deployment for the purpose of large in-space manufactured solar arrays. Drums of stowed panels can be relatively easily be stored for the production of multiple arrays or arrays that are exceptionally large. Unrolling of the panel works well in combination with a pushing mechanism that extends the 3D printed array structure. The produced solar array can look similar to ROSA as it was used in the in-space demonstration and as used on the ISS, but the STEM beams would be replaced with additively manufactured structures.

The type of panels used in SAFE also allow for use in combination with in-space manufacturing. Many of the before mentioned benefits also apply. The fact that a rolled-up panel allows for a more continuous deployment versus a folded panel gives it a slight edge. As well as the fact this panel type was chosen by NASA for large panels on the ISS. They say that ROSA has a higher energy generated per mass and per stowed volume compared to the panels currently in use [32].

2.5 Use cases

There are several cases for which a spacecraft needs lots of generated power, which is made possible with in-space manufacturing of solar arrays. Spacecrafts that require large amounts of power can be limited by the current capabilities for power generation and may benefit from the possibility to obtain large solar arrays after arriving in its desired orbit. High-power communication satellites for example. More generated power means that higher power signals can be transmitted. Spacecrafts with electric propulsion may also benefit from this possibility. Large, light-weight solar arrays would be produced using the manufacturing platform on the spacecraft. After completing the manufacturing process, the manufacturing platform is jettisoned to get rid of unwanted mass. The spacecraft can have a better performing propulsion system than what is possible using the current state of the art, because the solar arrays will be larger and lighter. Deep space spacecrafts with electric propulsion can benefit from this, for example.

It is obvious that the ISS would also be good candidate to use the opportunity for in-space solar array manufacturing, since the ISS currently has the largest solar arrays in space. The current solar arrays would have to be replace at some time in the future. Considering the large amount of solar array surface area required, in-space manufacturing would lower the amount of supply mission to the ISS that are required to deliver all materials. Alternatively, the manufacturing platform could be mounted to the ISS as its permanent location. That way the manufacturing platform can benefit from all facilities that are already present on the ISS, such as propulsion systems and an initial power source. Perhaps even one of the robotic arms on the ISS can be used for installation of the manufactured solar array onto the receiving satellite. A manufacturing platform would also make restocking missions easier. A separate docking location on the manufacturing platform is not required, since the ISS already has the facilities for this. Also, the ISS is already occasionally restocked by supply missions, so supplies for the manufacturing platform can be included in those missions.

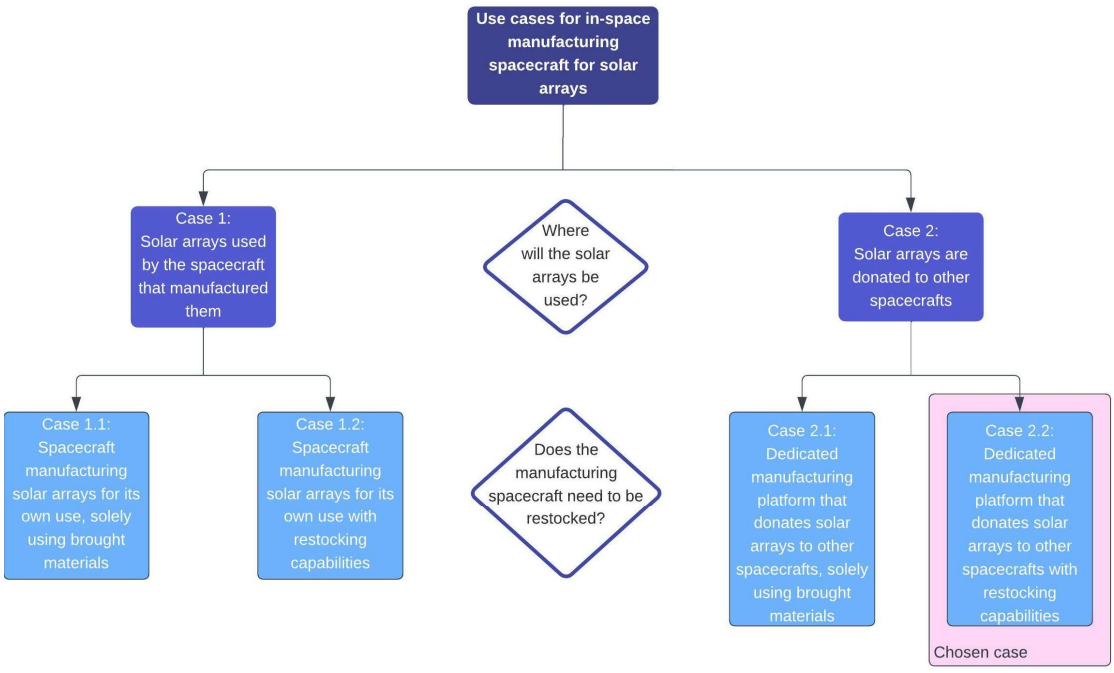

Figure 11: Block diagram of different use cases for in-space manufacturing of solar arrays

There are two main criteria that differentiate the use cases for an in-space solar array manufacturing platform. These are: operating location for the solar arrays and restocking capabilities of the manufacturing platform.
Regarding the operating location of the solar arrays, the first option is that the spacecraft with manufacturing capabilities can use the in-orbit manufactured solar arrays for its own goals. A spacecraft that has some kind of mission and purpose that has a high energy demand can be equipped with manufacturing facilities. Once arrived in orbit, this spacecraft will manufacture solar arrays that are large enough to meet its power needs. After the manufacturing phase has been completed, the main mission or operation can start. The second option is that a manufacturing platform can be created that works as a dedicated manufacturing facility with the sole purpose of manufacturing solar arrays for other spacecrafts. Other satellites would have to rendezvous with the manufacturing platform where the robotic arm can install the newly manufactured solar array onto the receiving satellite. It may be more economical to make a dedicated manufacturing platform, because the facility will be used multiple times in that case. It would have to be restocked occasionally with more filament material and stowed solar panels to make multiple arrays.

The other choice to be made is restocking capabilities. The most obvious choice for a spacecraft that manufactures solar arrays for its own use will in most cases not require restocking, as this is an exceptionally costly decision. However, to create the massive sizes that in-space manufacturing is capable of, restocking may be required nevertheless. For a dedicated manufacturing platform that donates the produced solar panels, it is clearer that restocking missions are beneficial. Still, in some cases it can be more economical not to create a spacecraft that is capable of receiving supplies. This simplifies the system. There would be no need for a docking station and systems for swapping empty material spools for new full ones.

The four cases that have been explained are summarized in Figure 11. The use case that was chosen to base this research on is case 2.2: a dedicated manufacturing platform with the purpose of donating the produced solar array to other spacecrafts, capable of being stocked with new materials for production. This use case is the one that is most in line with NLR's desires for the project. Choosing a dedicated spacecraft may me more difficult, than being connected to the ISS for example, but it allows for a great deal more freedom in designing the system. Also, enabling restocking capabilities makes the most sense in the future of the project. It is the most economical way.

2.6 Concept architecture

A schematic figure has been made to present a simplified overview of the proposed manufacturing platform, see Figure 12. An image provides a lot of context, so this will help with understanding the concept that is explained in this section.

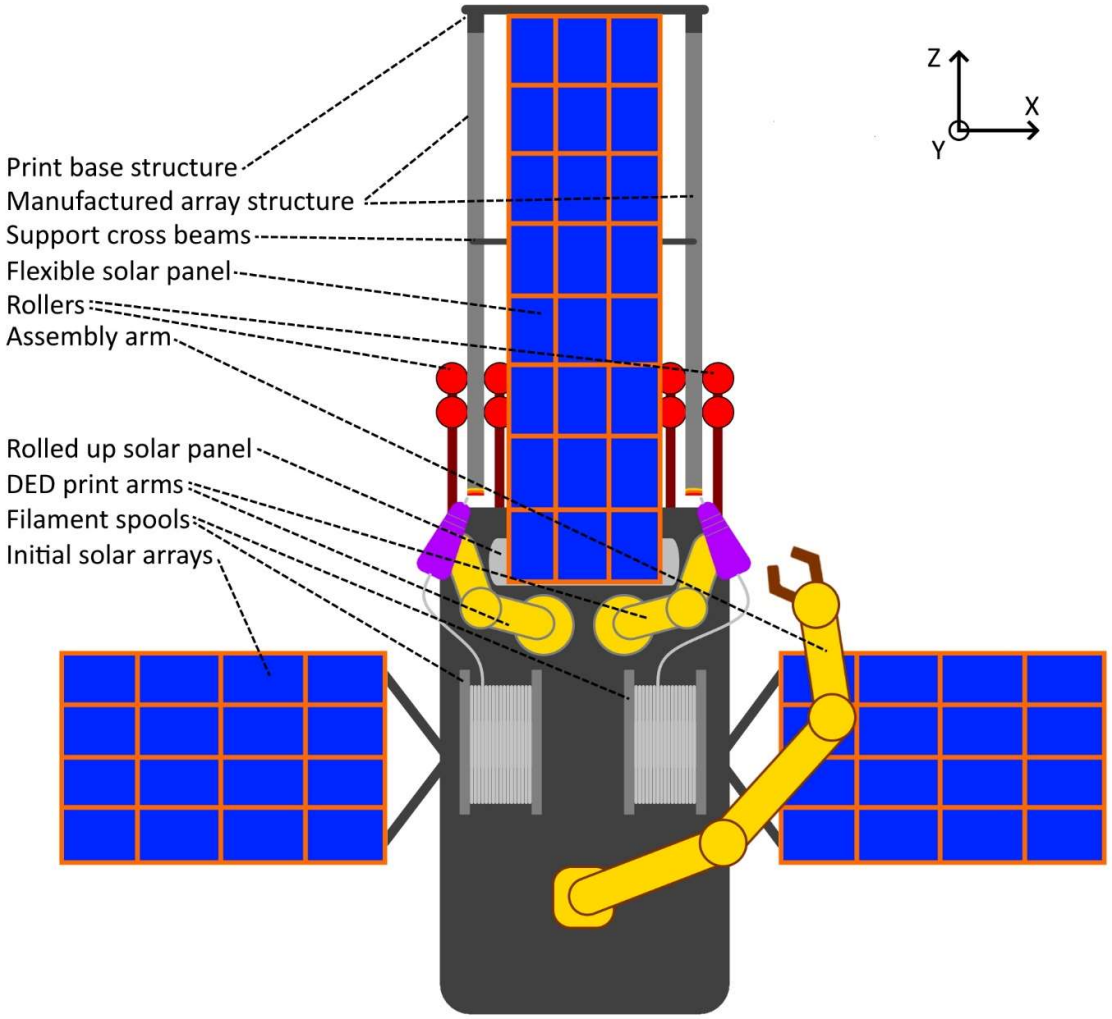

Figure 12: Schematic representation of the proposed manufacturing platform

A manufacturing platform is analysed here which is in an orbit around Earth. The type of orbit for this satellite remains undecided in this research as this is application dependent. This satellite is capable of manufacturing solar arrays autonomously by combining additive manufacturing machinery and prefabricated flexible solar panels. Raw material and semi-finished products will be launched together with the platform. Raw material and semi-finished products can be packed much more densely and robust than (deployable) finished products. Therefore, more material can be shipped to orbit and larger arrays can be achieved. Feedstock wire wound around spools is used as raw material for the DED process. The flexible solar panels are rolled up in a drum, which unrolls as it is pulled out by the manufactured array structure.

Optimized structure geometry will not be researched in this thesis, so a simple tubular design will be used for the structure geometry in this research. Two hollow tubes on either side of the rolled out flexible solar panel, possibly with crossbars at certain points for stability. The crossbars can be printed with the same DED printer. This array design is similar to ROSA's, but the STEMs are replaced by additively manufactured tubes. The goal is not to improve or replace ROSA, but the choosing ISM over deployable booms for the solar array structure allows for different applications, because of inherently different characteristics. Manufacturing in space allows for lighter-weight structures, because launch loads are not experienced by the structure. Extremely large array sizes can be achieved, larger than deployable structures, since the raw material is packed more densely. ISM is more flexible. It is possible to determine how big the solar array needs to be and to change the structure geometry after the spacecraft has been launched, whereas ROSA has a predetermined shape that is unchangeable. However, a major benefit for a deployable array is that no heavy manufacturing equipment is required.

Two wire-based directed energy deposition machines are installed on the platform for the production of the support structures for the solar array. Printing the tubes on both sides with one printhead is possible, but a lot more movement needs to be made to do this. This increases manufacturing time greatly, requires more energy and creates complication in the DED process. This AM technique is not good at starting a print, but works significantly better if printing occurs continuously at a constant speed. Therefore, printing each circular tube with its own DED printer is the best solution for getting the optimal results.

Additional activities can be performed with the assistance of a robotic arm. Mounting the solar panel to the printed structure, replacing empty rolls of solar panel or filament with new material rolls, and installing a fabricated solar array onto another spacecraft are all activities that may require the need of a robotic arm. It is not definitive that these actions require the arm. Smarter solutions could be found where a robotic arm is not needed. Also, not all applications for this manufacturing platform have the same needs. Though, incorporating a robotic arm for handling purposes in the system architecture is interesting to explore. To clarify, this would be a separate robot from the arms that move the DED printheads. The printhead only needs to make small translations, thus requiring a small arm, whereas the handling robotic arm needs to have a lot more reach. Therefore, separate systems would be better.

To print the object, either the subject is kept still and the printhead moves, the subject moves and the printhead is kept still or a combination where both parts move. To create large array sizes, the structure as a whole must be moved while the additive manufacturing process is in progress. The DED nozzle is attached to the spacecraft and has no way of moving far away. Additionally, it is easier to have the printhead do translations in the other directions than the printing direction. Therefore, the printhead will be moved to create X and Y translation and the printed solar array structure will be moved to create Z translation in the print path.
That raises the question of how the structure will be moved and held in place during printing. The proposed solution here is to use rollers. Somewhat similar to how rollercoasters clamp to the track, several roller wheels clamp onto the tube structures. By motorizing a wheel, the structure can be held in place and moved forwards and backwards. Obviously, such an idea needs to be refined, but this is a top-level choice for the system architecture.
The end of the rolled up solar panel needs to be attached to the end of the array structure. The panel unrolls from the storage drum as the structure is moved in the printing process. More connections between the solar panel and the structure may have to be made at intermediate locations for stability, considering the large size of the panel.

A connection is required between the solar panel and the 3D printed structure. The start of a 3D printed structure generally happens on a base plate. This also applies for DED, it is impossible to print in open space, since the deposited material must adhere to something. On Earth, DED commonly prints on a securely mounted thick metal baseplate which needs to be cut off in post-processing. It is not required to print on a plate however. For example, DED is also

used for objects that require repair or objects that are supposed to be part of the print. Different shapes can be used as a base on which the print starts, so a decision is to be made here. A start of the array structure can be manufactured on Earth, making it easier the begin the printing process. This starting object can possibly already be installed in the roller system that extends the structure, to lower the amount of required handling procedures for start-up. The proposed idea is to start on a piece that is connected to the solar panel and also has two beginnings of the tube structure. The 3D printing of the structure will take place on these small tube sections and the printing will extend this tube shape to long lengths. The object on which the additive manufacturing starts is called 'print base structure'. See the schematic in Figure 12 for the shape and location of the part.

Additive manufacturing and robotics do require a good amount of power. Although it seems like a solar array manufacturing platform would be able to create the resources to obtain enough power, the operation has to start without the massive solar arrays it will be capable of creating. Energy required to do this can be sourced from a small conventional solar array, or possibly another type of spacecraft power source. As solar arrays are the most often used power source for satellites, these will be used as the initial power source for the manufacturing platform. These will be common, small panels without any use of in-space manufacturing techniques. Section 2.7 will go more in-depth on the platform's power consumption and the needs for the initial power source.

2.7 Power analysis

A power analysis is done to gain better understanding about the limiting factors of a manufacturing spacecraft. An additive manufacturing system requires a lot of power for spacecraft standards. In this section the components in the system that draw power are examined to determine what can be expected for the total power requirement and what impact this has on the power generation system.

2.7.1 Subsystems

Commonly, a spacecraft is divided into eight different subsystems. These are: propulsion, GNC, ADCS, communications, C&DH, thermal, power and structures & mechanisms [33]. In addition to the standard subsystems of a spacecraft, a manufacturing platform has an additional subsystem for the components needed for manufacturing activities. This can also be seen as the payload of the spacecraft, as manufacturing is the prime function of the spacecraft and all other subsystems are only there to support this function. The functions of each subsystem are briefly explained in Table 4.

Table 4: Manufacturing spacecraft subsystems and their principal functions [33]

System	**Principal functions**
Manufacturing system	Equipment for manufacturing activities
Propulsion	Adjust orbit and attitude & manage angular momentum
Guidance, Navigation & Control (GNC)	Orbit determination and control
Attitude Determination & Control (ADCS)	Attitude determination and control & spacecraft pointing
Communications	Uplink and downlink & spacecraft tracking
Command & Data Handling (CDH)	Command processing & data processing/formatting
Thermal	Equipment temperature control
Power	Power generation/distribution
Structures & Mechanisms	Support structure, booster adaptor and other moving parts

The manufacturing system comprises of all parts that are required to fulfil the in-space additive manufacturing tasks. Referring back to the concept image presented in Figure 12 in Section 2.6, this includes all components except for the black base of the spacecraft and the initial solar arrays. The components that are accounted for in this subsystem are: the roller system, two DED printers, filament spools, flexible solar panel, print base structure and the assembly arm. The DED printers consist of an arc welding power source, a filament feeder and a robotic arm. Unless the arc welding power source can be combined for two printers, two of each part is required for the two printers.

Structures and mechanisms are needed to provide a functional platform for all other subsystems to be mounted on. It provides rigidity to survive the loads experienced on launch. Mechanisms are in place to perform certain functionalities, such as initial solar panel deployment and positioning, antenna pointing mechanisms and a separation system to release the spacecraft from the launch vehicle. A mechanism that is specifically required for the proposed concept is a docking station. The use case that was chosen is a dedicated manufacturing platform that donates solar arrays to other spacecrafts with restocking capabilities. For donating an ISM array, the other spacecraft ideally connects to the manufacturing platform. The same applies for restocking of materials. A mechanism to dock (small) spacecrafts needs to be included in the platform.

Thermal control is more demanding on a manufacturing spacecraft. Besides temperature control that may be needed for all common spacecraft components, like batteries, thrusters, sensors and mechanisms, specific attention is required for the manufacturing system. The arc welding power source generates heat due to losses, as all power supplies do. In a later stage of the project the impact of such a power source in space needs to be investigated and a suitable solution for thermal control needs to be found. Additionally, heat dissipation systems can be used to cool down the printed material. The simplest solution is to wait for the material to cool down, but adding a thermal control system for the printed material will reduce the idle time, which means that higher production rates can be achieved. What kind of systems are suitable and what the impact of that is needs to be investigated in future research.

The power system must be designed to be able to generate sufficient power to the subsystems that require power. How large the demand is for the power generation system depends on all powered components on the spacecraft. For a manufacturing spacecraft, it is likely that the manufacturing system is a significant part of the power requirement. Other subsystems are expected to have a commonly found power requirement for similarly sized spacecrafts. The power equipment for a manufacturing spacecraft is not different than for other spacecrafts, but the total power requirement is relatively large. A power analysis is done in the next section.

GNC, ADCS, CDH, propulsion and communications subsystems do not have to cater to specific needs created by implementing in-space manufacturing capabilities on a spacecraft. The requirements for these subsystems are obviously specific to this spacecraft's mission and technical parameters, but can be designed in the same way as for other spacecrafts.

2.7.2 Manufacturing system power consumption

Various sources were found for the energy consumption of GMAW WAAM aluminium printers. The paper of Shrivastava et al. [34] found a constant power consumption of $5303\ W$ during the welding process and $110\ W$ during idle time of the machine. Raju et al. [35] found an energy consumption of $197.7\ KJ$ during their 246 seconds during experiment. This is solely welding time. This results in a power consumption of $803.5\ W$. Figure 46 shows a summary of the power consumption of various DED-GMA (same as GMAW WAAM) experiments. The data points range between $3000\ W - 5000\ W$, with one outlier around $8500\ W$.
It can be seen that the data on WAAM power consumption vary greatly. The highest and lowest power consumption are an order of magnitude apart. The power consumption for the 3D printer is extremely large considering common spacecraft power consumption numbers. More power consumption directly increases the demand on the power generation system. Solar arrays would have to be bigger, which increases mass and cost. For these reasons, the power consumption of the 3D printer will have be optimized for a space application. That means that it can be expected that the power consumption will be at the bottom end of the range of power consumption for GMAW WAAM printers on Earth. Excluding the bottom-end outlier at $803.5\ W$, the best performance sits around $3000\ W$. It will be assumed that this is the operating power consumption that can be expected for each of the two GMAW WAAM printers on the manufacturing spacecraft. During idle time, $110\ W$ of power is assumed, which is adopted from the experiment by Shrivastava et al.

The mass of light-weight GMAW welders ranges between $5\ kg - 12\ kg$ [36]. These are not weight-optimized, yet more features and strength are expected to be required for a space application. A mass of $7\ kg$ per unit shall be assumed.

Interesting comparisons for the assembly robotic arm are the Canadarm2 and European Robotic Arm (ERA), which are robotic arms that are installed on the ISS. Canadarm2's average operation power is $1360\ W$, peak power is $2000\ W$ and keep alive power is $435\ W$ [37]. ERA's average operation power is $475\ W$, peak power is $800\ W$ and keep alive power is $420\ W$ [38]. The Canadarm2 is longer than ERA at $17.6\ m$ versus $11.3\ m$. The handling capacity is also much higher for the Canadarm2, at $116000\ kg$ versus $8000\ kg$. Nevertheless, it is not expected that the longer length nor handling capacity is required for the proposed spacecraft, considering that its needs will be less than for the ISS. Additionally, ERA is much newer, so it uses newer technologies. Therefore, the data for ERA will most likely be more suitable as a first assumption for the expectations for an assembly robotic arm for the manufacturing spacecraft. It will be assumed that a robotic arm similar or equal to ERA will be used on the manufacturing spacecraft. The mass of the ERA is listed as $630\ kg$.

The DED robotic arms can be much smaller. A reach of $0.5\ m$ is sufficient to reach the whole cross section of the beam, even for more complicated shapes. Commercially available robotic arms are examined to find relevant data for the DED robotic arm. Only high-precision robotic arms with a reach between $500\ mm - 700\ mm$ are included. The findings are summarized in Table 5. For the empty cells in the table no data was found.
None of the robots were designed for space. For space applications, mass and power consumption will be optimized, so the expected parameters lay in the lower end of the range. For the printer robotic arm and controller combined, a mass of $30\ kg$ and average power consumption of $150\ W$ is assumed.

Table 5: Data summary of commercially available small, high-precision robotic arms

Robot	**Controller**	**Robot mass (kg)**	**Controller mass (kg)**	**Average power consumption (W)**
Fanuc CR-4iA [39]	R-30iB Plus	48		500
IRB 14050 [40] [41]	OmniCore C30	9.5	24	
Elibot EC63 [42]	ERB1K6-220/110	13	15	150
Siasun SCR3 [43]		18		250
Staubli TX2touch-60 [44]	CS9	51	38	
AUBO-i3 [45]		16	10	150

Table 6: Overview of estimated average operating power consumption and mass of manufacturing system components

Component	**Amount**	**Average operating power consumption (W)**	**Average idle power consumption (W)**	**Mass (kg)**
GMAW WAAM printer	2	3000	110	7
Printer robotic arm	2	150	0	30
Assembly robotic arm	1	475	420	630
Roller system	2	150	0	50

For the roller system, it is difficult to assign a power consumption and weight, because the system is yet to be designed and there are no commercial systems available that are similar. A rough estimation for the power and mass that will be used is $150\ W$ and $50\ kg$.

A summary of the found power consumption and mass of components in the manufacturing system is presented in Table 6. The most important moment of operation for which power consumption needs to be calculated is during the

printing process. Other moments of operations, such as transferring the solar array using the assembly arm, are less important, because lower power consumption is expected. Also, the spacecraft will spend the most time in printing operation.
The calculation of power consumption will be based on the printing speed that was found in the thermal simulation in Section 4.2.4: 61.6 seconds of printing and 120 seconds idle per layer. Considering the determined $1.5\ mm$ layer height in that simulation, this results in 11.4 hours of printing time and 22.2 hours of idle time per meter of structure. Average power consumption for the printing process is:

$$P_{print} = \frac{(P_{printers} + P_{Printerarms} + P_{rollers}) * \tau_{print} + P_{idle} * \tau_{idle}}{\tau_{total}} \quad (1)$$

$$P_{print} = \frac{(2 * 3000 + 2 * 150 + 2 * 150) * 11.4 + 2 * 110 * 22.2}{11.4 + 22.2} = 2385\ W$$

2.7.3 Spacecraft power system

Suitable equipment must be installed on the spacecraft to satisfy the power needs of the components installed on the spacecraft. In Section 2.6 solar panels were assumed as the power source of the spacecraft. Large differences between peak power and average power can be expected for the manufacturing system. This is because printing is paused between each layer deposition to allow the material to cool down. Also, power surges are expected for such high-power equipment. Besides the power electronics required to supply these high power ratings, batteries need to be installed on board to provide enough power for peak power draw and when the solar panels do not receive (enough) radiation from the Sun.

The total spacecraft power requirement is estimated using an estimation equation based on data from flown missions. No manufacturing spacecrafts are currently in operation, so no data is available for a similar spacecraft. Instead, data from communication satellites is used, as this is the most similar alternative type of spacecraft. Both types of spacecrafts require high amounts of power for their payload. For the manufacturing spacecraft, the manufacturing system can be regarded as the payload. The estimation equation for total power of communication satellites is as follows [33]:

$$P_t = 1.1148 * P_{PL} + 384.2 \quad (2)$$

Where P_t is the estimated total spacecraft power and P_{PL} is the payload power, both in Watts. For $P_{PL} = 2385\ W$ this results in the following total power:

$$P_t = 1.1148 * 2385 + 384.2 = 3043\ W$$

This is a large amount of power for a spacecraft and requires a large solar array. Based on data from various flown spacecrafts, solar arrays deliver between $50\ W/m^2 - 300\ W/m^2$ with an average around $100\ W/m^2$ [33]. ROSA, the deployable solar panel referenced earlier in this report, achieves $3\ kW$ BOL on a $5.4\ m$ x $1.7\ m$ panel [3]. This results in $327\ W/m^2$. A large solar array, at least $10\ m^2$, is required to satisfy the power needs for this spacecraft.
A choice can be made for this power generator. One option is to equip the spacecraft initially with the required solar arrays, that are able to provide enough power for operation. That way, once the spacecraft is in orbit and deployed, it

can start manufacturing arrays in normal operation immediately. However, on top of the already high power requirement, eclipse time, deteriorating cell efficiency and margin need to be accounted for. That means that the demands on the initial solar arrays are extremely high.

There is an alternative approach than installing large deployable arrays as the manufacturing spacecraft's power source. This spacecraft is capable of producing its own solar arrays. The spacecraft can be equipped with small initial solar arrays. Using this smaller power source, the manufacturing platform is able to produce solar arrays, albeit at a slower rate. It is perfectly possible to pause the manufacturing process. Therefore, the manufacturing system can be active as long as there is energy available in the batteries. Once the energy runs out, the manufacturing process stops and the spacecraft recharges its batteries using the small initial solar panels. When the batteries have sufficiently been recharged, the manufacturing process resumes, and this cycle repeats. The first solar array that is produced is then installed on the manufacturing spacecraft itself, using the assembly robotic arm. Once the in-space manufactured solar array has been installed, the manufacturing spacecraft is capable of utilizing its full potential. Using either of these two options allows for the spacecraft to not be power limited in regular operation.

3 Material and design

This chapter looks into the optimal material for producing solar array structures in space using directed energy deposition. This requires consideration of the manufacturing process, space environment, application and more. The important material properties are explored and listed for use in the selection process. A structured material selection process is used to objectively find the best material. Additionally, considerations for the structural design aspect are highlighted, such as surface roughness and dimensional accuracy of the manufacturing process.

3.1 Desirable material properties

To find the best material in a methodical way, it is necessary to find the needs for the structure. This results in desirable traits for the material, which are dictated by a variety of inputs. Stakeholders, technology, performance and the application environment are all examples of inputs for needs. Requirements with exact values cannot be made in this stage of the project. This is because there is no client who expresses needs and no clear goal yet from NLR or Maana Electric for the platform's purpose. Nevertheless, it is extremely useful to find a suitable material, because detailed material information is required for the thermal model. Without the exact material information, it is impossible to go into depth on the manufacturing platform's capabilities. This process needs to be iterated in the future when more choices for the platform have been set.

The desirable material properties have been divided based on the source that imposes the desires. These are the stakeholders, the manufacturing process, performance, environment and non-technical parameters.
The desires coming from the stakeholders have been expressed by them. Manufacturing process driven desires are determined by the behaviour and limitations of applying directed energy deposition for structure manufacturing. Some materials cannot be processed using this technique and some material properties impact the performance of manufacturing process. The performance driven desires are found by investigating which parameters influence the structure's functionality, relating to the application. The space environment and expected events during the structure's lifecycle are harsh and impose needs for the material. Lastly, non-technical desires come from parameters that have no impact on the application, but on practical aspects of realising the system.

3.1.1 Stakeholders

As was mentioned in Section 2.2.2, the stakeholders in this project do not have many needs. NLR has expressed no preference or need for the structure material. Maana Electric, as the potential supplier of raw material, does have a preference. Aluminium and silicon have their preference, as they have experience in refining these materials. This is not a requirement, other materials are negotiable.

3.1.2 Manufacturing process driven desires

The process of directed energy deposition causes limitations and considerations for the to be chosen structure material. DED in space means that the process will happen in a vacuum. This is beneficial to the process, because

oxygen and water vapour exposure to the weld pool causes oxidation of the material and spattering, resulting in low quality welds with porosity and contaminations. However, that also means that there will be no convection happening. This is a limitation to the ways heat is dissipated. DED is a process that takes place at high temperatures, the melting temperature of the material is exceeded. The deposited material must cool down again to solidify into its permanent shape. Out of the existing types of heat transfer, only conduction and radiation are relevant for this case in space. Conduction occurs from the build object to the print base structure and spacecraft. Radiation happens from the hot material into space and from celestial bodies to the structure.

The challenging part of heat dissipation in DED is the fact that hot layers are placed onto each other. The current and previous layers must have cooled down enough before the next layer can be applied. If this is not done properly, the structure can disform because of its softness or thermal strain can cause distortions. This would lead to a complete failure of the print if the printhead and disformed structure no longer align. Obviously, the other end of the spectrum is printing too slowly. This would not be an issue for the manufacturing process, but preferably the print happens as quickly as possible, especially for printing massive solar arrays. It is at this stage not yet known what the limiting factor is to speed for applying DED in space. Heat dissipation is one critical factor.
For heat dissipation, material properties are important. The relevant variables can be seen in Equation 3 and Equation 4 for thermal radiation and conduction, respectively. Emissivity is a material property that impacts the radiation component. Similarly, the thermal conductivity is relevant for heat conduction. The material temperature is a variable to both heat transfer components. This is in this case related to the melting temperature of the material. Additionally, melting temperature plays more important roles. When the material melting temperature is higher, more energy is required to heat it up to this temperature. Larger energy generation requirements add complexity and mass to the system. Also, high melting temperature means more time is required for heating the material. This results in slower printing speeds.
In conclusion, melting temperature, conductivity and emissivity will be taken as relevant material properties in material selection.

$$Q_{rad} = \varepsilon * \sigma * A * T^4 \tag{3}$$

Heat dissipation by radiation where Q_{rad} is in J/s, ε is unitless emissivity, σ is the Stefan–Boltzmann constant ($5.67 * 10^{-8}\ W/(m^2 * K^4)$), A is the surface area in m^2 and T is the object temperature in K.

$$Q_{con} = -\kappa * A * \frac{T_2 - T_1}{L} \tag{4}$$

Fourier's law where heat dissipation Q is in J/s, κ is the thermal conductivity in $W/(m * K)$, A is surface area in m^2 and $T_2 - T_1$ is the temperature difference in K with L the distance between those points in m.

Specific heat capacity is another material property that is important in this application. This parameter quantifies the amount of energy that is required to heat $1\ kg$ of material by $1\ K$. The definition is shown in Equation 5. The amount of energy a material needs to dissipate depends on the specific heat capacity, as well as mass and temperature change, but those last two are not material properties. Therefore, the material will dissipate energy faster, thus perform better in DED, with a lower specific heat capacity.

$$c_p = \frac{Q}{M * \Delta T} \tag{5}$$

Specific heat capacity definition where c_p is the specific heat capacity, Q is the heat in J, M is the mass in kg and ΔT is the temperature change in K.

In addition to specific heat capacity, there additional heat required to do the phase change from solid to liquid. This is called latent heat of fusion. The specific latent heat can be multiplied with the material mass to find the energy required to do the phase change from solid to liquid.

$$Q_L = L_f * M \tag{6}$$

Latent heat definition where Q_L is the latent heat of fusion in J, L_f is the specific latent heat of fusion in J/kg and M is the material mass in kg.

Directed energy deposition cannot use all materials as feedstock. A hard requirement is that the feedstock needs to be in the form of filament. Even though ceramics are used in powder-based DED, ceramics in filament form do not work because of their brittleness. This rules out the material families ceramics, as well as glasses, in the selection process. Ceramic filaments do exist in compound forms where polymers are added. This is used in fused filament fabrication (FFF), however such compound filaments require post-processing treatments. This is not feasible for large scale space structures and DED was specifically chosen for not needing post-processing.
Generally speaking, all metals that can be welded can be used for DED. This includes (stainless) steel, aluminium, titanium, Inconel, tungsten, niobium and more. Certain DED processes also work with polymers. The line between FFF and DED becomes thin when talking about polymers, making them hard to differentiate in some cases. Based on DED capabilities, polymers are not excluded.

3.1.3 Performance driven desires

Any structure's primary goal is to provide strength to a system. The structure is designed to withstand any load that is expected to be experienced. In this case of in-space solar arrays, the structure provides stiffness to the solar panels. To do this, the structure is enduring a certain tension. Also, the spacecraft will most likely use its propulsion system to stay in the desired orbit and attitude. A small amount of drag force will otherwise cause the spacecraft to descend or tilt. Propulsion will induce a force on the spacecraft and therefore on the solar arrays as well. The array structure must be able to withstand this force.
An additional goal for structures is to create a particular geometry or size. A clear example for this in another application is when sensors have to be located at a distance from the spacecraft to reduce any interference. For the solar array, the structure keeps the flexible solar panels in the right position, which would otherwise drift into undesired shapes, since they are flexible.
So, strength is a critical material property that must be considered. Generally speaking, stronger materials are also heavier materials. Due to high launch costs, heavy materials are extremely unwanted in spaceflight, so the mass must be kept low. The mass is determined by the material density and the object volume, see Equation 7. Since the volume is dependent on geometry and geometry is not material dependent, density is the only important material property that influences mass. Though, volume will inevitably be related to strength, because enough material in the right shape is required to withstand expected forces. Regarding the remark that strength and density often go hand in hand, the goal here is to find the strongest yet lightest materials. Therefore, high specific strength is what is needed. The structure may not deform during the application, so yield strength is the relevant strength property. Specific yield strength is the property that is used in material selection.

$$M = \rho * V \tag{7}$$

Equation for mass where M is mass in kg, ρ is density in kg/m^3 and V is volume in m^3.

High stiffness is required in large space structures to improve control and stability [46]. Stiffness is an object property that is dependent on both the material and shape, as can be seen in the example equation for compression and tension stiffness, Equation 8. The relevant material property for stiffness is the elastic modulus or Young's modulus E, generally expressed in GPa. Similarly, bending stiffness also relates to the elastic modulus and geometrical properties. Since structure geometry remains undefined at this point, the goal to achieve maximum stiffness is to maximize E during the material selection.

$$S = \frac{E * A}{L} \tag{8}$$

Axial stiffness equation for compression or tension with S in N/m, Young's modulus E in Pa, area A in m^2 and element length L in m.

3.1.4 Environment driven desires

An aspect of the environment in space that has serious consequences, is the thermal cycles that are experienced. The large changes in temperature are caused by the changes in irradiation, mostly by the Sun. When an object is orbiting the Earth, it is periodically in direct visibility of the Sun. Since there is no atmosphere blocking the radiation, the orbiting object significantly heats up. However, when the orbiting object reaches the backside of the Earth, in respect to the Sun, all radiation is blocked. Without significant irradiation, the space environment is extremely cold. Therefore, the spacecraft temperature will cycle between hot and cold every orbit. Space equipment is commonly put through thermal cycling tests on Earth before being launched into space to do verification of the part's performance in this environment. Many aspects of the spacecraft impact the exact temperatures that will be experienced, such as shape, materials, surface finish and more. Dever said the following about parameters that impact the thermal cycles:

The range of temperature which a material experiences during thermal cycling depends upon its thermo-optical properties (solar absorptance and thermal emittance), its view of the Sun, its view of the Earth, its view of other surfaces of the spacecraft, durations of time in sun and in shadow, and the influence of equipment or components that produce heat. (Dever, 2005, p. 487) [47]

Calculations can be done to simulate the temperatures that will be experienced. However, system details lack in this case. Temperature variations from $-120℃$ to $120℃$ are often taken as a rule of thumb for designing a spacecraft [48].

For the material, this means that it should be capable to handle both a high and low operating temperature in its solid form without structurally breaking down. Even if solutions such as a heat shields are applied, materials will experience a temperature range between launch and operation. This temperature range can be especially difficult working with polymers, because the mechanical properties of polymers often are strongly dependent on temperature. This could mean that the structure made out of a polymer is weaker in sunlight than during the dark period of its orbit. Besides operating temperature, the thermal expansion coefficient is important, because this can create internal stresses, both in the structure and in the solar panel it is supporting. If this is high enough, they could break. The difficulty in assessing the impact of thermal expansion is that one needs to know the geometry to see if the expansion and shrinkage is critical. Since the geometry remains unknown at this stage, the impact of thermal expansion will not be investigated. This is an interesting topic for future research on the geometrical design of in-space additive manufacturing of solar arrays.

The thermal cycling can be critical inside of materials as well. The extreme temperatures and thermal cycling are a problem for composite materials, made out of two or more materials with a close bond. Composite materials and coated materials risk cracking and delamination. This is caused by the different thermal expansion coefficients of the materials. Different rates of expansion will induce internal stresses. This is also a problem for polymers [47]. Polymers experience damage caused by radiation in space. The radiation damage diminishes with thickness of the object. The damage affects the material properties. The material becomes more vulnerable to impacts and loads as the mechanical properties worsen. A mismatch in thermal expansion coefficient can be created due to the varying levels of degradation over the material, causing internal stresses while it is experiencing thermal cycling.

For the selection procedure, limits are set for operating temperature to make sure the selected material is able to handle both the hot and cold temperatures. For reference, during the on-orbit validation mission of the Roll-Out Solar Arrays the booms were tested before launch in thermal cycles between $-65℃$ to $90℃$ [27]. During the actual mission the maximum temperatures measured on ROSA were $-46℃$ to $77℃$. Inflatable Torus Solar Array Technology (ITSAT) is another similar type of deployable solar array which is used for small satellites (see Figure 13). The deployed configuration was tested from $-85℃$ to $70℃$ in vacuum conditions for 56 hours during its on-Earth testing phase [49]. As mentioned earlier, specifics are required to determine precise temperatures that can be expected. Those are unavailable for this research. Therefore, the rule of thumb taken from NASA's researcher's guide is used as operating temperature limits, which state $-120℃$ to $120℃$ [48]. Note that these operating temperatures relate to the material's solid state in which it provides its structural function. Higher temperatures will be experienced, since the material is melted during the DED process.

Figure 13: ITSAT solar array [49]

On Earth the solar radiation is partially absorbed into the atmosphere and ultraviolet (UV) is completely absorbed. But this does not happen for spacecrafts in orbit. These need to be able to withstand the incoming UV radiation. This has a degrading effect on materials. Polymers often contain bonds that are able to absorb the ultraviolet radiation. This causes reactions with effects like discoloration and deterioration of mechanical properties. However, according to Dever et al. (2005): "*It is generally thought that most polymers absorb approximately 95% of incident radiation below* $250\ nm$ *within* $0.3\ \mu m$ *from the surface. … For polymer films whose thickness is significantly greater than the UV attenuation depth (the depth within which the majority of UV light as absorbed), the undegraded portion of the polymer*

thickness provides support to a degraded surface." Therefore, it can be concluded that UV radiation does not degrade polymers in structural parts enough for them to lose their functionality.
Glass and ceramic materials also undergo effects caused by UV radiation. The light can darken the material surface, also called solarization. Although this effect does not have consequences to mechanical properties, in some applications the change in colour has negative effects. Darkening of glass worsens optical properties and darkening of metals changes thermal properties, like emissivity. Since the presented application is not optical and thermal properties post-manufacturing are not critical, UV radiation is not an issue for glass and metals.

Ionizing radiation is another concern for materials in space. This includes charged protons and electrons, and energetic photons like X-rays and gamma rays. If the energy of the particles is high enough and the material is susceptive to it, the material atom will get ionized. Large amounts of ionizing radiation will degrade certain materials if it is exposed to it for a long time. Therefore, to determine the risks of ionizing radiation, the material and mission duration must be considered. Like for UV radiation, it is mostly polymers that are susceptive to ionizing radiation. Physical and mechanical properties will degrade if the radiation dose, expressed in the unit gray (Gy), is high enough. This is generally only a problem for thin films, like tape and blankets. Also, coating layers may suffer from this type of radiation, but that is not a concern for the application. For structural purposes, ionizing radiation will not have significant impact to cause problems.

Atomic oxygen can cause material related issues in low Earth orbit (LEO) [47]. No exact orbit has been determined yet, but since LEO is an important option for the manufacturing spacecraft's orbit, this potential problem needs to be considered. Atomic oxygen is formed by photo dissociation of diatomic oxygen. Ultraviolet in the solar radiation is able to break the diatomic bond. This requires sufficiently long free path, which is about $10^8\ m$. Therefore, atomic oxygen is the most abundant atom in LEO altitudes around $180\ km$ to $650\ km$. These particles can cause damage to the surfaces of spacecrafts in LEO. Atomic oxygen contains enough energy to break down most organic polymer bonds. Polymer materials will erode in its presence. Mitigations strategies for this are: applying a protective layer, surface modification of the part and using special polymers that contain metal atoms to create a protective layer upon exposure [47]. All of these techniques add too much complication to the process for the current state of technology. Because operation in LEO is a possibility, polymers are rejected in the material selection.
Carbon and metals will react too when exposed to atomic oxygen. It will oxidize metal surfaces to create a layer of non-volatile metal oxides. This is a protective effect however, because the oxidized layer will act as a shield for the underlying material. Most metal structures will not experience issues for that reason.
Certain composite materials can also be printed with DED. As many composites incorporate polymers, these are undesirable too. Other composites, such as metal-metal composites, are included in the selection pool.

3.1.5 Non-technical desires

Cost is a relevant parameter for virtually all design processes. Choosing an extremely expensive material for the solar array structure would infeasible, even if it would be the best choice. However, for the first selection stage no limit on cost is set. Firstly, applying in-space additive manufacturing in the chosen application is something completely new and unprecedented. When dealing with innovation, the first design or demonstrator is never completely optimized. As the technology matures, the cost will come down generally due to changes that happen over time. So, even though cost will be high at this stage, that does not mean the technology will never be financially feasible and should not be explored. Secondly, in the documentation stage of the selection process cost is looked into. In this stage a number of top materials have been identified and are further explored. With a limited amount of options, it is easier to assess more material information that could not have been incorporated in the material indices and limits that roughly

determine the performance of material options. More information on the selection procedure is found in Section 3.2. Extreme outliers, for example materials like gold, can investigated then. Cost per kilogram can be weighed against the amount of material required and the feasibility is determined.

Besides cost, the availability of the material is another interesting non-technical parameter. This relates to the difficulty of obtaining the material filament. Cost and availability are often correlated, but are definitely not the same. Some materials may be hard to get, as the market is limited. Others are not yet being produced in filament form and require new tools and machinery for a specialty order. It is common in the space industry to order custom parts that do not follow standard sizes or manufacturing procedures. However, this does add complexity and thus time and cost. Commonly found materials are preferred.

3.1.6 Important material properties overview

In Table 7 the previously explained relevant material parameters are summarized. If possible, the parameter symbol is given. It is listed what aspect of the system the parameter is related to. The desired value or outcome of the material parameter is mentioned, which is required for setting up material indices and selection in material graphs. And lastly, the stage of the material selection procedure is provided in which the parameter is evaluated. The stages of the material selection are: performance index, limits and documentation. More explanation about what each of the stages in the material selection mean is given in Section 3.2.

Table 7: Summary of relevant material parameters for material selection

Label	Parameter	Symbol	Related to	Desired value	Considered for which stage
S1	Preferred material	-	Stakeholders	Aluminium/silicon	Documentation
M1	Emissivity	ε	Manufacturing process	High	Performance index
M2	Thermal conductivity	κ	Manufacturing process	High	Performance index
M3	Melting temperature	T_m	Manufacturing process	Low	Performance index
M4	Specific heat capacity	c_p	Manufacturing process	Low	Performance index
M5	Specific latent heat of fusion	L_f	Manufacturing process	Low	Performance index
M6	Feedstock in filament form	-	Manufacturing process	Yes	Documentation
P1	Yield strength	σ_y	Performance	High	Performance index
P2	Young's modulus	E	Performance	High	Performance index
P3	Density	ρ	Performance	Low	Performance index
P4	Operating temperature	$T_{o,max}$ $T_{o,min}$	Environment	Outside of limits	Limits
N1	Cost	-	Non-technical	Low	Documentation
N2	Availability	-	Non-technical	Good	Documentation

3.2 Material selection

Now that the problem has been analysed and relevant material properties have been identified, the selection process can start. The method that is applied for material selection is taken from the book *Materials Selection in Mechanical Design* by M.F. Ashby [50]. This method creates indices that provide a numerical value for the performance of each material. Indices are made using relevant formulas, which can be anything from strength, thermal, volumetric equations etc. The indices consist of material properties, like density, expansion coefficient and flexural strength and these relevant properties and formulas are based on the application. A software package is used to make it easy to collect all the relevant data for each material. Graphs and tables containing the material data can be generated using this software, from which conclusions can be drawn. The software is called GRANTA EduPack [51].

The next step is to select the desired materials for the selection pool. Ceramics, glasses, polymers and elastomers have been identified to be inapplicable for this application. This leaves metals and certain composites. These material categories are selected in the database of GRANTA EduPack and are considered in the material selection process. First, the materials are tested for the desired 'performance'. The performance index is put into the program and the computer simply calculates this for all materials in the pool using information of material properties in its database. These are then plotted in the desired graph. The generated images are called 'bubble charts'. A material property (or a combination of properties/index) is plotted on the x and y axis of the chart. Each material or material (group) has a value range for the plotted properties. This creates a bubble on the chart. The chart is generally plotted with logarithmic scales, since the properties of all materials vary greatly. The logarithmic scale compresses them together to create a more compact chart. Lines of constant performance can be plotted on the chart using the performance index to find the best material for a certain application. Also, limits are set for certain properties. This rejects materials which have undesirable properties. Operating temperature is a limit that is set, for example.

Thereafter, documentation for the top material candidates are researched to learn about these materials and their properties that could not be included in the first stage. Finally, the best material is chosen based on the pros and cons found in this research.

It does not matter for this methodology that the application is in space. It bases the performance on equations, which apply to any application if used correctly. Limitations could be experienced in the data that is available in the database. Materials that are not in de database are not included in the selection process.
The hardest part is determining the index, as there is some flexibility in determining what the best index is. The index is based on the application and desires for the material. Therefore, these have to be carefully considered. Good argumentation must be made for why certain properties are desired and which are more important than others. The same applies to finding the right equations. These are driven by the application, but strength can be expressed in many different ways: bending, compression, torsion, and then what shape does the sample have and in what direction is force applied. Determining the right equations requires thorough argumentation.

3.2.1 Material indices stage

Now the material indices are created. The problem is summarized in Table 8:

Table 8: Problem summary for material selection of AM solar array structures

Function (what does the component do?)	AM structural supports for solar arrays in space
Constraints (What non-negotiable conditions must be met? What negotiable but desirable conditions are there?)	Tube length Tube diameter Tube thickness Tube strength Tube stiffness
Objective (what is to be maximized or minimized?)	Minimize heat input required for melting and density Maximize conductivity
Free variables (what parameters of the problem is the designer free to change?)	Material choice

In this material selection problem, it is assumed that the shape and dimensions of the structure are determined. It was determined that the shape is assumed a round tube. The thickness of the tube is especially important, because the thickness will be determined by chosen nozzle size for the DED process. The thickness needs to remain one layer to optimize the manufacturing process. This means that the cross-section of the tube is made by drawing on circle for the printhead path, as opposed to multiple circles to make the tube thicker. The tube length is constrained, because this will be known beforehand, based on how big the solar array needs to be for its use case. Dimensions values are not actually known, but set as constraints. This is possible, because for the material selection process, only material properties are evaluated.

The other constraints in this problem are strength and stiffness. The structure needs to be capable of dealing with the stresses and vibrations it is going to endure without failing. Based on details, such as solar panel mass and expected spacecraft manoeuvres, requirements will follow in the future for these performance parameters. Currently, specific values are unknown. They are considered constraints, but are not required to find te best material. This is because the materials are weighed relative to each other.
One of the objectives for material selection is to minimize the energy it takes to melt the material from its solid state as a wire to a liquid droplet that is deposited on the part. This is necessary to minimize spacecraft's energy consumption and thus lowering the needs for power systems on board of the spacecraft.
It is difficult to theoretically determine the relative importance for thermal properties, such as thermal conductivity and emissivity. Therefore, the thermal model created in Section 4.2.3 is used to obtain more information on this. High conductivity was found to be an objective as well, because this is beneficial in the manufacturing process. This will reduce the thermal gradients that might cause the manufacturing process to fail. Lastly, the parameter that remains undetermined is material choice, which is aimed to be found in this section. So, all material properties in the equations that follow are variables.

Stiffness

First, an index for (vibration) stiffness is considered. The equation for stiffness of a beam is:

$$S = \frac{F}{\delta} = \frac{C_1 * E * I}{L^3} \geq S^* \tag{9}$$

Where $S\ (N/m)$ is the stiffness, $F\ (N)$ is the force applied, $\delta\ (m)$ is the deflection, C_1 is an unitless constant determined by the mode of loading, $E\ (N/m^2)$ is the flexural modulus, $I\ (m^4)$ is the second moment of inertia, $L\ (m)$ is the beam length and S^* is the required stiffness is that must be achieved. The required stiffness value is unknown right now, but will be an important requirement in a more advanced stage of the project.
Considering a round tube is the shape of the beam, the mass, area and second moment of inertia can be calculated with the following formulas:

$$A = \pi(r_o^2 - r_i^2) \approx 2\pi * r * t \tag{10}$$

$$M = V * \rho = A * L * \rho = 2\pi * r * t * L * \rho$$

$$I = \frac{\pi}{4}(r_o^4 - r_i^4) \approx \pi * r^3 * t \tag{11}$$

Where $M\ (kg)$ is mass, $V\ (m^3)$ is volume, $\rho\ (kg/m^3)$ is material density, $A\ (m^2)$ is the cross sectional area, $r_o\ (m)$ is the tube's outer radius, $r_i\ (m)$ is the tube's inner radius, $r\ (m)$ is the centre radius for a thin walled tube, $t\ (m)$ is tube wall thickness and $I\ (m^4)$ is the second moment of inertia. Now, substituting I in the equation for stiffness and rewriting it for r:

$$S = \frac{C_1 * E * \pi * r^3 * t}{L^3} \quad \rightarrow \quad r = \sqrt[3]{\frac{S * L^3}{C_1 * E * \pi * t}}$$

r is now substituted in the equation for mass:

$$M = 2\pi * t * L * \rho * \sqrt[3]{\frac{S * L^3}{C_1 * E * \pi * t}} = \left(2\pi * \sqrt[3]{\frac{S}{C_1 * \pi}}\right)\left(\frac{L^2}{\sqrt[3]{t}}\right)\left(\frac{\rho}{\sqrt[3]{E}}\right)$$

Here, the first term in brackets contains the functional parameters and constants, the second term contains geometrical parameters and the last term contains the material properties. Considering that the mass needs to be minimized, we obtain the following index that must be maximized to find the material with the highest stiffness to mass ratio for a beam in bending load:

$$N_1 = \frac{\sqrt[3]{E}}{\rho} \tag{12}$$

Strength

Next, strength is considered. The beam must have sufficient strength to handle the loads that will be experienced, mainly induced by spacecraft attitude control. The creates, most importantly, a bending load on the beam.
The equation that describes the force at which a beam fails in bending loads is:

$$F_f = \frac{C_2 * Z * \sigma_f}{L} \tag{13}$$

Where F_f (N) is the force at which the beam fails, C_2 is an unitless constant that is determined by the mode of loading, σ_f (N/m^2) is the flexural strength at which the material fails and L (m) is the beam length.
Z (m^3) is the moment of inertia in the Z direction, which is equal to the second moment of inertia I divided by the maximum distance to the edge of the object y_m, measured from the centre of the beam. For a round tube, this is:

$$Z = \frac{I}{y_m} \approx \frac{\pi * r^3 * t}{r} = \pi * r^2 * t \tag{14}$$

Z is inserted in the equation for maximum bending force and the equation is rewritten for r.

$$F_f = \frac{C_2 * \pi * r^2 * t * \sigma_f}{L} \quad \rightarrow \quad r = \sqrt{\frac{F_f * L}{C_2 * \pi * t * \sigma_f}}$$

Same as for stiffness, mass is found by multiplying volume with density. The equation found for r is inserted in the equation for mass.

$$M = V * \rho = A * L * \rho = 2\pi * r * t * L * \rho$$
$$M = 2\pi * t * L * \rho * \sqrt{\frac{F_f * L}{C_2 * \pi * t * \sigma_f}}$$
$$M = \left(2\sqrt{\frac{\pi * F_f}{C_2}}\right)\left(\sqrt{L^3 * t}\right)\left(\frac{\rho}{\sqrt{\sigma_f}}\right)$$

The first term contains the functional parameters and constants, the second term contains geometrical parameters and the last term contains the material properties. Same as before, the mass is minimized by maximizing the following material index:

$$N_2 = \frac{\sqrt{\sigma_f}}{\rho} \tag{15}$$

Thermal performance

Thermal properties are crucial to the application of additive manufacturing in space. Energy is limited, so heat input needs to be minimized. Thermal gradients in the manufacturing process must be minimized to prevent warping and unwanted stresses. The material needs to cool down again as quickly as possible to produce solar arrays as fast as possible. The energy input required to melt the material is calculated using the following equation:

$$Q_{melt} = c_p * M * dT + L_f * M \tag{16}$$

Where Q_{melt} (J) is the heat required to melt the material, c_p $(J/(kg * K))$ is the specific heat capacity, M (kg) is the object mass, dT (K) is the temperature difference between start and end of the heating process and L_f (J/kg) is the specific latent heat of fusion. Mass is equal to volume V (m^3) times density ρ (kg/m^3). It is assumed here that the object geometry (tube radius, thickness and length) is known. Therefore, volume is a functional parameter and is

irrelevant for the material index. The end temperature is taken as the melting temperature of the material, because the material is deposited in its fluid state. This is a good reference for the temperatures that are actually experienced. The start temperature is something that cannot be exactly determined at this stage, as it is dependent on currently unknown system specifics. $T_0 = -50°C$ is used. This is an estimate based on the minimal temperature that was experienced during the on-orbit validation experiment for ROSA [27], which was $-46°C$. Unfortunately, the start temperature is a parameter that cannot be eliminated in the equation, so the estimate needs to be worked with.

$$\begin{gathered} Q_{melt} = c_p * V * \rho * (T_m - T_0) + L_f * V * \rho \\ V = 2\pi * r * t * L \\ Q_{melt} = (2\pi * r * t * L)(c_p * \rho * (T_m - T_0) + L_f * \rho) \end{gathered} \tag{17}$$

Here the first term in brackets contains constants and geometrical parameters. The second term is the index consisting of material properties (and one functional parameter) and must be minimized to obtain the lowest heat input Q_{melt}. This results in the following material index that must be maximized to find the best material:

$$N_3 = \frac{1}{C_p * \rho * (T_m - T_0) + L_f * \rho_P} \tag{18}$$

Additionally, it was found that thermal conductivity κ plays an important role. This material property must be maximized for optimal additive manufacturing performance. This can be seen as the fourth material index:

$$N_4 = \kappa \tag{19}$$

Since bubble charts are two-dimensional, it is only possible to plot on two axes. Therefore, material index N_1 and N_2 are going to be combined into one index. Currently, there is no reason to value stiffness differently than strength, because no specifications are known yet for these parameters. For that reason, the two indexes are valued equally. This is done by multiplying the two indexes.

$$N_{12} = N_1 * N_2 = \frac{\sqrt[3]{E}}{\rho} * \frac{\sqrt{\sigma_f}}{\rho} = \frac{\sqrt[3]{E} * \sqrt{\sigma_f}}{\rho^2} \tag{20}$$

The same method and reasoning are applied for the thermal material indices. These are valued equally and multiplied with each other to obtain a single, combined material index.

$$N_{34} = N_3 * N_4 = \frac{1}{C_p * \rho * (T_m - T_0) + L_f * \rho_P} * \kappa = \frac{\kappa}{C_p * \rho * (T_m - T_0) + L_f * \rho_P} \tag{21}$$

A brief sensitivity analysis is done in Section 3.2.3 to see the sensitivity of the assigned index weight and if this has an impact on the material choice.

3.2.2 Limits stage

A selection pool of materials is created by taking all possible materials in the GRANTA EduPack database, excluding the ones that have properties or characteristics outside of the set limits. The limits that are set are confined to material family limitations and operating temperature.

Certain aspects to the application that create reasons to set limits to the material pool have been determined in Sections 3.1.2 and 3.1.4. The conclusions regarding material families was that polymers are excluded due to atomic oxygen degradation. Ceramics and glasses are excluded because of their unavailability in wire feedstock due to their brittleness. Only certain (metal) composites could be compatible with DED. Lastly, elastomers are not suitable in strong, stiff applications for structures. This results in metals and partially composites being the only possible material families in the material selection pool.
Another limit that is set is operating temperature. The structure will have to endure both extremely hot and cold temperatures in space and must not fail under those conditions. The minimum operating window that is set is $-120℃$ to $120℃$. It was found in Section 3.1.4 that this is often taken as a rule of thumb in spaceflight. ROSA tested its structure on ground between $-65℃$ and $90℃$ [27], and ITSAT performed its thermal cycle tests from $-85℃$ to $70℃$ [49]. Based on this information found in the literature, the chosen temperature operating window is expected to be suitable with an additional margin.

3.2.3 GRANTA EduPack

All previous mentioned selection parameters are entered into GRANTA EduPack. A chart is generated using material index N_{12} on the y-axis and material index N_{34} on the x-axis. Limits are added to the stage. Materials that do not meet those limits are hidden on the chart. This creates the chart in Figure 14. Note that the chart has logarithmic axes. The colours of the bubbles represent the material family of the material. The colours are irrelevant for this material selection. The material indices need to be maximized to find the best material, so the best materials can be found in the top right corner of the chart. On this chart, commonly applied materials in DED are labelled, as well as top performing materials. A dotted line is added to give an idea of how materials rank versus each other. Materials on this line have equal performance if the indices on the x and y axes were weighed equally. Also, note that the units for the performance indices are extremely elaborate. These do not have a physical meaning, other than for being used as a performance benchmark.

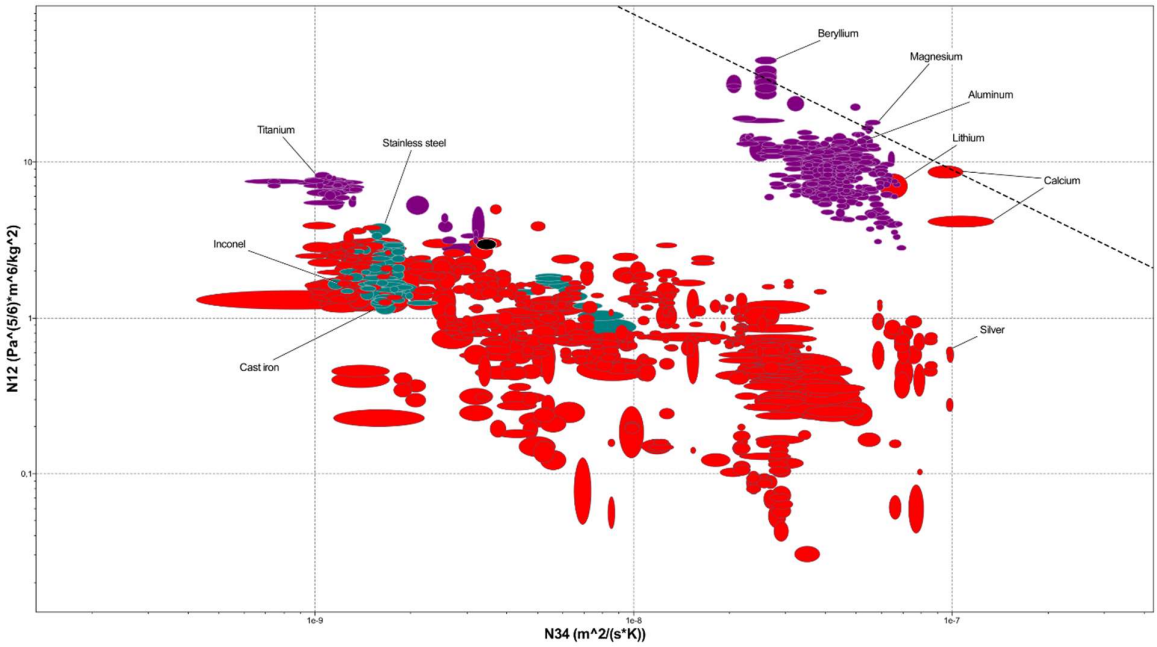

Figure 14: Bubble chart for N12 and N34, limited to metals with operating temperatures outside of -120°C to 120°C

The whole purple island of material bubbles in the top right corner consists only of aluminium, magnesium and beryllium alloys. Also, the pure metals lithium and calcium are in that same area of the chart. Interestingly, out of the metals known to be used with directed energy deposition, only magnesium and aluminium appear to be good candidates for a space structure application. Other popular DED materials, such as titanium, (stainless) steel and Inconel all perform significantly worse. Besides titanium, all of these materials score worse on the specific strength and stiffness index. Thermal performance is even worse. These DED materials score an order of magnitude worse on the performance index, meaning they are not even close to being a contender to be the chosen material.

To make sure no materials are overlooked when a selection is made for further investigation, a new chart is made where the material indices are combined into one index. This does not hold any value to the material selection procedure, but a list can be made with names, sorted on best index values. The top section of this list can be found in Figure 15. Looking through the names of this list, one can make sure no materials are overlooked, which could be hiding under other bubbles in the first chart. The results of this new chart can be seen in Figure 16.

As can be seen in Figure 14, this selection of top performers on this chart are in a league of their own. These materials form an island that is separated from the rest of the materials. The fact that there is a group of materials that is significantly better is confirmed in the chart in Figure 16. A gap is found between the performance of the worst aluminium alloy and the next best option, which is a silver-copper alloy.

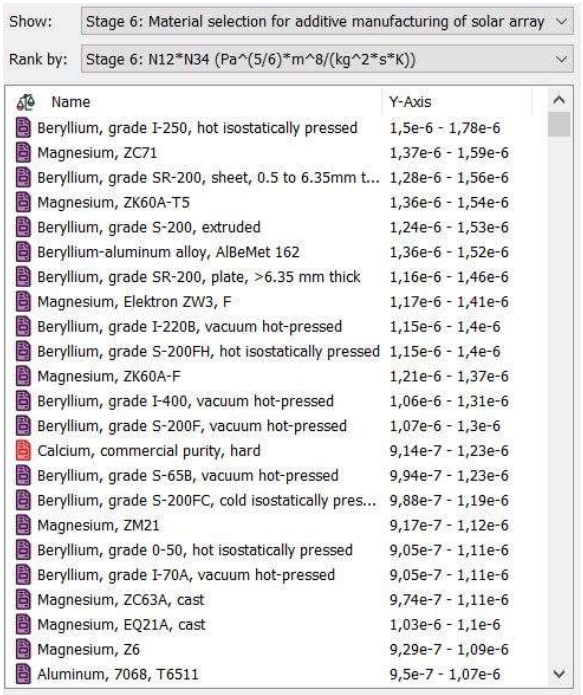

Name	Y-Axis
Beryllium, grade I-250, hot isostatically pressed	1,5e-6 - 1,78e-6
Magnesium, ZC71	1,37e-6 - 1,59e-6
Beryllium, grade SR-200, sheet, 0.5 to 6.35mm t...	1,28e-6 - 1,56e-6
Magnesium, ZK60A-T5	1,36e-6 - 1,54e-6
Beryllium, grade S-200, extruded	1,24e-6 - 1,53e-6
Beryllium-aluminum alloy, AlBeMet 162	1,36e-6 - 1,52e-6
Beryllium, grade SR-200, plate, >6.35 mm thick	1,16e-6 - 1,46e-6
Magnesium, Elektron ZW3, F	1,17e-6 - 1,41e-6
Beryllium, grade I-220B, vacuum hot-pressed	1,15e-6 - 1,4e-6
Beryllium, grade S-200FH, hot isostatically pressed	1,15e-6 - 1,4e-6
Magnesium, ZK60A-F	1,21e-6 - 1,37e-6
Beryllium, grade I-400, vacuum hot-pressed	1,06e-6 - 1,31e-6
Beryllium, grade S-200F, vacuum hot-pressed	1,07e-6 - 1,3e-6
Calcium, commercial purity, hard	9,14e-7 - 1,23e-6
Beryllium, grade S-65B, vacuum hot-pressed	9,94e-7 - 1,23e-6
Beryllium, grade S-200FC, cold isostatically pres...	9,88e-7 - 1,19e-6
Magnesium, ZM21	9,17e-7 - 1,12e-6
Beryllium, grade 0-50, hot isostatically pressed	9,05e-7 - 1,11e-6
Beryllium, grade I-70A, vacuum hot-pressed	9,05e-7 - 1,11e-6
Magnesium, ZC63A, cast	9,74e-7 - 1,11e-6
Magnesium, EQ21A, cast	1,03e-6 - 1,1e-6
Magnesium, Z6	9,29e-7 - 1,09e-6
Aluminum, 7068, T6511	9,5e-7 - 1,07e-6

*Figure 15: List of top performing materials for N12*N34*

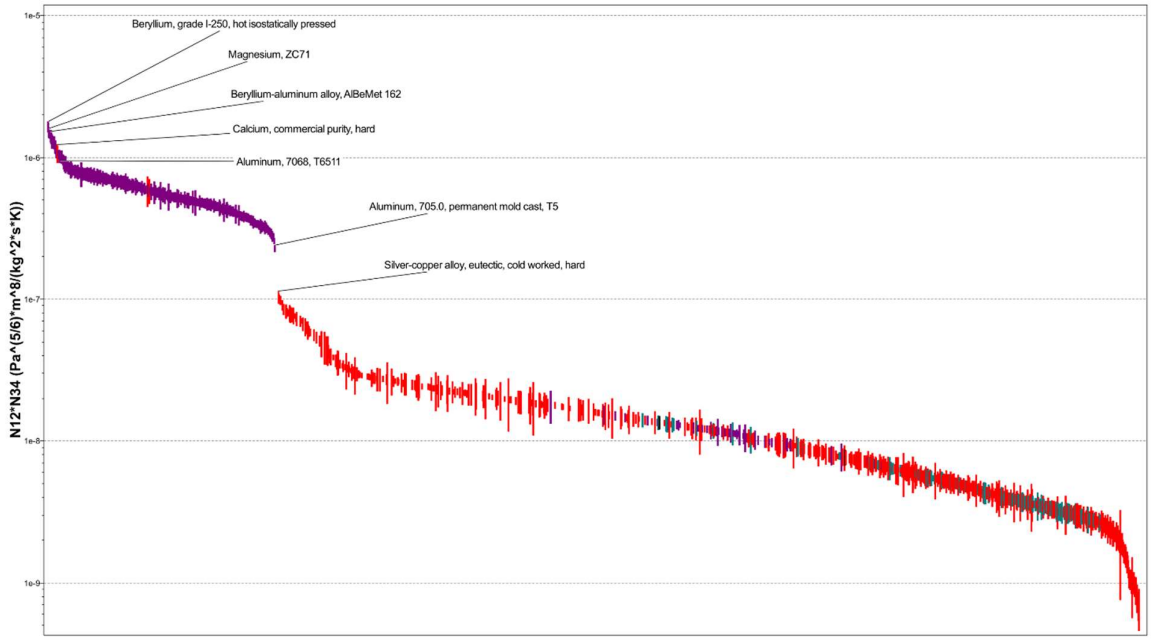

*Figure 16: Material performance chart for N12*N34*

Now, the top performers are further examined. Figure 17 shows a zoom-in of the materials in the top right corner of the bubble chart. Beryllium alloys score the best overall on the N_{12} index. They provide the best strength and stiffness in an application where bending loads are applied, while having the lowest mass. Second best is a magnesium alloy, which is closely followed by an aluminium alloy. Lithium and calcium fall in a different category, being a pure metal instead of an alloy. Yet, they still perform equally well on the N_{12} index as some magnesium and aluminium alloys. There is about an order of magnitude in performance difference between the best beryllium alloy and the worst aluminium alloy on this chart.
The thermal performance ranges approximately within an order of magnitude as well. For N_{34} the worst performer in this selection is a beryllium alloy. Beryllium in general scored about equally to the worst thermal performers for aluminium and magnesium alloys. The best performing beryllium alloy is a beryllium-magnesium combination. This material scores about equal to the better thermal performers for aluminium and magnesium alloys. Lithium scores better than this material group and calcium even better than that.

All of these materials are taken into the next phase: documentation. Aluminium, magnesium and beryllium alloys, as well as lithium and calcium are investigated more thoroughly in Section 3.2.6.

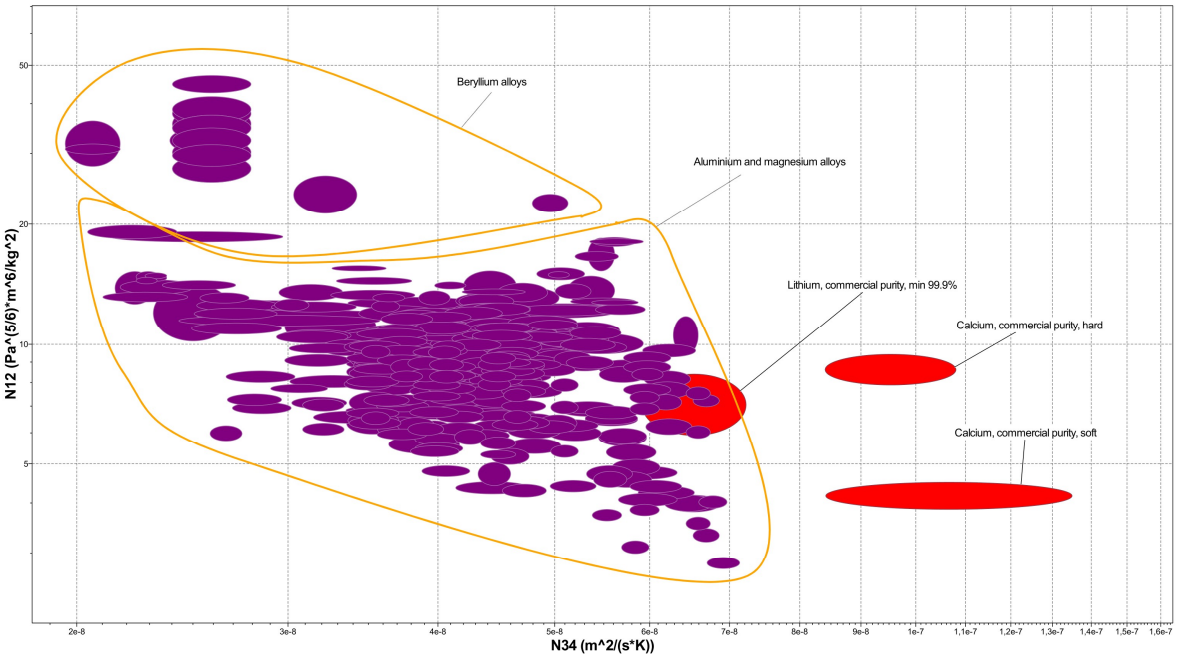

Figure 17: Zoom in on the top performers in the bubble chart for N12 and N34, limited to metals with operating temperatures outside of -120°C to 120°C

3.2.4 Sensitivity analysis

When the material indices N_1 and N_2, as well as N_3 and N_4 were combined into a single material index, the assumption was made that both of the indices have the same weight. One index would not be more important than the other, so conductivity is not valued greater than heat input for example. A sensitivity analysis is done to find out if a different index weight would have caused a different material to be the best choice. This increases the confidence in the found material and also shows that the found material can be the best option for slightly different mission requirements. Charts have been generated with alternative weights for each of the indices. This is done by keeping the chart the same as the chart in Figure 14, but with one index altered. The weight is changed by taking the squared of the respective index in the combined index. So, for example, $N_{12} = N_1^2 * N_2$ instead of the previously used $N_{12} = N_1 * N_2$. Doing this for each of the four indexes resulted in the charts found in Figure 18, Figure 19, Figure 20 and Figure 21.

Giving extra weight to stiffness and strength, Figure 18 and Figure 19 respectively, does not seem to change much in the outcome of the charts. The general distribution of material bubbles remains the same and one needs to look closely to find any materials that have climbed the performance scale. Whereas increased stiffness weight does not seem to have any significant change, increased strength weight drags the materials out a little in the y-direction. Lithium is one of the few materials that gains some rankings. Nevertheless, the differences in results are so small that a different weight, within margin, given to strength or stiffness does not change the outcome of the material selection significantly.

Doubling the weight for the thermal indices shows more impact. The top performers selection remains the same, but their relative ranking shifts slightly. Looking at Figure 20 where the required heat input is emphasised, is can be seen that the beryllium alloys get a lower relative thermal performance score. One reason for this is the high melting point

close to 1300℃. Lithium and calcium gain in relative ranking. For an increased weight of thermal conductivity in Figure 21 the opposite happens. The berylliums gain slightly and lithium and calcium lose slightly. For both changes, aluminium and magnesium seem to stay in the centre of the top performers. They show less change with different weights, meaning the material properties for those materials are better balanced between strength, stiffness, density and thermal properties.

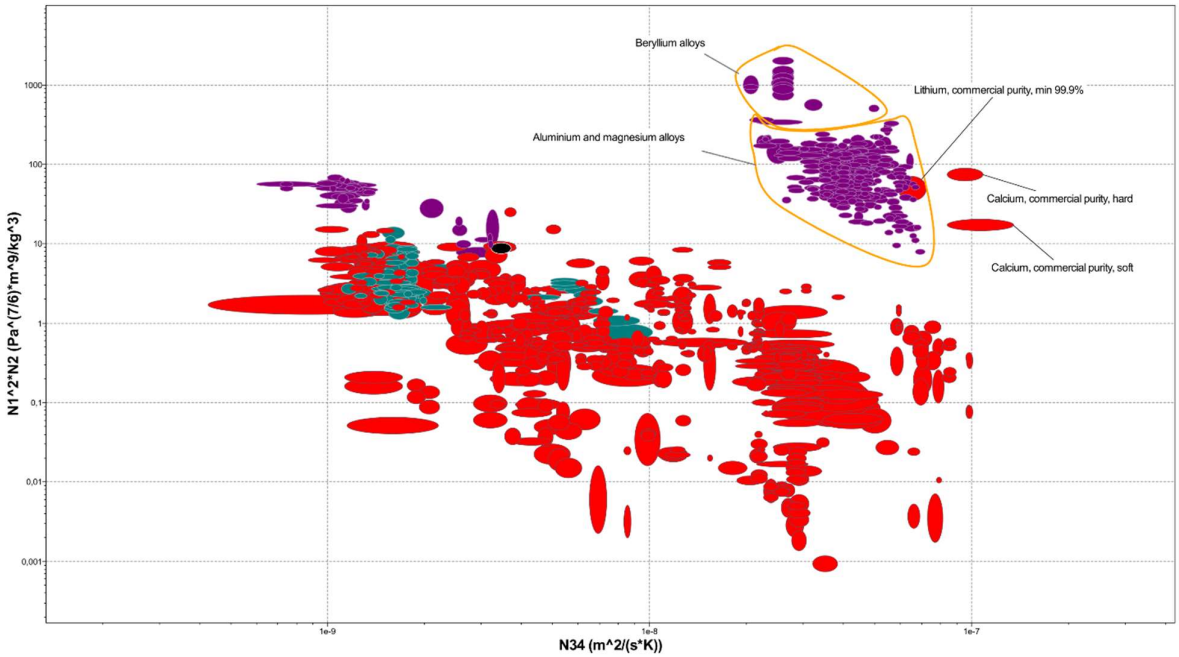

Figure 18: Bubble chart sensitivity analysis - stiffness

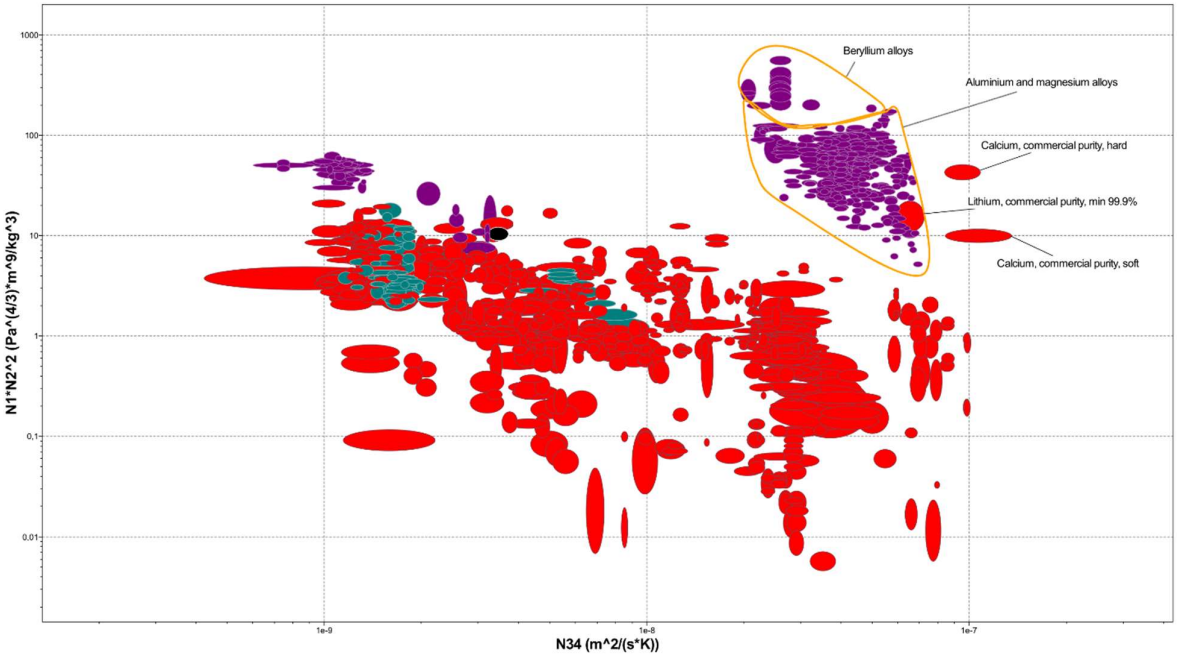

Figure 19: Bubble chart sensitivity analysis - strength

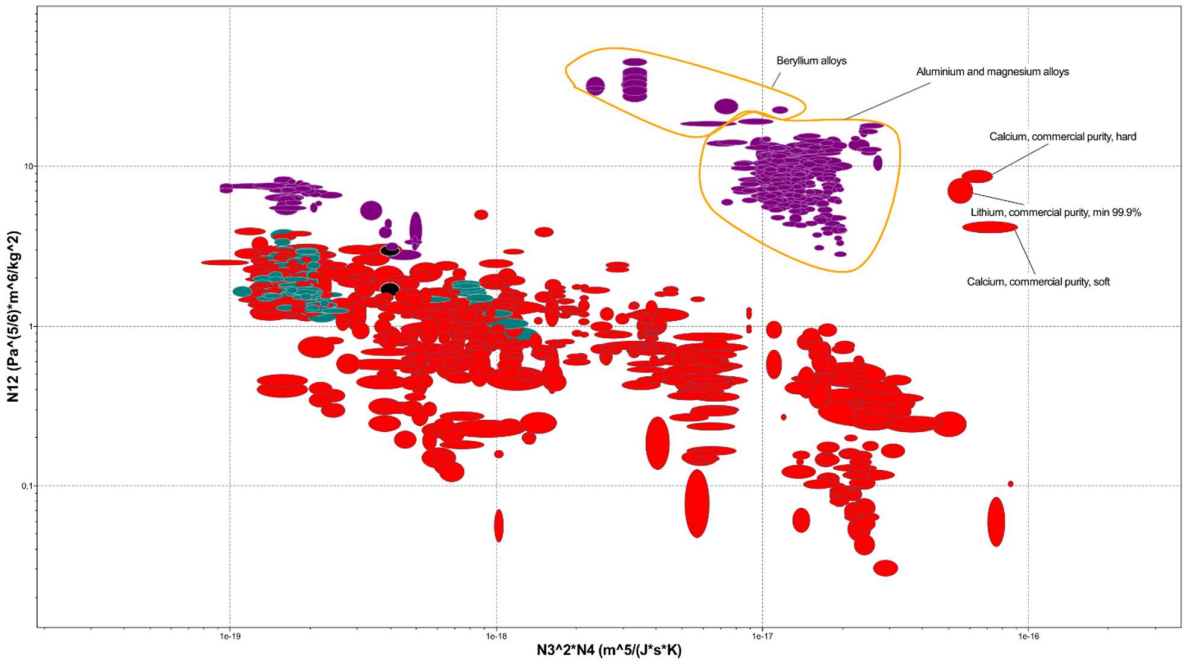

Figure 20: Bubble chart sensitivity analysis - required heat input

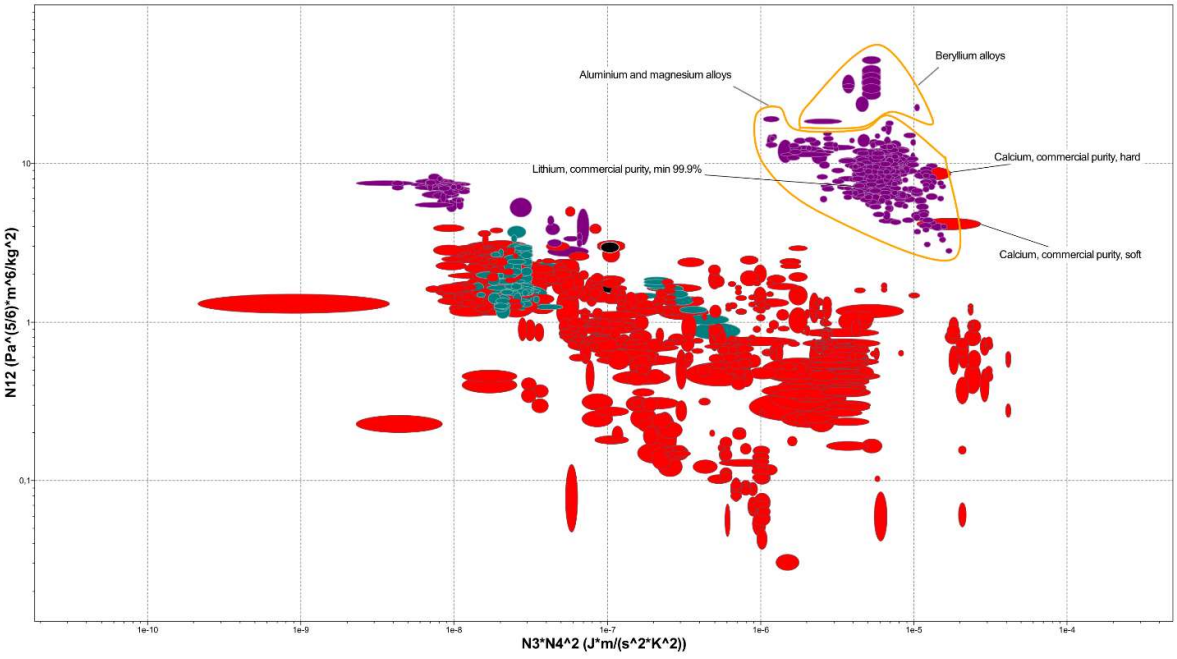

Figure 21: Bubble chart sensitivity analysis - thermal conductivity

3.2.5 Interesting alternatives

For some interesting findings, the chart for performance indices N_{12} and N_{34} is provided without any limits selected in Figure 22. This reveals materials that were not considered in the previous charts. Looking at this chart, it can be made sure no good materials are overlooked by assumptions made in the limits.
The purple cloud of bubbles in the top right is the same group of beryllium, aluminium and magnesium alloys, for reference. The red bubbles are the same metals that were seen in the previous charts. Out of all materials in the database, which is nearly all materials known to men, the top performers found in the first chart are still among the best. Regarding the other high performing material bubbles in this chart: green is foam materials, brown is composites and yellow is ceramics. Grey bubbles are materials that do not meet the operating temperature limit, many of which are polymers and natural materials.

There are only few materials that show better performance. These materials are labelled in Figure 22. The problem with all of these competitive materials is their manufacturability in combination with DED. These materials include carbon fibres, carbon reinforced aluminium and magnesium, and diamond. Unfortunately, carbon fibres cannot be incorporated using directed energy deposition. This reason simply makes it an impossible material for the desired application. The same applies to diamond. Diamond cannot be moulded with DED. Another obvious problem is the super high cost of diamond. It was said that, within reason, cost should not be a limiting factor to innovation, but diamond exceeds limits and is completely unfeasible. Among the beryllium, aluminium and magnesium alloys, more composites are found. Though, the same complications are experienced. These composites cannot be manufactured using directed energy deposition, but require different, often more complicated manufacturing methods.
In conclusion, the best material options found in the results in the first chart are indeed the best options possible. No materials were overlooked during the selection procedure.

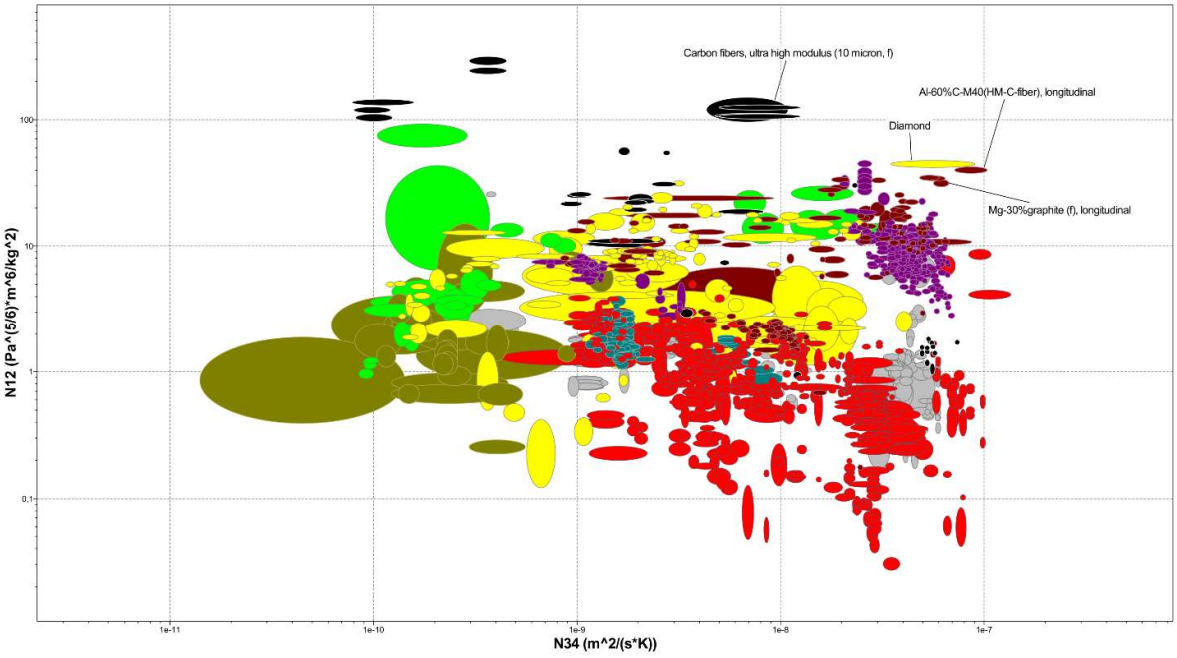

Figure 22: Bubble chart of all materials for N12 and N34 without limits

3.2.6 Documentation stage

The top selection that resulted from the findings gathered using the bubble charts is: beryllium alloys, aluminium alloys, magnesium alloys, calcium and lithium. These materials are further researched to find arguments why one is a better choice over another. The material indices only provide a part of complete picture, so other aspects that could not be incorporated into these indices are investigated. This is done by looking into documentation for these materials. This includes non-numerical attributes of the materials. The values for the material indices, as well as the important material properties are listed in Table 9. In this table, the best performing material per property is marked green.

Emissivity is a parameter that could not be summarized into a general numerical value. This needs to be investigated per material what the expected range can be. Another important aspect that was not able to be expressed differently in the material indices for strength and stiffness is the fact that tube radius is not defined in those equations. Radius was substituted to be able to combine the equations for strength and stiffness with the equation for mass. Therefore, the final equation for mass did not contain r, meaning that the radius was not a geometrical constant in those equations. This means that materials with the same performance for N_{12} do not necessarily have to have the same diameter. Looking at the equations r found earlier, it can be found how much bigger the radius needs to be for one material over another.

$$S = \frac{C_1 * E * \pi * r^3 * t}{L^3} \quad \rightarrow \quad r_s = \sqrt[3]{\frac{S * L^3}{C_1 * E * \pi * t}} \quad \rightarrow \quad r_s \sim \sqrt[3]{\frac{1}{E}} \tag{22}$$

$$F_f = \frac{C_2 * \pi * r^2 * t * \sigma_f}{L} \quad \rightarrow \quad r_f = \sqrt{\frac{F_f * L}{C_2 * \pi * t * \sigma_f}} \quad \rightarrow \quad r_f \sim \sqrt{\frac{1}{\sigma_f}} \tag{23}$$

$$\frac{r_{s_1}}{r_{s_2}} = \frac{\sqrt[3]{\frac{1}{E_1}}}{\sqrt[3]{\frac{1}{E_2}}} = \frac{\sqrt[3]{E_2}}{\sqrt[3]{E_1}} = \sqrt[3]{\frac{E_2}{E_1}} \tag{24}$$

$$\frac{r_{f_1}}{r_{f_2}} = \frac{\sqrt{\frac{1}{\sigma_{f_1}}}}{\sqrt{\frac{1}{\sigma_{f_2}}}} = \frac{\sqrt{\sigma_{f_2}}}{\sqrt{\sigma_{f_1}}} = \sqrt{\frac{\sigma_{f_2}}{\sigma_{f_1}}} \tag{25}$$

In Table 9 the radius required to have the same strength and stiffness is provided. This is given as the factor relative to the radius of magnesium. The provided factor is a range of the lowest and highest possible values, based on the range in flexural modulus and flexural strength.
Looking at the results, it can be seen aluminium and beryllium alloys require a smaller tube radius to have the same strength and stiffness as magnesium alloys, except for the lowest values of flexural strength. Calcium and lithium require a bigger radius, in some cases by a lot. Note that whether stiffness or strength is the limiting factor depends on the requirements. Also, the range can be very wide, because within a certain alloy family a big difference is found in property values. Looking only at the maximum values of flexural strength and modulus, it is found that aluminium requires about 1.3x smaller radius, beryllium 1.1 - 1.9x, calcium 0.4 - 0.8x and lithium 0.1 - 0.5x. Radius size directly impacts print speed. Therefore, this is a highly valued material parameter.

Table 9: Important material property values for the top materials selection found in the bubble charts

Property\Material	Magnesium alloys	Aluminium alloys	Beryllium alloys	Lithium	Calcium
N_{12} $(Pa^{5/6} * m^6/kg^2)$	9.37 - 19.8	2.75 - 14.5	14.6 - 47.2	5.92 - 8.4	3.86 - 9.44
N_{34} $(10^{-8}\ m^2/(s * K))$	2.15 - 6.58	2.18 - 7.13	1.96 - 5.29	5.92 - 7.21	8.41 - 13.5
$r_{s_{magnesium}}/r_{s_x}$ (-)	1	1.10 - 1.32	1.56 - 1.99	0.46 - 0.51	0.72 - 0.81
$r_{f_{magnesium}}/r_{f_x}$ (-)	1	0.23 - 3.41	0.56 - 2.97	0.05 - 0.18	0.17 - 1.04
Density ρ (kg/m^3)	1730 - 1950	2490 - 2960	1840 - 2230	530 - 540	1540 - 1560
Flexural modulus E_f (GPa)	40 - 47.3	63 - 92	179 - 315	4.6 - 5.2	18 - 21
Flexural strength σ_f (MPa)	65 - 440	24- 756	136 - 575	1 - 2	12 - 70
Thermal conductivity κ $(W/(m * K))$	50 - 155	75 - 249	88.4 - 216	70 - 85	125 - 200
Specific heat capacity c_p $(J/(kg * K))$	950 - 1110	833 - 1080	1390 - 2220	3450 - 3600	630 - 655
Melting temperature T_m (℃)	420 - 650	450 - 680	632 - 1290	177 - 182	827 - 840
Specific latent heat of fusion L_f (kJ/kg)	350 - 375	239 - 550	305 - 1360	420 - 450	205 - 225
Cost (€$/kg$)	2.28 - 16.8	1.46 - 13.9	366 - 564	61.4 - 68.3	2.02 - 2.97
Maximum service temperature (℃)	130 - 310	80 - 300	255 - 830	150 - 160	57 - 140
Minimum service temperature (℃)	-273	-273	-273	-273	-273

Magnesium alloys

Magnesium is already being used for additive manufacturing. Magnesium is a material with one of the lowest densities out of the metals used for structural purposes [52]. The low density is the reason this material is chosen for most of its applications. Although its modulus is lower than many counterparts, such as aluminium and steel, its specific modulus is similar to that of aluminium due to its low density. The specific strength of magnesium is higher than that of aluminium, though just the strength is slightly lower. Magnesium alloys' strength reduces somewhat at higher temperatures, starting around 93℃ [53]. Magnesium alloys have relatively poor creep properties. Fortunately, the structure does not endure a continuous force in the application of solar arrays in space.
Although pure magnesium is known to be a flammable material, magnesium alloys are considered safe. The additives in the alloy make the material non-combustible, making most alloys safe.

Aluminium alloys

Within the group of structural metals, aluminium alloys offer high stiffness and strength per unit of mass [54]. Though, just like magnesium, flexural modulus and strength are lower than many other metals. In a lot of ways aluminium alloys are similar to magnesium alloys. Both are used for applications where light, strong parts are required. The thermal properties are also similar. In particular, aluminium is a good thermal conductor. It can be seen in Table 9 that specific heat capacity and melting temperature are very similar. Thermal conductivity and latent heat of fusion are also close but show a bit more variety.
Aluminium corrosion will create a white powder-like layer on the surface that protects itself from further oxidation. Certain alloys or heat treatment will make the material more corrosion resistant. In space corrosion will not be a big problem due to the lack of an atmosphere.
Aluminium is often highly reflective. Radiant energy will partly be reflected because of this. In one way this is beneficial: lower incoming heat from the sun will cause smaller thermal gradients in the part. As was mentioned in the heat source selection in Section 2.3.3, reflective materials will have issues when combined with a laser as a heat source in additive

manufacturing. In that same section laser was not chosen as the heat source to continue this project with, so reflectance is not a problem for the additive manufacturing process.
Aluminium has a lower fatigue strength compared to other metals such as steels. This is the amount of stress under which no failure occurs. Over this limit, the material can only handle a certain amount of stress cycles before it fails. As opposed to creep, where a sustained stress is causing failure, fatigue stress is more important in a space application. The structure is expected to undergo vibrations, because of less dampening that happens in a space environment. The vibrations are a source of stress cycling.

Beryllium alloys

Beryllium is only used in high performance applications, such as space, defence and medical fields. Beryllium is transparent to X-rays. An important limitation to this material is its high cost. An example is the use of beryllium O-30-H as the material used to make the mirrors for the James Webb Space Telescope (JWST) [55]. Beryllium has a very low coefficient of thermal expansion, which makes it a suitable choice for high precision applications.
Beryllium is especially interesting for its high flexural modulus. It is used for applications where stiffness is important. Its strength is slightly higher than for magnesium alloys and slightly lower than aluminium alloys. Combined with its low density, beryllium achieved the highest values for the strength-stiffness material index.
Beryllium did not score high on the thermal material index. Its thermal conductivity is good, but the energy required to melt beryllium is high. This is because of both the high specific heat capacity and melting temperature, and to a smaller degree the high latent heat of fusion.
Although not impossible, beryllium is not commonly combined with additive manufacturing. Beryllium is not common in general because of its high cost. Beryllium is a toxic material. Machining of beryllium releases small particles. Inhaling beryllium particles is harmful to human health.

Lithium

Whereas magnesium alloys are the lightest structural metal, lithium is the lightest metal overall. Lithium is highly reactive. In open air it will oxidize with the atmospheric nitrogen. It also reacts with water and several other materials. Lithium is flammable and produces an extremely hot flame. On Earth it is stored in a hydrocarbon to insulate it from water and nitrogen [56]. However, as it is not dense enough to sink in mineral oil it is commonly stored in petroleum jelly. The highly reactive nature of lithium makes it completely unsuitable to be used as a structural material in space. Although it would not be as dangerous in space, because of the inert vacuum environment, the risks of getting it into space are massive. Storing it in a sealant while on the spacecraft on Earth would be completely impractical. This adds mass, complexity and risk to the mission.
The material indices showed good performance, but the reactivity of this material make it unsuitable for this application. Other properties of this material do not need to be considered.

Calcium

Calcium has the same issue as lithium: it is highly reactive. It reacts aggressively with water, which releases the flammable hydrogen gas. On Earth it has to be stored in an inert environment to prevent it from reacting. Calcium is mostly used as an additive for steelmaking and not as a structural material on its own. Calcium has advantageous thermal properties, but because of its reactive nature it is not suitable as a structural building material.

3.2.7 Material selection conclusion

Lithium and calcium were found to be unsuitable. That leaves magnesium, aluminium and beryllium alloys as the best options for in-space additive manufactured structures for solar arrays. Magnesium is unfavourable because it requires more volume to achieve the same performance as the other two material families. Assuming that the printer is not able to print any faster due to different thermal properties, an equal size solar array with a magnesium structure takes between 1.10 - 1.99x longer to print than an aluminium or beryllium structure. For a manufacturing station that has the sole purpose of production, this has significant impact on how many arrays it is able to produce in its lifetime. Additionally, it may become an issue for launching lower density material into space, because the payload volume is limited.
Besides volume related reasons, magnesium does not score notably better on thermal properties. Their performance for additive manufacturing and energy consumptions is extremely similar. There is no benefit to choose magnesium over aluminium for thermal performance and no reason to choose magnesium over beryllium for strength and stiffness performance. For these reasons, magnesium is not the best material option.

Comparing beryllium to aluminium alloys, it can be seen that there are some distinct characteristics to each of them. Beryllium scores significantly higher for stiffness. This can be beneficial to mitigate problems with vibrations. For a stiffness limited design, beryllium will require less volume than aluminium. In a strength limited design, it is for certain aluminium alloys possible that less volume is required than for beryllium. Generally speaking, their strength is similar. Aluminium is better than beryllium in thermal performance. It has a lower specific heat capacity, melting temperature and latent heat of fusion. Looking at the complete material families, aluminium and beryllium achieve similar thermal conductivity values. Though, the best aluminium alloys can achieve higher values than what is possible for beryllium.

It is not possible to obtain values for emissivity with enough certainty to base a conclusion on. Emissivity is dependent on the surface finish, which cannot be determined at this stage. Additive manufacturing often has a rough surface, but for wire-based DED shiny surfaces can be found as well, depending on process specifics. In particular, emissivity values for 3D printed parts could not be found. For some kind of reference, values found in The Engineering Toolbox are provided [57]. This source states an emissivity coefficient of 0.07 for aluminium rough and 0.18 for beryllium. These values are not certain enough to be considered, so they will not be used for this conclusion on material selection. In the future, practical tests need to be performed to obtain meaningful values for emissivity, as this is a property that has a big impact on the cool-down behaviour of AM in space.

A big difference between aluminium and beryllium is cost: $1.46 - 13.90$ €/kg for aluminium versus $366 - 564$ €/kg for beryllium. It was said earlier that cost should not limit innovation, but that does not mean cost should be neglected. The difference in cost must be worth it. It must be considered that not only the cost of material required for the structure is important, but also the cost of development. Industry and institutes may feel held back by the fact that practical testing is expensive. This may extend the development time and postpone the moment when this futuristic application can become a reality.
An additional inconvenience for development is the safety hazard of working with beryllium. Expensive air filtration systems need to be installed, protective gear must be used and contaminations in the air must be monitored.

Another argument can be made about sustainability. In the literature study done in preparation for this thesis research [1], space debris was mentioned as problem that can be partially solved by in-space manufacturing. Materials found in space debris can be reused for new application through recycling processes. In-space manufacturing is required to obtain the right object for a new application. There are ways to combine the proposed application with recycling. It is possible that recycled wire is delivered to an in-space manufacturing platform, which is then used for the production of

solar arrays. Now, coming back to material selection, aluminium is the most used material for spacecrafts found in space. Basing a manufacturing platform on the use of aluminium makes the project more future-proof for combining in-space manufacturing with space debris recycling. Beryllium is found in space, often for optical systems, but in way smaller amounts than aluminium. Therefore, it is probably not interesting to create a recycling station in space for beryllium, at least not given the current state of technology.

In conclusion, because of all previously mentioned arguments, aluminium alloys are considered the best materials for in-space additive manufacturing for solar array structures. This selection procedure was done without bias by including all materials possible. Performance was based on the application and advantages and disadvantages for the best performing materials were explored. The summary of arguments can be found in Table 10.

Table 10: Overview of arguments for material selection

Material	**Argument**
Lithium	• Highly reactive
Calcium	• Highly reactive
Magnesium	• Slightly worse thermal performance than aluminium • Requires more volume than aluminium • Worse strength and stiffness performance than beryllium
Beryllium	• Has the best performance on the strength and stiffness index • Worse thermal performance than aluminium • Costs ~2 orders of magnitude more per kilogram than aluminium • Working with beryllium can be a safety hazard • Has had little development for additive manufacturing • Not suitable for recycling of space debris
Aluminium	• Good thermal performance, but lower strength and stiffness performance • Cheap • Lots of information available on WAAM/welding • Lots of aluminium in space, so suitable for combining with space debris recycling

The next step is to determine what aluminium alloy specifically is the best for WAAM in space. This is a hard problem to answer accurately, because there are many factors that come into play when deciding on one alloy over another. Some important aspects are addressed here and a choice is made based on these findings.
Figure 23 shows where the different aluminium alloys place on the bubble chart for $N12$ and $N34$. Here, the beryllium alloy material family is also included to include beryllium-aluminium alloys in this chart. On the chart two lines of equal performance are included for reference: equal performance for $N12 * N34$ and $N12 * N34^2$. This chart demonstrates the superior performance of beryllium alloys, but even the beryllium-aluminium alloys are significantly more expensive than regular aluminium alloys.
Figure 24 lists the best performing aluminium alloys for $N12 * N34$. In this figure it is found that the 7xxx, 6xxx and 2xxx series offer the best performance within the aluminium material family. Though, an important factor that is relevant here is what hardening process was used in the production of the material. Work hardening or solution hardening and ageing procedures will give better properties to the materials in the bubble chart, but melting the material for additive manufacturing will make the material lose some of these benefits. The distribution of alloying elements will change upon heating of the material. These hardening processes are difficult or impossible to do in space and generally not worth the complexity. Langebeck et al. [58] found during their test where specimens where produced using DED in aluminium 7075 T6 that their ultimate tensile strength was $222 \pm 17\ MPa$, while conventionally produced material of this aluminium alloy has an ultimate tensile strength of $572\ MPa$. For this reason, it is bad practice to base alloy

performances solely on property values in the database. This phenomenon extends to all metals that have undergone hardening processes.

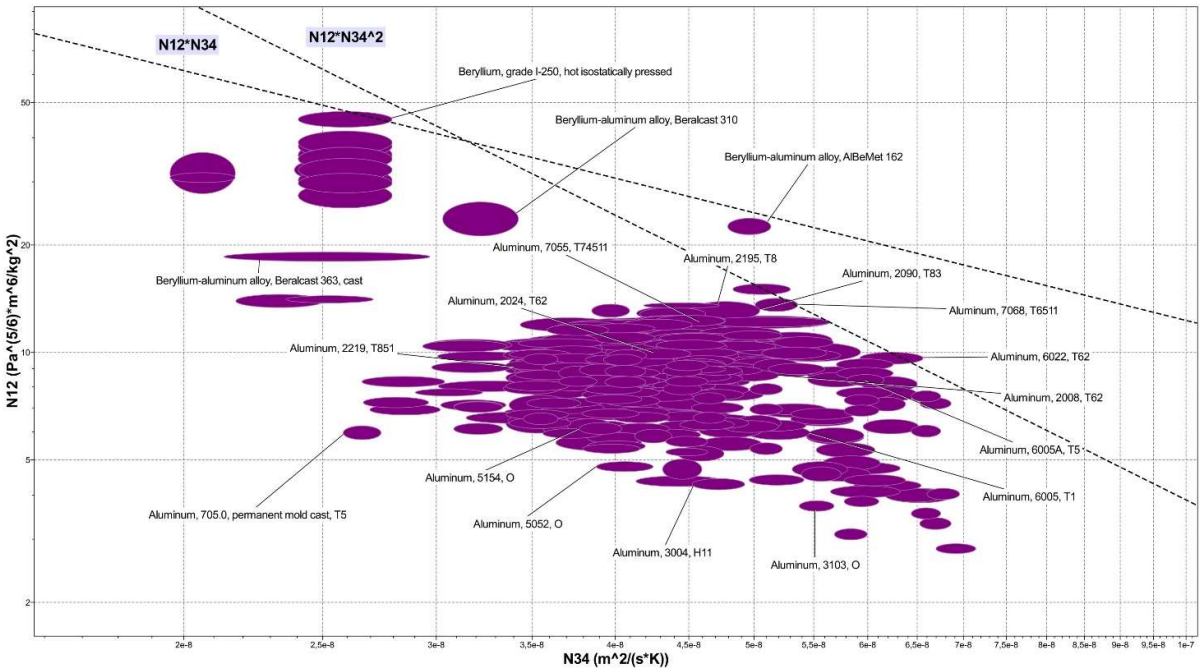

Figure 23: Bubble chart for N12 and N34 limited to aluminium and beryllium alloys

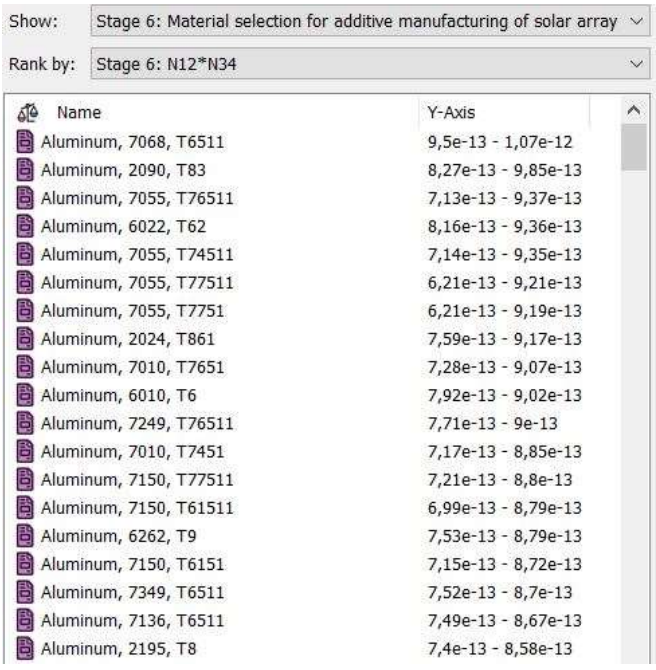

*Figure 24: Top performing aluminium alloys for N12*N34*

Most of the alloys in the 1xxx, 3xxx, 5xxx, 6xxx and medium strength 7xxx series can be welded with the MIG (GMAW) process [59]. Therefore, they should also be suitable for GMAW DED additive manufacturing. Especially the 5xxx series have good weldability. Alloys with high strength, such as 7010 and 7050, as well as 2xxx series are less suited for welding. These alloys suffer problems with liquation and solidification cracking.
Haselhuhn et al. [60] have found in experiments with different aluminium alloys for GMAW WAAM (a.k.a. MIG WAAM), the chosen DED method in this research, that the 4000 series aluminium showed the best performance.
Vimal et al. [61] have summarized a number of papers that contain research on aluminium WAAM. The 1100, 2319, 4043, 4047, 4943, 5087, 5183 and 5356 aluminium alloys have been demonstrated in experiments where their performance was researched. In this paper, levels of porosity, energy input and strength are discussed based on the results from experiments with these materials. The focus lays on understanding how the process affects the behaviour of these materials, so there is no best material determined.

The biggest problems with aluminium DED applications are porosity and cracks that are created in the material during the manufacturing process. Another issue is residual tensile stress, which impacts the fatigue strength of the 3D printed object. There are many techniques known to help with these issues. They are often incorporate complex procedures for how the wire of current is delivered, special filler materials in the wire and cleaning steps of the subject. There is a lot to explore in this field, however, this does not fall within the scope of this research.

It is difficult to choose the best aluminium based on these findings. There is not one that is a clear winner, many alloys can be chosen for different reasons and still function great in this application. For the purpose of this of this report, aluminium 6005A T5 is chosen to move forward with. This alloy contains a small fraction of magnesium and silicon. The material is weldable, making it suitable for wire DED. This is the best performing alloy based on the material indices that is not quenched in water. Instead, T5 means that it is air cooled. Therefore, it is deemed to have material properties that are truer to when the material has been used in additive manufacturing. Still, discrepancies can be expected between air-cooled and cooled in space, but it is expected to be more comparable than quenched materials. The material properties for aluminium 6005A T5 are listed in Table 11.

Table 11: Material properties of aluminium 6005A T5, taken from GRANTA EduPack [51]

Property	**Value**
N_{12} $(Pa^{5/6} * m^6/kg^2)$	8.06 – 8.79
N_{34} $(10^{-8}\ m^2/(s * K))$	5.45 – 5.97
Density ρ (kg/m^3)	2680 – 2730
Flexural modulus E_f (GPa)	67.5 – 71
Flexural strength σ_f (MPa)	208 – 243
Thermal conductivity κ $(W/(m * K))$	185 – 201
Specific heat capacity c_p $(J/(kg * K))$	874 – 910
Melting temperature T_m (°C)	630 – 655
Specific latent heat of fusion L_f (kJ/kg)	384 – 393
Cost (€$/kg$)	1.63 – 1.83
Maximum service temperature $T_{o,max}$ (°C)	130 – 150
Minimum service temperature $T_{o,min}$ (°C)	-273

3.3 Geometrical accuracy

When a part is printed multiple times using additive manufacturing processes, it is common that the results show differences in shape. Print reliability is currently one of the biggest problems in perfecting AM on Earth. In space, print reliability is even more important, because human interference to change something is not an option. Thermal distortions can cause all kinds of unwanted deformations and internal stresses. Improving print quality happens for a large part through simulating models. But, making these models behave exactly like the real process is extremely challenging. There are a great deal of parameters that influence the process. When these models are able to provide a good prediction of the print, they are able to give information about whether a certain print will be successful or not. Even better would be to use simulations to predict which areas of the object will experience thermal deformations and compensate for them before they happen. This will improve print quality greatly, but is no easy feat.
On Earth, perfecting additive manufacturing is already challenging enough as it is. It is possible to make multiple test prints and calibrate the simulations based on the outcome. However, for space purposes, things need to be perfect. There is no option to waste a lot of precious material for calibration purposes. This requires extensive research in the parameters that are important for the system in space and achieving models with high certainty.

High level accuracy cannot be expected for DED. To a certain extend this has to be expected and accounted for in the design. Figure 25 shows an overview of typical part accuracy and surface roughness that can be expected for various manufacturing technologies [62]. Wire-based DED is among the worst manufacturing methods for dimensional accuracy. Deviations in part geometry of millimetres can be expected for small parts (in the order of centimetres), up to centimetres for large part (in the order of metres). A surface roughness in the order of $1\ mm$ can be expected, which is caused by the layering effect. For most applications, DED is seen as a near net shape manufacturing method. Post-processing, such as milling, is used to obtain high precision measurements.

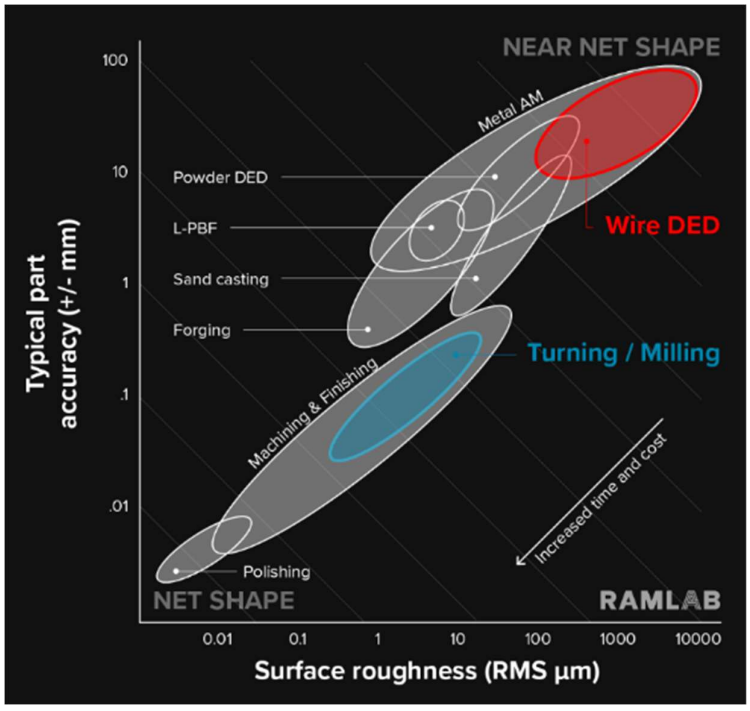

Figure 25: Common accuracy and surface roughness for various manufacturing processes [62]

The most prominent factor that causes the AM part geometry to differentiate from the original design is the characteristic of DED that material is deposited in layers. These layers are clearly visible in the final product, as can be seen in Figure 26, where an example of wire-based DED is demonstrated. As bigger layer heights are chosen, more dimensional inaccuracy can be expected [63]. A thicker wire results in a bigger welding bead, which creates a more prominent layering effect in the part. This creates a trade-off between deposition rate and accuracy. Since powder-based DED technologies deposit smaller layer heights than wire-based, typically ten times better accuracy can be expected for powder-based DED [13]. The other side of the coin is that wire-based DED is able to achieve higher production rates.

A lot of effort has been put into the research on effects of welding parameters on the welding bead shape. Although improvements can be made in the surface roughness using better modelling techniques, the surface of a DED part will never be perfectly smooth without post-processing due to inherent characteristics of the process. GMAW WAAM performs slightly worse in surface roughness than other wire-based DED processes, because the weld bead geometry is not uniform over the whole length of the layer. Start and end regions of the weld are particularly difficult to attain high geometrical accuracy, which is clearly visible in Figure 26. It is possible to improve this by locally changing welding parameters, such as current and printhead speed. It is best to minimize regions where non-constant movement occurs, such as end points and sharp corners, to prevent issues from occurring. Circular print paths with continuous movement are preferred to achieve the best geometrical accuracy.

Figure 26: Example subject of WEAM demonstrating the layered surface [18]

Besides surface roughness, part accuracy needs to be accounted for. Due to thermal stresses and inconstant conditions during the process, the shape of the part will deviate from the intended shape. Because additive manufacturing builds layer upon layer, errors will build upon one another. As part size increases, bigger dimensional errors can be expected. That is the case, unless a feedback system is incorporated. Process monitoring will be a key functionality for applying AM in space. This means that through image and sensor data processing the quality is monitored constantly throughout the process. Based on the data, parameters can be tweaked during the process to achieve the best result. More information on process monitoring can be found in Section 2.5 of the literature study on in-space manufacturing: ‘Qualification’ [1].

Geometrical accuracy of DED is not good, but fortunately, high accuracy is not needed for the proposed application. The solar array structures merely have to provide functional stiffness and strength. There is plenty of space around the solar panel, so in that regard it does not matter is the shape is slightly off. The only parts that require good tolerance would be the locations where the solar panel is mounted to the structure. In the concept, a prefabricated base structure attached to the solar panel is used to solve the difficulty of the start of the print. So, in this location printing accuracy is not relevant. A simple solution for mounting the flexible solar panel at intermediate locations on the structure would be to weld little metal pieces on the panel to the structure using the DED printer. From a mechanical point of view, this would require an accuracy of about one centimetre. This can be achieved by process monitoring. Research needs to be done in this area, as well as in understanding the effects of input parameters of AM on the outcome quality. Good models to predict the process behaviour, combined with process monitoring is the only way to reliability produce AM structures for solar arrays in space. What improvements can be made in geometrical accuracy using this strategy is difficult to say at this stage. This technology is in low TRL, so this will follow from future research.

4 DED in space

In this chapter the effects of using directed energy deposition in space is discussed. The environment in space is significantly different than on Earth, which will have large effects on the manufacturing process. The most impactful environmental differences are the vacuum, microgravity and thermal fluctuations. The vacuum has the consequence that there is practically no thermal convection. DED is a process where a lot of heat is generated for shaping of the object, which has to dissipate for the material to set. No thermal convection means that an important part of heat dissipation is taken away. The impact of different thermal characteristics in space is quantified by creating a thermal model for DED. Also, impacts of vacuum, microgravity and thermal fluctuations are discussed.

4.1 Impact of the space environment on DED

The environment in space is vastly different from the environment on Earth. Therefore, in this section, the effects of the most important differences in environment are discussed. The most important differences are: microgravity, vacuum and thermal fluctuations. This is particularly important, because metal additive manufacturing has to the date of publication of this report not been performed in space.

4.1.1 Microgravity

Microgravity has a great influence on the behaviour of the weld [21]. Fluids in microgravity behave differently than on Earth. Buoyancy and fluid convection in the liquid metal in the weld, caused by locally different densities, are diminished in space. These factors disappearing causes surface tension to be the most prominent factor in fluid behaviour in space. The effects of surface tension are enhanced in comparison to weld behaviour on Earth. Arguably, the most challenging aspect of experimentally proving the functionality of applying DED in space is to simulate a microgravity environment. On Earth it is not possible to create a microgravity environment for a prolonged period of time. Parabolic flights and drop towers are mostly used to experimentally verify a project's functionality in microgravity. This allows experiments to be performed seconds to minutes in microgravity. Evidently, the functionality of DED in a microgravity needs to be thoroughly investigated through simulations first. This is a much cheaper option than experimental testing.

The functionality of 3D printers in microgravity has already been proven through multiple missions, both on Earth and in space. The ISS is currently equipped with a polymer FDM printer, manufactured by Made In Space, that is used by NASA and also commercially available [64]. This is called the Additive Manufacturing Facility. Prior to that, the 3D Printing in Zero-G Technology Demonstration proved that additive manufacturing in space is possible [65]. This did not require significant hardware changes compared to hardware designed for use on Earth. Metal additive manufacturing has not been demonstrated in space yet. The fact the additive manufacturing was proven to be possible in microgravity for polymers, it can be expected that metal additive manufacturing is also possible. More research and a flight demonstration are required to achieve the readiness level needed to make the proposed application in this thesis realistic. There are multiple projects ongoing on this topic, such as VULCAN by Made In Space [66]. For more information on this and other relevant projects, the reader is referred to the literature study on in-space manufacturing [1].

4.1.2 Vacuum

The vacuum in space actually has a lot of benefits for metal additive manufacturing. The specific DED method that was chosen, GMAW WAAM, requires a shielding gas for applications on Earth. Oxygen in the air causes the metal to oxidize at the high temperatures in the weld. Additionally, the shielding gas protects the substrate from contaminating particles that negatively impact the weld quality. The same problems extend to all other wire-based DED processes. WEAM is actually always performed in a vacuum.
A shielding gas or an enclosed vacuum environment are not required for an application in space. In the space environment these issues do not exist, because there is practically no oxygen and contaminating particles. In that regard, the space environment is ideal for metal additive manufacturing.

Vacuum does have an effect on the behaviour of the weld pool in DED. The surface tension of aluminium has a dependency on the environment it is in. A polluted or oxidized aluminium surface, which occurs in an atmospheric environment, has a significantly lower value for surface tension than for perfectly clean aluminium in a high vacuum environment [67]. Melting temperature is, although merely to some degree, dependent on the pressure as well. Exact numbers for the correlation between atmospheric pressure and melting temperature for aluminium could not be found in the literature.
Another effect that is relevant is evaporation aluminium in the welding process. GMAW is normally performed with a shielding gas, so in a pressurized environment. Metal evaporation is already a factor that needs to be accounted for in accurate models. At the low pressure in space, it can be expected that the effect of metal evaporation in the welding process becomes more prominent.

All of these properties that change in the vacuum environment in space need to be well understood to make metal AM in space possible. Welding in space has been researched extensively in the early stages of space travel. Welding has been proven to work in space through numerous successful missions. More information on welding in space can be found in the literature study on in-space manufacturing [1]. Considering that welding in space has been proven to be successful, there is no reason to think that DED in space cannot. The principle workings of these two methods are the same. The biggest differences between welding and metal AM in space are that there can be no human intervention and that errors add up in AM as the number of layers increase. Therefore, the behaviour of GMAW WAAM in a vacuum must be researched to a great extent.

4.1.3 Thermal fluctuations

The both high and low temperatures that are experienced by objects in space can have a serious effect. Materials expand and shrink during their cycles of being exposed to the Sun and being in the shadow of Earth. Also, the materials simply need to be able to deal with a high temperature and low temperature. However, this is not a new problem and plenty of suitable materials and solutions have been found to deal with the thermal fluctuations. What is new, is the effect of this on additive manufacturing. There are moments where the spacecraft is exposed to solar radiation and moments where there is barely any incoming radiation. In the first place, this can have negative effects on the DED machine. Components in the machine will expand and shrink and the machine still needs to be able to operate. In the second place, the 3D printed object is at times locally exposed to solar radiation and at times not. Both the fact that the irradiation on the object is nonuniform, as well as the fact that the object experiences different temperatures during its orbit are highly undesirable. During the printing process, this will cause thermal gradients, which will in turn cause

dimensional errors and residual stresses. The effect of incoming radiation from the Sun and Earth are examined in Section 4.2.3.

Thermal fluctuations also impact the filament that is used for the DED process. A positive aspect is that material preheated by the Sun will require less energy to heat it to its melting point. The downside is that the filament temperature is not constant during orbit. For the AM process to work during the whole orbit, it needs to have adaptive printing parameters, based on temperature. If the filament has a difference in temperature over one orbit, the printing quality would not be consistent if constant DED parameters are used. That is because the deposited material would be hotter if the filament is preheated by the Sun.
A preventive strategy is to equip the spacecraft with a sunshield. Blocking the incoming radiation will mitigate the magnitude of the thermal fluctuations. The downside to this is that a sunshield adds complexity and mass to the spacecraft. Nevertheless, based on the serious difficulties that are expected to make the system adaptive based on temperature, it is expected that finding a solution to perform the printing process out of direct exposure to radiation is inevitable.

4.2 Thermal modelling

Space is a high vacuum environment. Therefore, practically no thermal convection is experienced. On Earth convection is a significant element of heat dissipation. Taking that element away in space will have consequences to the way the molten material cools down. During the DED process, a lot of heat is generated. Most of this heat must dissipate before the structure is functional. More importantly, enough heat must have dissipated in the deposited material before the next layer can be deposited. If this does not happen, more heat will be put into the subject than is being dissipated, which will result in structural failure. As the subject remains soft at high temperatures, it may warp which will make the DED process fail to deposit the next layer in the right location. Also, cooling down a soft structure, if the manufacturing process has not failed yet, will not be geometrically accurate to the intended shape due to thermal strains that will be experienced in the cooling down phase. For those reasons it is clear that thermal control is highly important for the DED process. Especially in space, considering the challenging environment.
Currently, there is a complete lack of experimental data of how DED would perform in a microgravity vacuum environment. To learn more about how thermal behaviour will impact the manufacturing process and what aspects are important to thermal control, a thermal model is made to simulate the input and output of thermal energy in the DED subject. This will also give understanding about the limits to deposition rate regarding the thermal behaviour of DED in space. Insight is gained in the limitations of printing speed based on thermal behaviour. This can be used to determine what factor limits the speed of manufacturing structures, as other aspects to the system can also be the limiting factor, like mechanical or power limitations.

In the model, a simple case is described. There is no defined structural geometry at this stage of the project. The ideal geometry will be explored at a later stage of the in-space manufacturing project. A common type of structure for large light-weight applications is a tube system design where tubes are assembled into an assembly often forming triangles. See Figure 27 for an example of what this looks like. A crane is an example that uses a similar design, but this geometry was also found in many of the in-space manufacturing projects that were explored during the literature study [1]. For example, SpiderFab [24] and Archinaut One (OSAM-2) [68]. A simple round tube is chosen as the shape that is printed in the model. Figure 27 displays this shape for clarification. It is an ideal shape to print using DED, because a constant printing speed can be applied and the printhead never has to stop. Also, the more complex shapes, like trusses, can be achieved in the future by combining tube sections. Therefore, the round tube is a relevant geometry for the simulation, of which the data may be able to be used in future research.

Figure 27: Simple truss shape (left) and round tube shape (right)

4.2.1 Simulation software

Abaqus FEA [69] [70] is chosen as the simulation software to do additive manufacturing simulations in for this project. The additive manufacturing department at NLR had experience with AM simulations in Abaqus. Abaqus is a finite element analysis (FEA) tool capable of various engineering simulations, including static and dynamic mechanical strength, thermal, acoustic and piezoelectric simulations, as well as coupled simulations. There are a lot of possibilities in different material applications and defining material properties. Abaqus is a well-known software tool in the aerospace, industrial and automotive branches. Although there are no additive manufacturing capabilities in the software as installed, a plugin is available that enables AM simulations. This plugin, called AMModeler, is made available by the owner of Abaqus, Dassault Systèmes [71]. The plugin provides additional capabilities, based on Python scripts, to make it easier to simulate time-dependent material placement and a laser source.

The model geometry is created using the Abaqus graphical user interface (GUI). Basic model settings are selected as well. Afterwards, this information is written to a file with code, a .inp file. The rest of creating the model is done by adding and adjusting code in this so-called input file. The Abaqus code for the final model can be found in Appendix A. To use the AM plugin, additional input files are required for the deposition path. These were made using Matlab [72]. The code that was written to generate the path information can be found in Appendix B.

The additive manufacturing plugin caused a lot of difficulties at the start. This plugin is quite unknown and the source is difficult to find. There is hardly any tutorials or documentation available of how to work with this plugin. The only information accessible online is concise or hard to understand explanations for coding functions [73] [74]. Two employees at NLR, Jos Vroom and Tim Koenis, were able to answer questions and help to get the model started.

4.2.2 Basic model

The aim for this model is to set up a usable thermal model, with some simplifications, to gain the skills and learn about the influence of parameters to later make an advanced model. In the basic model a variety of parameters have been set. Starting with the geometry, a tube was chosen with an outer diameter of $100\ mm$. The thickness is $2\ mm$. Given that the average thickness for DED is $1-3\ mm$, as mentioned in Section 2.3.2 (Table 2), and the fact that no large forces are expected on the structure, these sizes were chosen. A single-pass structure is assumed to be best in this case. Multiple layers to make the tube thicker would complicate the printing process and it is not expected that more thickness is required.
The additive manufacturing happens on a print base structure, which is a tube section with the same diameter and thickness. A length of $200\ mm$ was chosen for this base tube section, which should be large enough to clamp in the roller system, yet no bigger than needed. On top of this base tube, an AM tube of $1\ m$ is printed, resulting in a $1.2\ m$ tube in total. The shape of the deposited material is simplified. The cross-section of one layer is rectangular and does not have rounded edged, which occur in practice. The end-result is a perfectly shaped tube without imperfections in its surface. As for additive manufacturing parameters, a layer height of $1.5\ mm$ was chosen. This is common for wire-based DED, see Figure 28 [13] [75]. The printhead is estimated to take three seconds to print one layer.

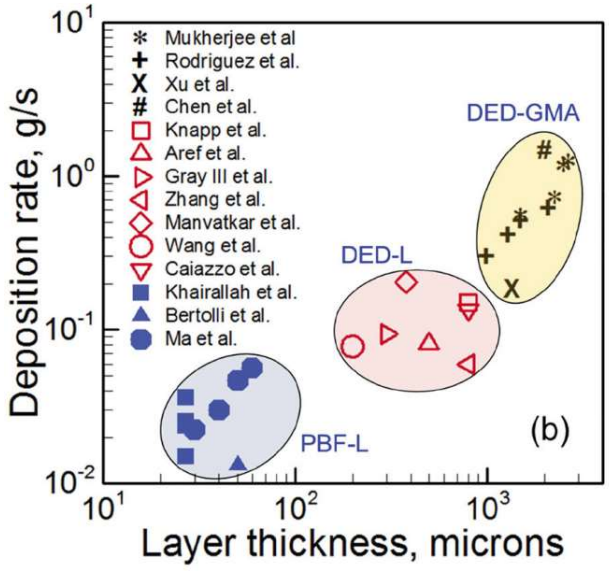

Figure 28: Datapoints on deposition rate and layer thickness for different AM processes [75]

The material that was chosen for this model is aluminium 7075. Aluminium is a common metal for space applications, as well as a common material that is used for DED manufacturing of parts. The material properties required for this simulation are the specific heat capacity, density and thermal conductivity. These are $960\ J/(kg * K)$, $2810\ kg/m^3$ and $130\ W/(m * K)$, respectively [76]. The emissivity coefficient is assumed to be 0.25 and radiates into space with a temperature of -270℃. For this basic model it is assumed that there are no other radiating sources surrounding the object, so for example effect of the sun are not included.

The heat input is for this model done by depositing hot material. No simulation of a laser or other heat sources are done here. Neither are other effects considered, such as the possibility of evaporating material. The chosen material has a melting temperature range of 477℃ to 635℃. A temperature for the deposited material was set at 600℃. This model considers a case where the structure is printed in the shadow with no incoming heat, as this is the simples to simulate. Therefore, the initial temperature for the base tube section is set at -50℃. This is based on the minimal temperature that was experienced during the on-orbit validation experiment for ROSA [27], which was -46℃.

Next up are the model related parameters. To do a FEA, the part must be meshed into small elements. As advised by the simulation experts at NLR, the part was seeded to create element sizes that are half the size of the smallest details. This is because if a larger size is chosen, accuracy is too low to obtain meaningful results. A smaller size will result in more unwanted processing time without gaining much more accuracy in the model. The smallest details in this part are the layer height and tube thickness.
One layer is divided into a circle of 100 elements and is two elements thick, so 200 elements in total per layer. The element height is chosen as half the layer height, which is $0.75\ mm$. Figure 29 displays the part divided into elements. The total time to print is 2000 seconds. This is determined by the time per layer and length of the printed part. After the print time, 500 more seconds are added to the simulation to be able to analyse the cooldown behaviour.

After the shape and mesh have been created in Abaqus, more settings have to be set and lines of code have to be added to the file to enable additive manufacturing. In Abaqus, the material properties are inserted, an assembly is generated, a step is made and initial temperatures and loads are set. The step defines the length of the simulation and how many increments are done in this time period. More increments creates more accuracy and detail in the model,

but this requires more processing time. Most of these parameters can also be adjusted in the input file that is generated from the model. This input file requires some sections of code for the enabling of additive manufacturing and its parameters. The AM plugin has no interface from which everything can be adjusted. In this code parameters are inserted, such as selection of AM part, bead size, material path file, radiation for AM part and more. The non-geometric code of the input file can be found in Appendix A.

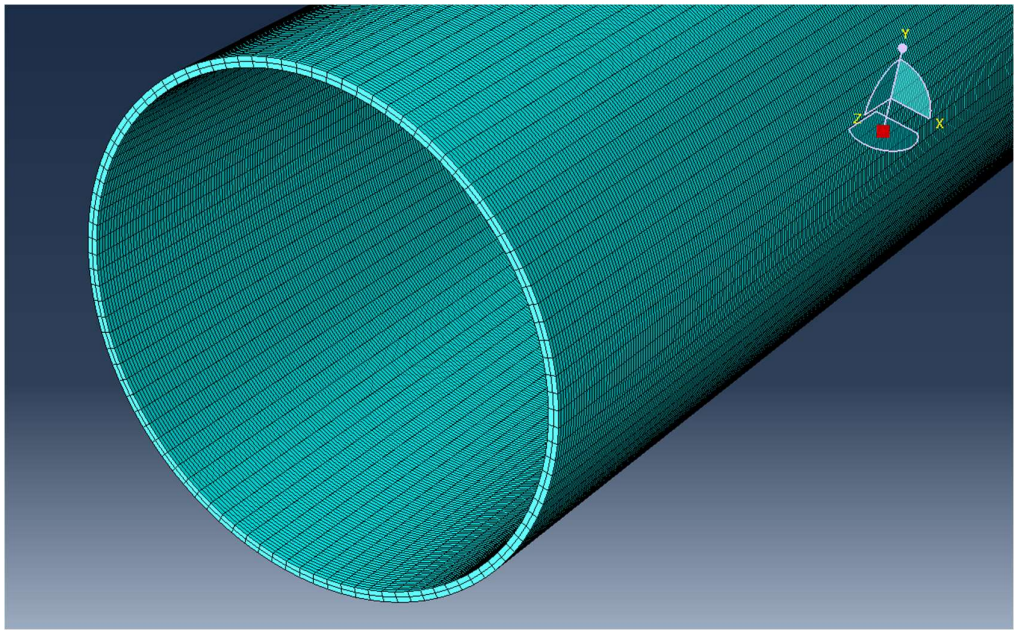

Figure 29: Meshed part for the basic model

Visual results of the simulation after 12 hours of computing time are shown in Figure 30. Each figure shows a moment of the printing process at a different time. A timestep can be found in the orange text in the top right corner of each figure, named 'Total time', which is in seconds. The different colours of the tube relate to the temperature in that area. A legend that relates the colours to temperatures can be found on the left in each figure.
Figure 31 demonstrates the heat patterns that are generated by the additive manufacturing. The three images are each one step apart, which translates into two seconds. It can be seen that the hottest part, in dark orange, moves over the circle. This is the printhead going around the tube, depositing hot material.

The results of the basic model show the functionality of this model. The foundation of the basic model is used for the simulations performed in the next section: 4.2.3 Weight of thermal properties. This model is kept simple to be able to perform many simulations with alterations in material properties, to reduce computing time. Also, the basic model is used as the basis for the advanced model in Section 4.2.4, where improvements are made.

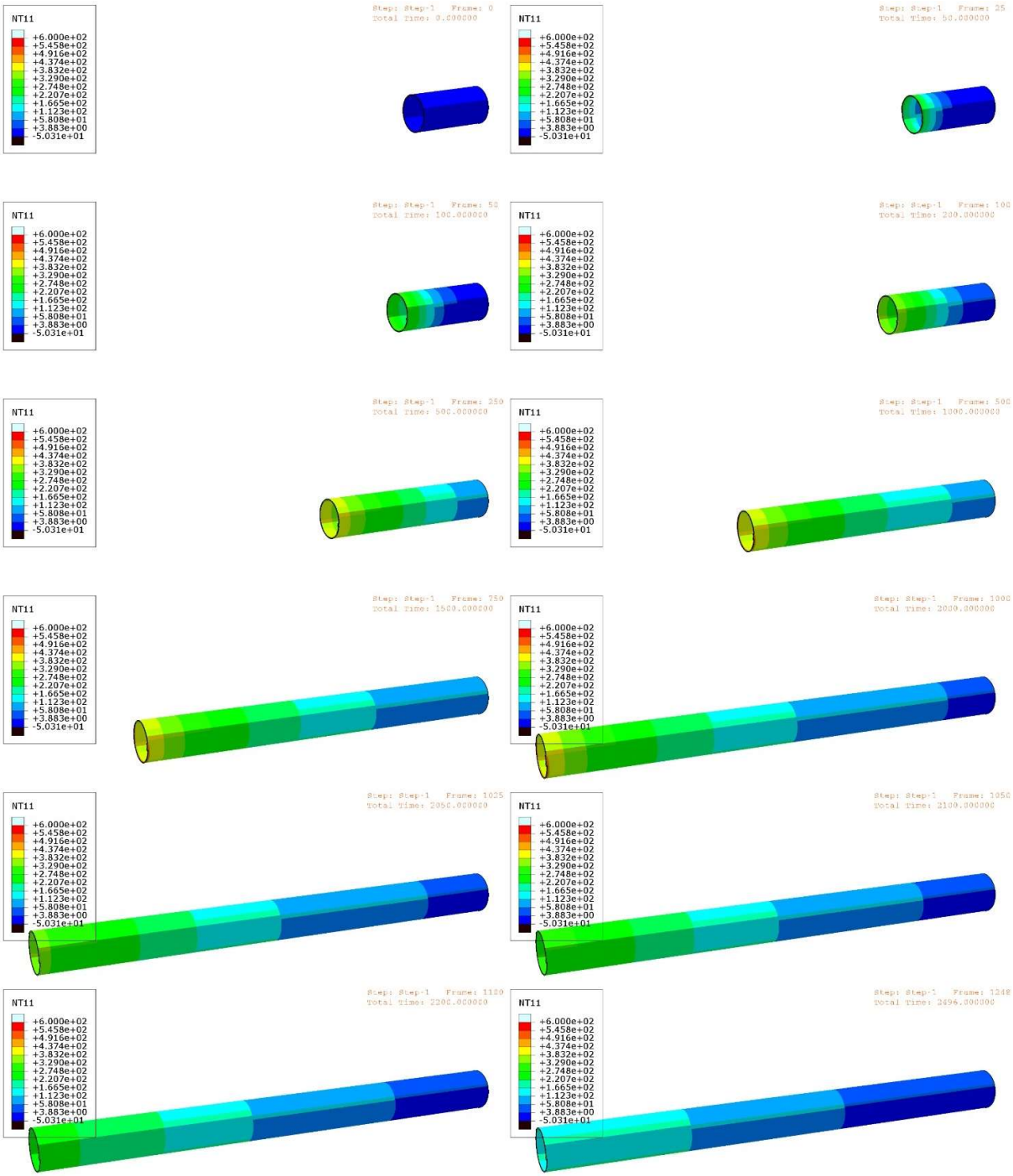

Figure 30: Various timesteps of the basic thermal simulation (see top right corner)

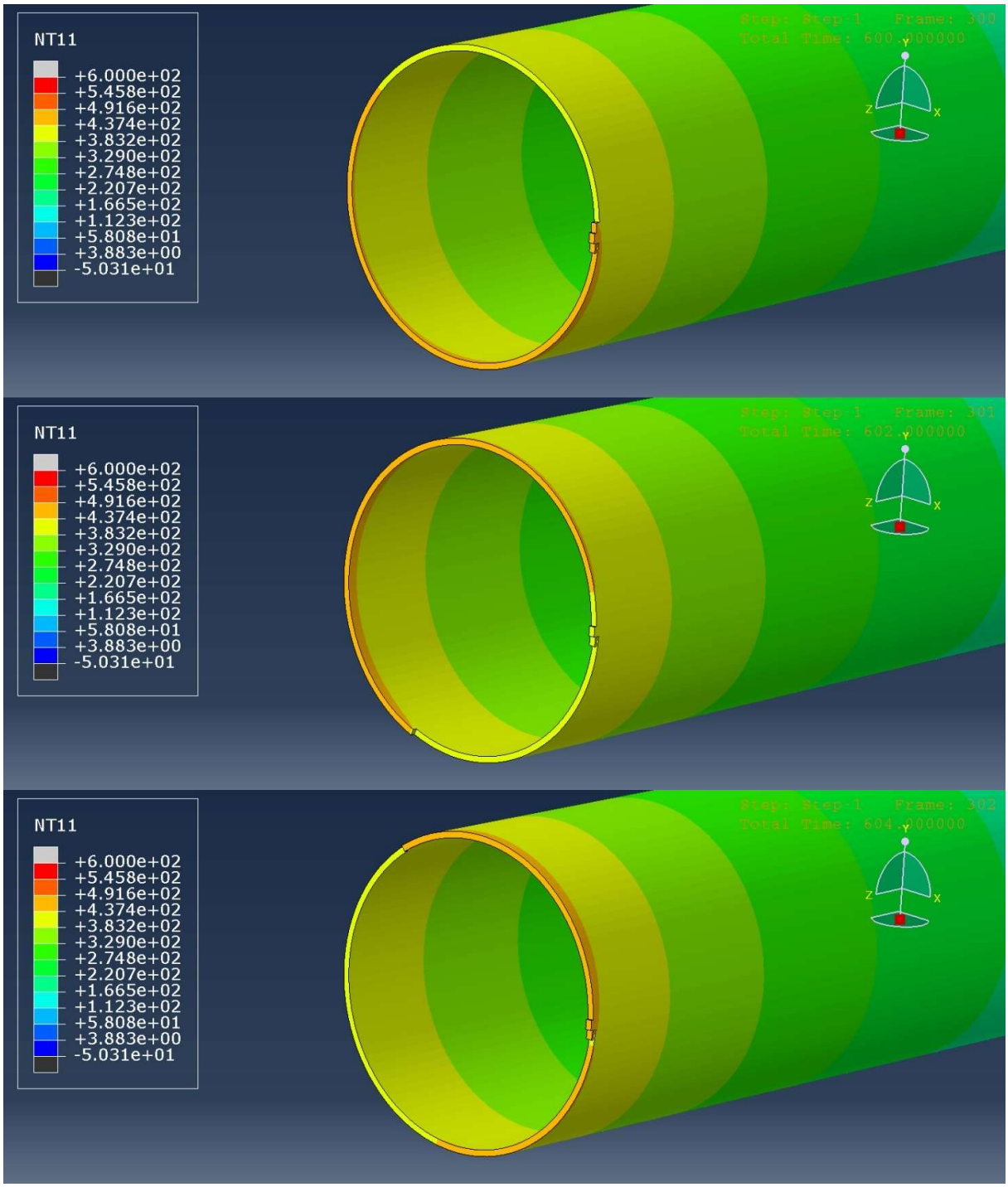

Figure 31: Close-up showcasing the heat input of the newly deposited hot material

4.2.3 Weight of thermal properties

The simulated process is used to get a better feeling for the relative weight between the thermal properties of the material. Simulations are performed based on the Basic Model from Section 4.2.2. Many simulations are done, each with one material property value changed from the initial conditions. Doing this over a range of values for each material property individually, the effects of the material property on the thermal behaviour is found.
One thing was changed from the Basic Model, which is the length of the part. The base tube was shortened to $0.1\ m$ and the printed tube was shortened to $0.1\ m$ as well. This was required to significantly reduce processing time of the simulation and to be able to perform several simulations.
The two metrics that are used to measure the significance of the thermal properties are volume weighted average temperature (VWAT) and the thermal gradient. The former is basically the average temperature of the complete part: base and printed tube. Abaqus contains a function that calculates this using the size and temperature of each element. This is demonstrated in Figure 32. The thermal gradient must also be looked at. Average temperature says something about the total part, but local hot-spots are just as bad in additive manufacturing. It was chosen to measure the thermal gradient at the moment when the print has finished, between two nodes at the top end of the part $15\ mm$ apart. In this end region of the tube, the biggest thermal gradient is experienced. This is done by finding the temperature difference of the two chosen nodes.

The thermal parameters that are evaluated are:

- Emissivity
- Thermal conductivity
- Specific heat capacity

Two values for the material properties are chosen that are located near the ends of the spectrum in possible values, considering the remaining materials in the selection pool. Property values are taken from the database of GRANTA EduPack. Additionally, two values between these outer values are chosen and simulated to find out of the relation is non-linear.
For thermal conductivity, the materials with extreme values are silver and titanium alloys. Titanium can reach a thermal conductivity as low as $5\ (W/(m*K))$ and silver as high as $420\ (W/(m*K))$.
Specific heat capacity has gold at the low end of the spectrum, with around $120\ (J/(kg*K))$, and magnesium on the high end, with $1100\ (J/(kg*K))$.
There is no data available in GRANTA EduPack for emissivity. Emissivity is greatly dependent on a number of variables, including the surface finish, process parameters, manufacturing environment etc. In space no post-processing treatment will be applied, so the surface will be as-manufactured. The whole range from 0 to 1 is simulated to find the impact for a wide range of materials. For example, The Engineering Toolbox lists an emissivity of 0.07 for rough aluminium, 0.79 for oxidized steel, 0.19 for polished titanium and 0.90 - 0.97 for plastics [57].

The results are summarized in Table 12, Figure 33 and Figure 34. Figure 35, Figure 36 and Figure 37 showcase the overall part temperature map for high and low values of each material property. It was found that for specific heat capacity and thermal conductivity relate to the average part temperature exponentially. This mean that as the property value gets higher, lesser effect is experienced on the part temperature. Part temperature behaves relatively linearly to change in emissivity.
Specific heat capacity and emissivity show a linear relation to the thermal gradient, but with a small effect. Thermal conductivity however shows an extreme effect on the thermal gradient, which behaves exponentially.

In conclusion, thermal conductivity has a massive impact on the thermal gradient and materials with low values must be avoided. Even though the average part temperature is lower for low-conductivity materials, this has no benefit if the print still fails due to local warping. Specific heat capacity must be minimized and emissivity must be maximized.

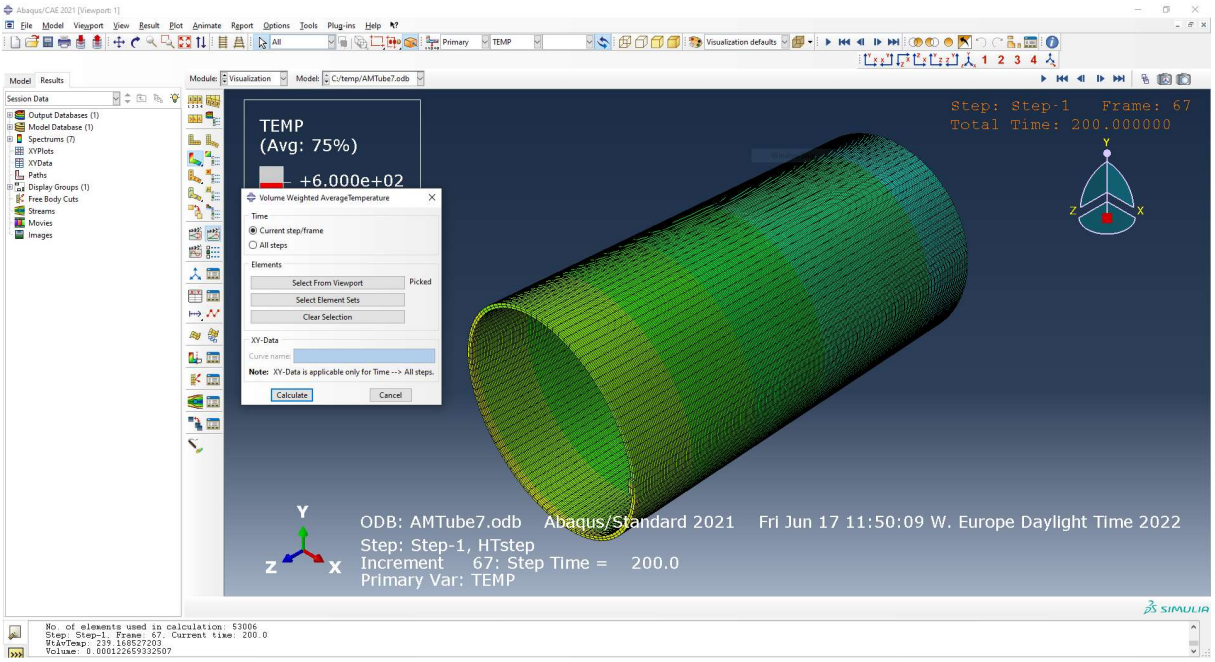

Figure 32: Calculating the volume weighted average temperature in Abaqus

Table 12: Thermal property values for thermal simulations to find relative weight

Property	**Value type**	**Value**	**Volume weighted average temperature (°C)**	**Thermal gradient 0-15mm from end (°C)**
Base model			**238.2**	**15**
Emissivity (-)	Low value	0	275.2	13
	Intermediate value 1	.33	228.7	15
	Intermediate value 2	.66	196.6	16
	High value	1	171.8	18
Thermal conductivity $(W/(m*K))$	Low value	5	200.8	56
	Intermediate value 1	150	239.2	13
	Intermediate value 2	300	241.8	7
	High value	420	242.4	5
Specific heat capacity $(J/(kg*K))$	Low value	120	135.6	2
	Intermediate value 1	450	213.1	8
	Intermediate value 2	780	232.7	12
	High value	1100	241.4	16

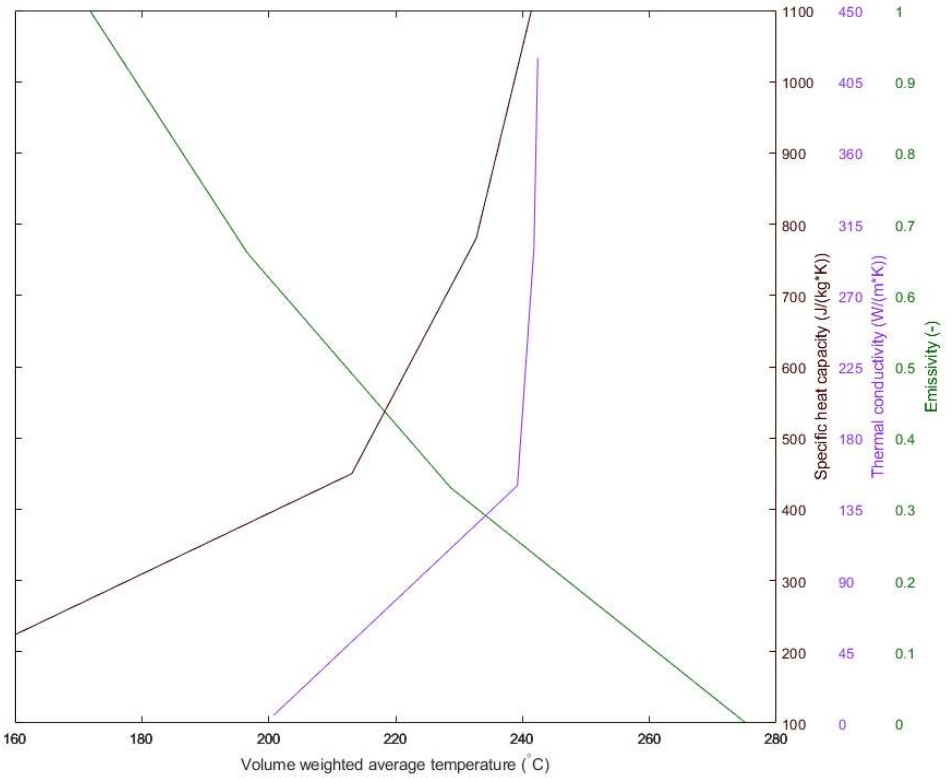

Figure 33: Plot for thermal property impact on volume weighted average temperature

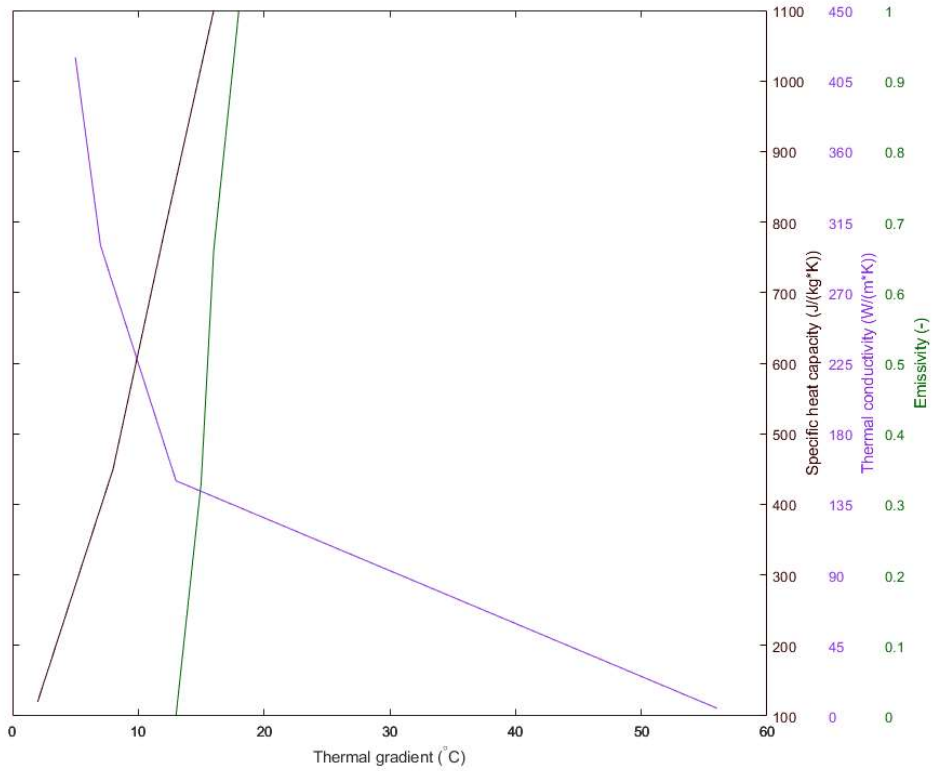

Figure 34: Plot for thermal property impact on temperature gradient between 0 and 15 mm from part edge at end of printing

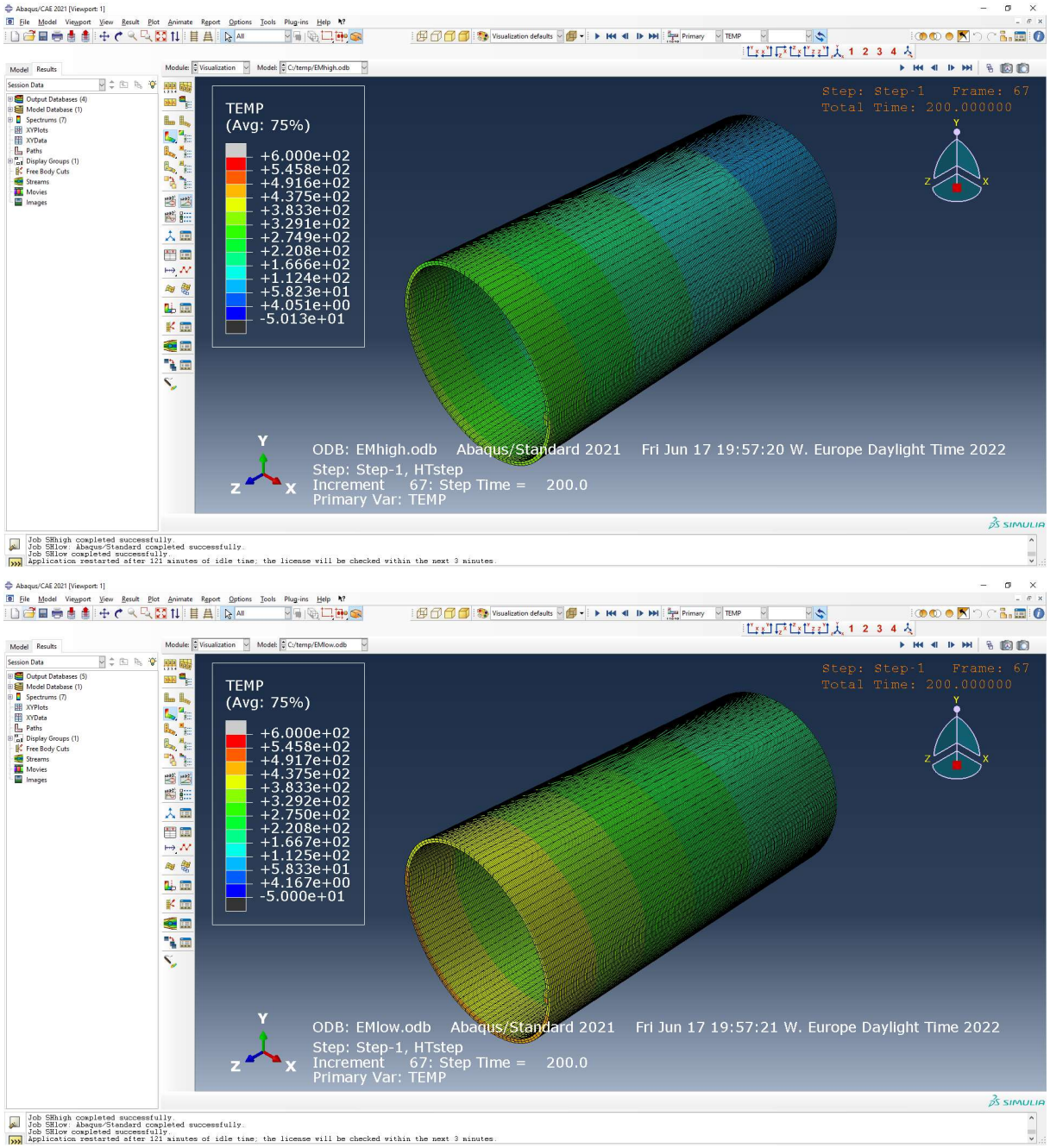

Figure 35: Thermal model with high (top) versus low (bottom) emissivity

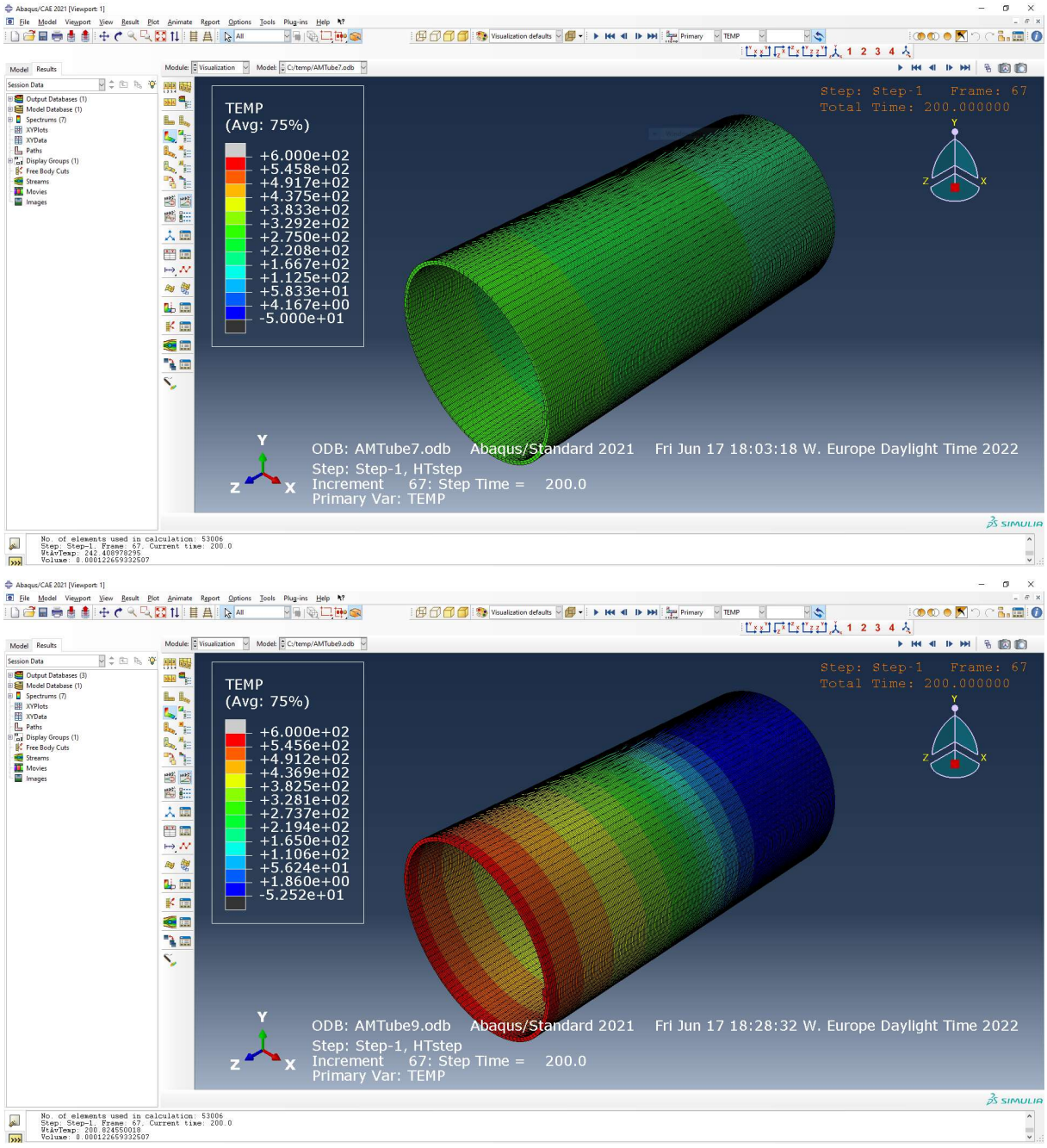

Figure 36: Thermal model with high (top) versus low (bottom) thermal conductivity

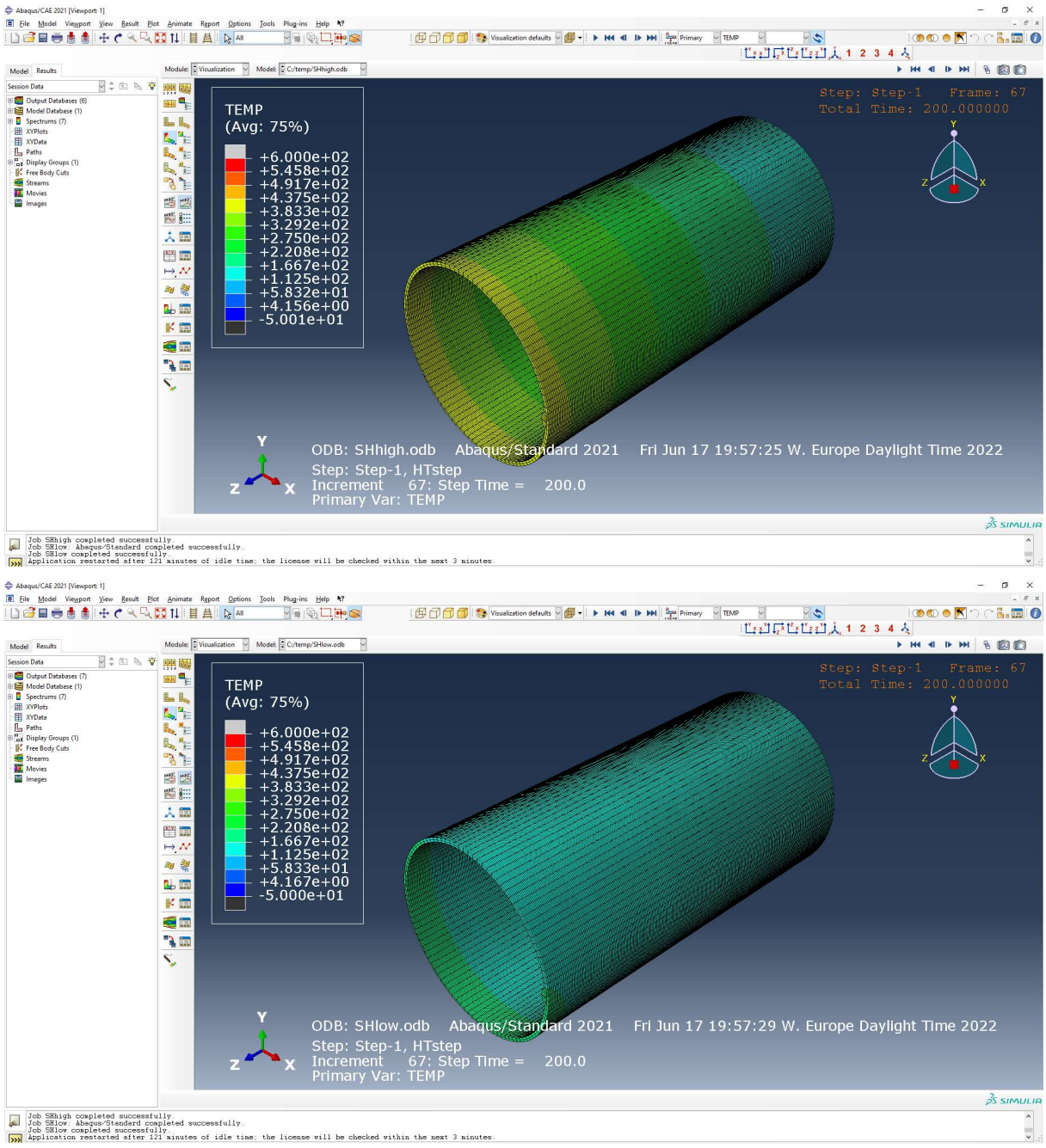

Figure 37: Thermal model with high (top) versus low (bottom) specific heat capacity

4.2.4 Advanced model

The advanced model builds upon the basic model to create a more accurate model. Whereas the basic model was created to obtain information and experience from a simplified, but working model, the aim for the advanced model is to create a more detailed model. In addition, the advanced model simulates a worst case scenario. The most important factor to the worst case of the incoming radiation from other celestial bodies. Firstly, in a process where heat input is already a limiting factor to the success of the production process, adding even more heat is highly undesirable. But the question is how big the impact is of this added heat. Secondly, incoming radiation from a heat source far away is not distributed uniformly over the surface of the object. Certain parts of the surface receive more radiation than others, which results in a thermal gradient. It must be investigated how big this thermal gradient is and if this results in problems for the manufacturing process.
More improvements are made to the model. The best material for applying DED in space for structures was found in Section 3.2. The material properties of this material are applied to the advanced model. The effects of latent heat of fusion is added to the thermal model. For a worst case scenario, the initial temperature of the material is higher. With the best heat source for DED that was found in Section 2.3.3 a better estimate of the temperature of the deposited material can be made. All these changes will result in a model that is truer to the real world and more useful to base conclusions about applicability of the proposed system on.

Temperature of deposition material for GMAW DED

The temperature of the deposited material is not exactly the melting temperature. This was the simplified assumption made for the basic model. The literature shows that the temperatures in the weld pool are significantly higher than the melting temperature. This is required to obtain a good quality weld. Without sufficient temperature, the added material would not mix with the existing layer well enough. Microstructure of the metal is also impacted by the temperatures. However, this topic exceeds the scope of this research.
Unfortunately, it is not possible to simulate an arc as the heat source in the Abaqus AM simulation. The temperature of the deposited material is dependent on many parameters, such as the arc waveform, current, frequency, material feed rate, travel speed of the printhead and more [77]. For the purpose of the simulation, an assumption will have to be made for the temperature of the deposition material.

Murphy [78] did a computational study on the weld pool for GMAW of aluminium, the same method and material as was chosen in this research. In the study by Murphy a numerical model was made to determine the temperatures and flow velocities in the weld pool area, including metal vapour which is often neglected in models. This was done for aluminium 5754. Although not exactly the same material, thermal properties are closely similar. For example, the melting temperatures are $600℃$ and $605℃$ for aluminium 5754 and 6005A, respectively, according to Thyssenkrupp [79] [80]. So, it is assumed that the findings for this material apply for aluminium 6005A as well.
Arc current, welding velocity, droplet frequency and more parameters specific to this model impact the temperatures. It is assumed that the temperature distribution in this case is one that represents nominal behaviour for GMAW. Therefore, the parameters are not particularly relevant anymore, because another environment with other parameters can produce a similar temperature profile. Even in space.

One of the results of the study is presented in Figure 38. This figure shows the temperature profile and flow velocity of the weld pool. Detailed parameters for this case can be found in the source [78]. The part that is most interesting for the Abaqus AM thermal model is the temperature of the deposited material. This is the area between $28.5\ mm$ and $30\ mm$ in the z-direction and $-2\ mm$ and $2\ mm$ in the y-direction. In lack numerical data, a conclusion is draw based

on visual inspection of this figure. This area averages at around $2000\ K$, which is $1726.85℃$. This is a big change from the melting temperature used in the basic model of $600℃$. This increased value for the deposition material temperature is used in the advanced model.

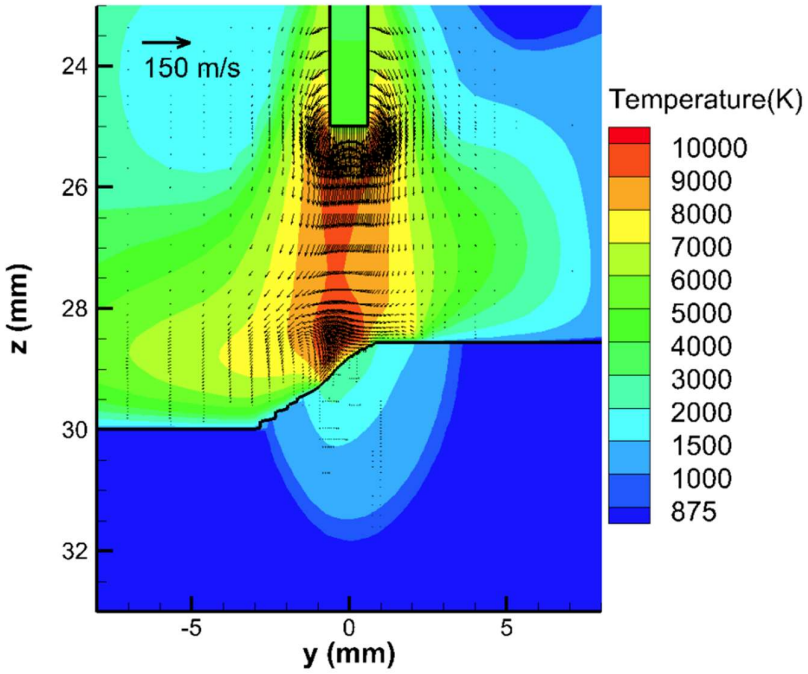

Figure 38: Computational model of the weld pool of aluminium GMAW: Temperature distribution and flow velocity vectors [78]

Improved material properties

The material properties can be used for the material that was found the best material for this application (Section 3.2). These are listed in Table 13. The material properties for this material that were found in GRANTA EduPack were listed as ranges, but Abaqus requires a single value. The average property value is taken. The solidus and liquidus temperature, required for implementation of latent heat, were taken from Apac's specifications of aluminium 6005A T5 [81]. In this model the effects of latent heat are included. In Abaqus this is a simple task of including the property values required for latent heat in the material properties assigned to the object.

Table 13: Material properties of aluminium 6005A T5 used for advanced Abaqus model

Property	**Value**
Density ρ (kg/m^3)	2705
Thermal conductivity κ $(W/(m*K))$	193
Specific heat capacity c_p $(J/(kg*K))$	892
Specific latent heat of fusion L_f (J/kg)	388500
Solidus temperature (℃)	607
Liquidus temperature (℃)	654

The property values in Table 13 are for room temperature ($22℃$). Thermal conductivity and specific heat capacity are actually significantly dependent on temperature of the material. Unfortunately, no temperature dependent data could be found for aluminium 6005A T5. Therefore, an estimate is made based on a similar alloy. GRANTA EduPack does have temperature dependent data for aluminium 6061 T6, an alloy of the same aluminium series. Both materials predominantly consist of aluminium with magnesium and silicon as alloying elements. Differences lay in the use of additional alloying elements in small fractions, in the order of $0.1 - 1\ Wt\%$. Since these materials are very similar, it is expected that the curve of specific heat capacity and thermal conductivity versus temperature is very similar as well. Their values at room temperature are not the same, however. Therefore, the data is scaled with a factor of $\frac{\kappa_{Al6005@22℃}}{\kappa_{Al6061@22℃}}$ for the thermal conductivity and $\frac{c_{p_{Al6005@22℃}}}{c_{p_{Al6061@22℃}}}$ for the specific heat capacity. The results of the estimation for temperature dependent thermal properties for aluminium 6005A T5 can be found in Figure 39. The Matlab script used to calculate the temperature dependent data can be found in Appendix C.

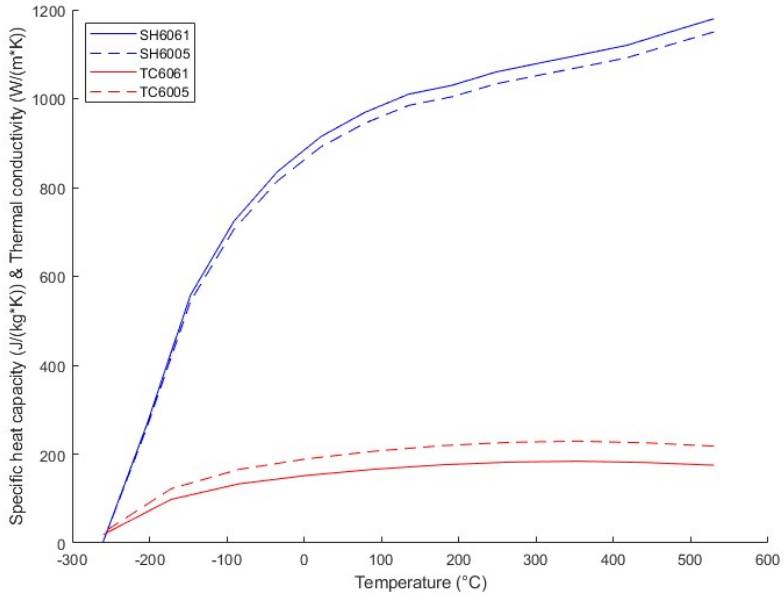

Figure 39: Plot of specific heat capacity (blue) and thermal conductivity (orange) versus temperature for aluminium 6061 T5 (solid line) and estimated for aluminium 6005A T5 (dashed line)

The data in GRANTA EduPack only goes up to $530℃$. However, temperatures of the liquid aluminium go a high as $2000\ K$, so more data is required. As agreed upon by various sources, the specific heat of aluminium is practically constant in its liquid state [82] [83]. Note that this research concerns elemental aluminium, but due to the lack of temperature dependent information for aluminium 6005A this data is used. Considering that aluminium 6005A is about 99% elemental aluminium, the properties cannot be far off. The values found by researchers are in the range of $1030 - 1180\ J/(kg * K)$. Four out of seven sources find near or exactly $1180\ J/(kg * K)$. Therefore, this value is used for the specific heat of aluminium in liquid state between $654℃$ and $1726.85℃$.
There is still a gap of data for specific heat capacity between $530℃$ and $654℃$. It is assumed that the thermal property values can be linearly interpolated in section.

Thermal conductivity shows a more drastic change when going into the liquid state. Leitner et al. [82] have created a graph that demonstrates the temperature dependence of the thermal conductivity of elemental aluminium using the

Wiedemann-Franz law, as well as comparing it to other studies. See Figure 40. This data is used and adjusted to fit data for aluminium 6005A. This is done by shifting the data on the temperature scale to make the melting temperature overlap with that of aluminium 6005A (903.65 K). This is $29.82\ K$ difference. Also, the thermal conductivity data is shifted with a constant offset to match the end of the GRANTA EduPack data with the beginning of the Leitner et al. data. This data only goes up to $1500℃$. The section after the phase change shows a linear relation, demonstrated by a red fit line. The data is linearly extrapolated to obtain data up to $1800℃$.
The complete profile of the thermal properties that are used in the Abaqus model can be found in Figure 41.

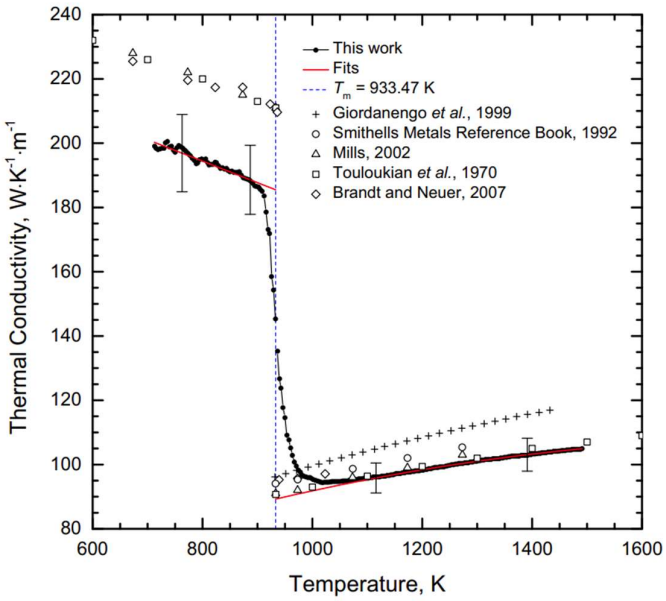

Figure 40: Thermal conductivity of elemental aluminium found by Leitner et al. and other studies

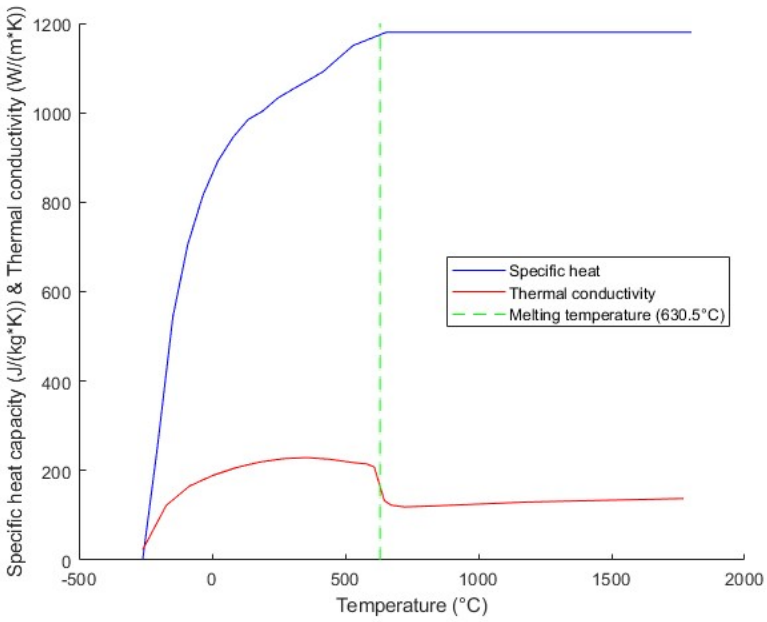

Figure 41: Temperature dependent thermal properties for aluminium 6005A

Evaporation of material and outgassing are more relevant in a space application. The low pressure in space aggravates these two phenomena. Losing mass generally has a significant impact on the thermal state of the subject. However, aluminium has relatively good outgassing properties. It is often used in ultra-high vacuum chambers for that reason. The effects are worse for liquid material, which is only a tiny surface in the melt pool. The temperature of the rest of the object is not high enough to make a big impact. The amount of mass lost due to evaporation and outgassing is small. For these reasons it is assumed that evaporation and outgassing have minimal effect on the thermal behaviour and are therefore ignored in the thermal model.
Nevertheless, outgassing does have some impact, as was demonstrated by Murphy [78]. It may be interesting for future, more accurate thermal models to include this. It is difficult to include this in simulations, because it adds a great deal of computing time. Still, it would be interesting to see the magnitude of the effects, especially in space.

The solidus and liquidus temperatures given in Table 13 are for an ambient environment with $1\ bar$ pressure. The application takes place in an ultra-high vacuum in space, however. The literature provides next to no information on the melting temperature of aluminium for different pressures. In the phase diagram of metals, it is common that the melting temperature is near constant over pressure, up until the triple point. See Figure 42. However, without any information available in the literature on the triple point of aluminium as well, it is assumed that the melting temperature of aluminium is the same in a space environment as in an Earth environment.

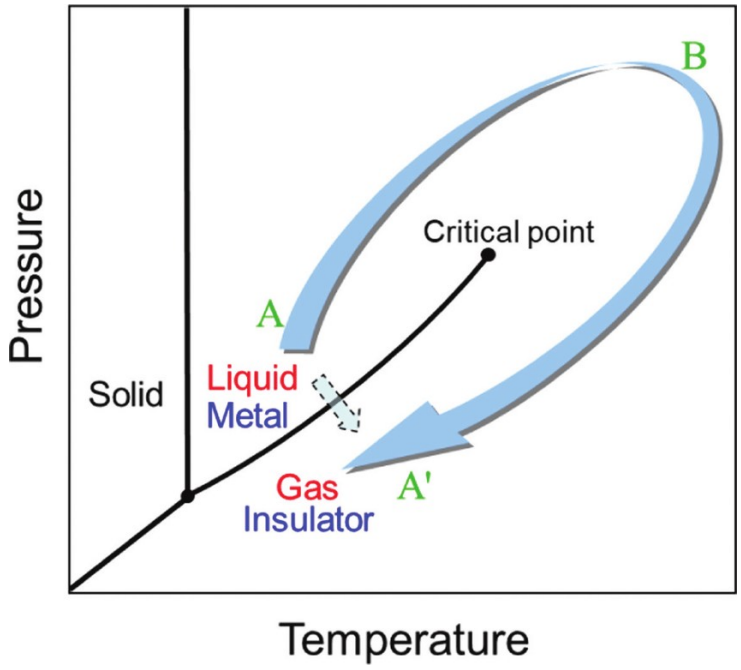

Figure 42: General phase diagram for metals [84]

Worst case

In the advanced model the incoming radiation from the Sun and Earth is included. Figure 43 shows a schematic overview of the different factors of radiation for a spacecraft in an orbit around a planet. These components are: direct solar flux, Earth's albedo and Earth's planetary radiation.
The solar constant describes the mean incoming flux density coming from the sun at one astronomical unit (AU) distance. This is approximately $1366\ W/m^2$ [85]. This amount does vary slightly depending on the relative position of

the Sun and Earth and the solar cycle, but this gives a good number to work with in the model as the variability in the solar irradiance is small. Not all of the incoming flux density is absorbed into the material. The absorptivity of the material must be accounted for. Just like the emissivity, it is difficult to determine an accurate value for this without all factors known. Also, absorptivity is dependent on the wavelength of the radiation, so absorptivity is specific to the sun's radiation in this case. According to Engineering Toolbox [86], the solar absorptivity for processed aluminium parts varies between $0.15 - 0.30$. 3D printed aluminium is rougher and without a post-processing surface finish, thus less reflective. For dark grey surfaces, a solar absorptivity is given of 0.50. This is the highest value that can be expected for aluminium, so considering a worst case is modelled, this is an appropriate factor to work with. Multiplying the absorptivity with the solar constant results in an absorbed solar radiation of $683\ W/m^2$.

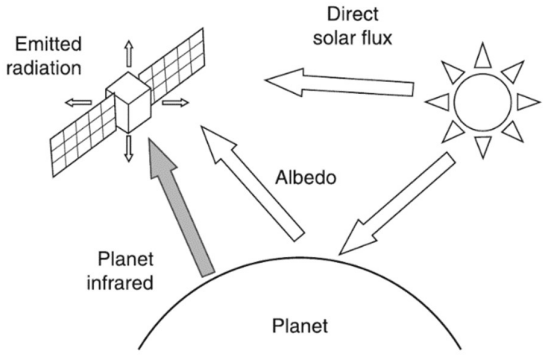

Figure 43: Incoming and outgoing radiation components for a spacecraft in orbit

The Earth also radiates onto the AM tube. This occurs through two different ways: albedo radiation and planetary radiation. Albedo radiation is the radiation from other sources that is reflected by the planet. For planets, the albedo radiation is practically solely the reflected radiation from the Sun. The average planetary albedo of the Earth is 0.30 [87]. This is the fraction of incident radiation that is reflected. The albedo varies for different orbits, because reflectivity can be highly local. For example, ice can have an albedo of up to 0.95. Albedo varies between 0.24 for equatorial orbits and 0.42 for polar orbits. Radiation is always stronger closer to the source. For geostationary orbits (GEO) albedo lows are small enough that they can practically be neglected. The thermal load is higher for LEO, so it needs to be accounted for.

Calculating how big the albedo radiation on the spacecraft is, is a difficult task that is usually done with specialized software tools. Many factors are important, so a lot of data needs to be combined. For estimations, a simplified equation can be used [87]:

$$q_{alb} = a * G_s * A * F_{SC-P} * \cos(\Phi) \qquad \text{for } -\frac{\pi}{2} \leq \Phi \leq \frac{\pi}{2} \tag{26}$$

Where q_{alb} is the albedo radiation (W), a is the planet albedo (-), G_s is the solar constant (W/m^2), A is the projected surface area (m^2), F_{SC-P} is the view factor between the surface and the planet (-) and Φ is the angle (rad) of the spacecraft's orbit around the planet. This angle causes the albedo radiation to be at a maximum at the sub-solar point and goes to zero when the spacecraft is in eclipse. The view factor is dependent on the orbit height. The maximum view factor for a LEO orbit at $300\ km$ is about 0.90 and for a GEO orbit at $35786\ km$ is about 0.023. For detailed calculations, the reader is referred to the paper by Li et al. [88]. Applying the view factors, the average Earth albedo, solar constant and $\Phi = 0$ for the maximum albedo radiation gives the following results:

$$\left(\frac{q_{alb}}{A}\right)_{LEO} = 0.30 * 1366 * 0.90 * \cos(0) = 368.8\, W/m^2$$
$$\left(\frac{q_{alb}}{A}\right)_{GEO} = 0.30 * 1366 * 0.023 * \cos(0) = 9.425\, W/m^2$$

It can be seen that albedo radiation in GEO is indeed very low and is negligible compared to the solar radiation. LEO is a possible orbit for this project. As this model is a worst case scenario, the LEO albedo radiation is used. A simplification that is going to be made is that this worst case remains constant. So, the spacecraft is in LEO permanently in the sub-solar point. This scenario is demonstrated in Figure 44. In reality, the spacecraft orbits the Earth and therefore, the incoming radiation continuously changes. This is particularly relevant for LEO, because at $300\ km$ height the spacecraft orbits the Earth every 1.5 hours. This simplification is done reduce the complication of creating the model, which would otherwise take too much time. In the future it would be recommended to simulate a scenario in an orbit.

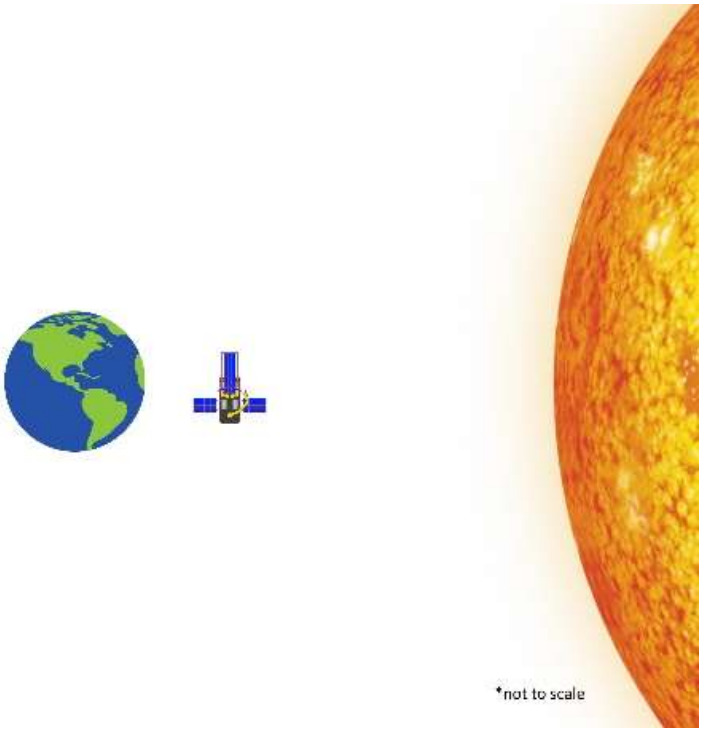

Figure 44: Positional scenario of the spacecraft in the advanced model

The last component is planetary radiation coming from Earth. This is infrared radiation emitted by the planet. Again, the exact amount varies in each location on Earth, because of different materials, population and more. An average is used, based on the assumption of thermal balance. This is not exactly true, but provides a good estimate. In this case, the absorbed solar radiation is equal to the blackbody equivalent temperature radiation.

$$G_s * \pi * r_p^2 * (1 - a) = 4 * \pi * r_p^2 * \sigma * T_p^4 \tag{27}$$

Where G_s is the solar constant (W/m^2), r_p is the planet's radius (m), a is the planet albedo (-), σ is the Stefan-Boltzmann constant ($W/\ (m^2 * K^4)$) and T_p^4 is the planet's blackbody equivalent temperature (K). For Earth this results in $T_p = 255\ K$. To calculate the incoming planetary radiation on the spacecraft, the following equation is applied:

$$q_p = \varepsilon * A * F_{SC-P} * \sigma * T_p^4 \tag{28}$$

Where q_p is the planetary radiation received by the spacecraft (W) and ε is the infrared emissivity of the spacecraft (-). In Section 4.2.2 an emissivity of 0.25 was used for aluminium. Using the view factor for LEO and GEO gives the following results:

$$\left(\frac{q_p}{A}\right)_{LEO} = 0.25 * 0.90 * 5.67 * 10^{-8} * 255^4 = 53.9\ W/m^2$$
$$\left(\frac{q_p}{A}\right)_{GEO} = 0.25 * 0.023 * 5.67 * 10^{-8} * 255^4 = 1.38\ W/m^2$$

Again, it can be seen that Earth's radiation is small enough to be neglected in GEO, but not for LEO. The fluxes from albedo radiation and planetary radiation are combined, as their direction is the same. Just like for the solar radiation, the absorptivity needs to be accounted for, because part of this incoming radiation is reflected on the spacecraft. Although wavelengths of the radiation may be different for Earth's radiation than the Sun's radiation, it is assumed that absorptivity is equal to 0.5 for both. In conclusion, the following incoming heat fluxes are absorbed in the spacecraft and are included in the simulation, coming from opposite directions:

$$\frac{q_{sun}}{A} = 683\ W/m^2$$
$$\left(\frac{q_{Eart}}{A}\right)_{LEO} = \left(\left(\frac{q_{alb}}{A}\right)_{LEO} + \left(\frac{q_p}{A}\right)_{LEO}\right) * abs = (368.8 + 53.9) * 0.5 = 211.4\ W/m^2$$

In Abaqus these heat fluxes are applied to the outer surface of the tube. The heat flux is distributed in a way that it is maximum on the surface perpendicular to the direction of the source, and zero on the surface that is parallel to the direction of the source and surface that is not visible to the source (the backside). The heat flux scales over the tube's surface with $\frac{q_x}{A} * \cos\left(atan\left(\frac{Y}{X}\right)\right)$. See Figure 45 for the result of this and reference axes. This is done for both the Sun's radiation and Earth's radiation, each on opposing sides of the tube.

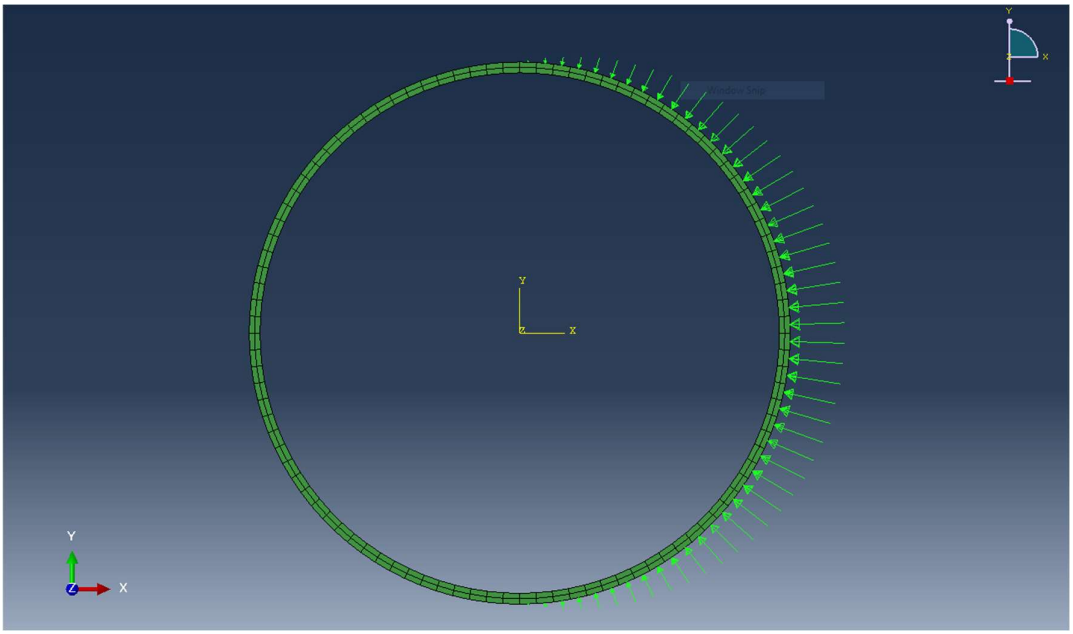

Figure 45: Heat flux magnitude distribution over the AM tube's surface

Another aspect that can change in the worst case scenario is the initial temperature of the base tube. In the basic model this was set at $-50℃$. This was chosen because a scenario was assumed where the spacecraft and its

components had cooled down in the Earth's shadow. If printing would start after the spacecraft has been exposed to the Sun, the base tube would be a higher temperature.
Again, the on-orbit validation of the Roll-Out Solar Array is used for temperature data of what can be expected [27]. The maximum experienced temperature of the deployed booms was $77℃$. Obviously, the exact temperature will be different, because many factors are different. For example, the ROSA boom is black and the aluminium structure is not. Alternatively, a simulation could be made to obtain a value for this specific case. However, some parameters are not exactly known, such as the orbit altitude. It was found in the basic model that the initial temperature of the base tube does not have a massive impact on the result. Within a few decimetres of printing, the structure found itself in an equilibrium state for temperature distribution. This means that the cooling effect of the base tube was no longer in effect.
In conclusion, based on the results found for ROSA an initial temperature for the base tube is set at $80℃$. This is assumed to be a good estimate, possibly on the high end considering the colour differences. This suits the worst case approach for the advanced model.

Printing speed and interpass temperature

A better estimate of the print speed is required for the model. Figure 46 summarizes data from multiple experiments on directed energy deposition. The chosen type of DED in this research is GMAW. In this figure this is named DED-GMA, but this is the same technology. The other types in the figure are laser-based DED and powder bed fusion (PBF). The required power and achievable the scanning speed are presented on a logarithmic scale. Scanning speed is the speed of the laser path or printhead. For DED-GMA it can be seen that the scanning speed ranges between $4\ mm/s$ and $10\ mm/s$. Another reference is the welding velocity used in the computational study on weld pool temperature [78]. Here, the welding velocity was set at $15\ mm/s$. Although the technology is the same, the welding application may require slightly different values than DED.
In the advanced model, $10\ mm/s$ is used as the first estimate. This can be changed later to optimize print speed. the chosen outer diameter of the tube is $100\ mm$. Considering the tube thickness is $2\ mm$ and the printhead moves over the centreline of the tube, the printhead will follow a circular motion with a radius of $49\ mm$. This results in a print time of $30.8\ s$ per layer:

$$p = 2\pi * r = 2\pi * 0.049 = 0.308\ m$$
$$\tau_{la} = \frac{p}{v_{printhead}} = \frac{0.308}{0.01} = 30.8\ s$$

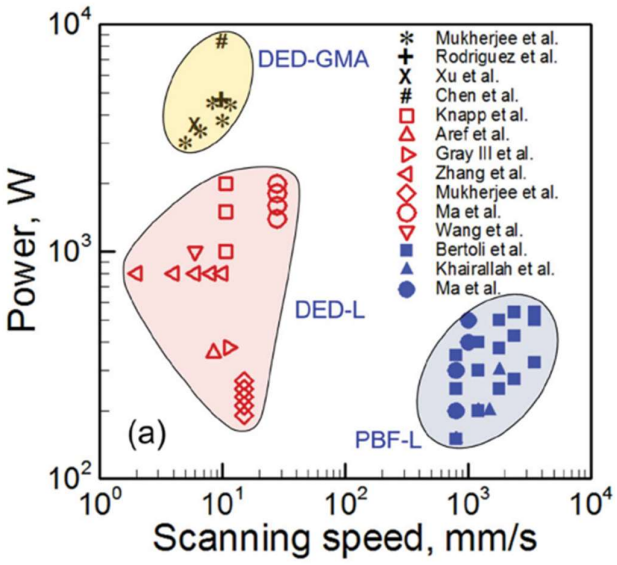

Figure 46: Summary of power usage and scanning speed of various DED processes and experiments [75]

In practice, the print speed is limited by the thermal behaviour of the part. This includes multiple factors: balance between heat input and output, thermal gradients and thermal effects on the material microstructure. For practical use, a parameter is used to indicate how hot the AM part can be in the process and when the part is ready for the next deposition layer. This is the interpass temperature. The interpass temperature is the temperature of the last deposited layer, right before material of the next layer is applied. This parameter is key for getting high quality AM parts, but it is also challenging to optimize since there are so many factors that are influenced by interpass temperature. The interpass temperature should not be too low. The thermal gradients increase as the interpass temperature decreases. However, if the interpass temperature is too high, other problems start to occur, such as inconsistent cross-sectional dimensioning [89]. For aluminium GMAW WAAM, higher interpass temperature samples ($100℃$) showed smaller pore sizes and better strength performance than lower interpass temperature samples ($50℃$) [90]. Geng et al. [89] found that the surface appearance of the DED part kept improving as the interpass temperature increased, up until $150℃$. At that temperature, geometrical accuracy starts to suffer. Spencer et al. [91] found similar results in an experiment where interpass temperature varied between $50℃ - 250℃$. A temperature of $150℃$ showed the best visual appearance out of the test subjects. This is also endorsed by Kozamernik et al. [92] in their study on interpass temperature control.

Based on the findings in the literature, the goal for interpass temperature during the process is set at $150℃$. This can be achieved in three ways: print speed adjustment, delay between layers and forced cooling/heating. During intermediate simulations it was found that the interpass temperature is too high for the conditions previously determined. Also, forced cooling is a complex solution. There are possibilities to connect the tube to a heat sink on the spacecraft, but this is not ideal. It is assumed that the temperature needs to be lowered by adjusting the process parameters. The print speed is lowered from $10\ mm/s$ to $5\ mm/s$, which is the low end of the spectrum for DED. Lowering this parameter further is undesirable and possibly not even possible. Print speed is dependent on the welding current and oscillation. These need to be within a certain range to perform a proper weld. Therefore, lowering the interpass temperature further needs to be done by adding idle time between layer depositions. After a layer has been applied, the printhead needs to stop for a certain time to let the part cool off. After the right temperature has been reached, which can be measured by a sensor, the next layer can be deposited.
In the thermal model, this idle time is added and adjusted by trail-and-error. The goal is to keep the idle time as low as possible, but the interpass temperature should be around $150℃$.

Finding the parameters to achieve the interpass temperature goal

First, the improvements and changes made in the advanced model were applied through intermediate steps. A test model was worked with that contains a smaller tube section of 10 cm base tube and 10 cm AM tube, which runs in a smaller amount of time. This allowed for intermediate checks and bug fixing, needed to confidently implement changes to the model. Additionally, the test model was used to examine what parameters were required to achieve the interpass temperature goal.

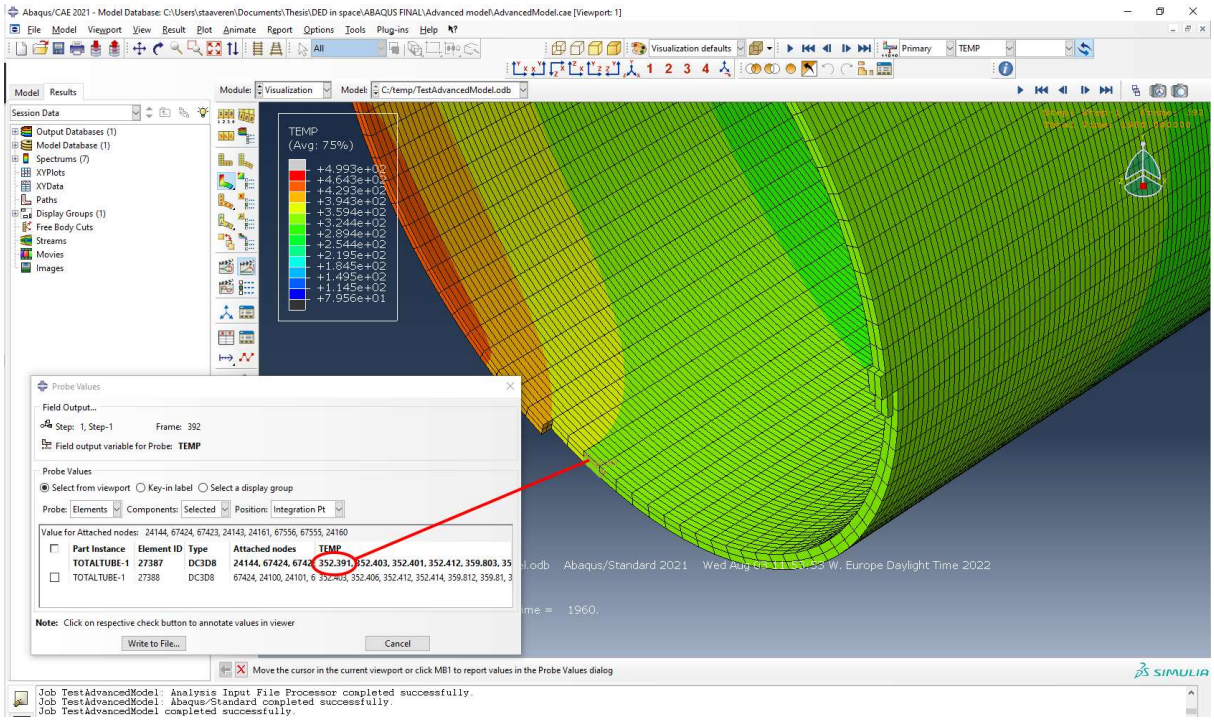

Figure 47: Interpass temperature of the advanced test simulation with initial conditions: 352 °C

The test simulation with the shorter tube is run with the initial parameters (model 1 in Table 14). The results of this simulation can be seen in Figure 47. The parameters used are common for GMAW WAAM on Earth, with the exception of the simulated environment. This results in an interpass temperature of 352℃, which is way higher than what is seen as appropriate in the literature. To lower the interpass temperature, the print speed is lowered from 10 mm/s to 5 mm/s. Additionally, to further lower the interpass temperature, idle time is introduced at the start of the next layer. This gives the part time to cool down before more heat is applied.
The aim is to reach an interpass temperature of 150℃. The idle time is increased in each simulation until this goal has been reached. The results of these simulations can be seen in Figure 48, Figure 49, Figure 50 and Figure 51. It was found that at a print speed of 5 mm/s, an idle time between layers is required of 120 seconds. The time it takes to print one layer at 5 mm/s is 61.6 s. This means that including the required idle time to reach an interpass temperature of 150℃ it takes about three time longer to print.

It must be noted that interpass temperature changes slightly over time when the idle time is kept constant during the print. This is because as the part is printed, the surface area increases and more heat is radiated out of the part. It is advised to use a closed-loop system that takes temperature measurements of the subject during the process. The interpass temperature can be measured and based on that data and the set goal for the interpass temperature, the next layer can be printed at the right time. That way no time is wasted and higher deposition rates can be achieved.

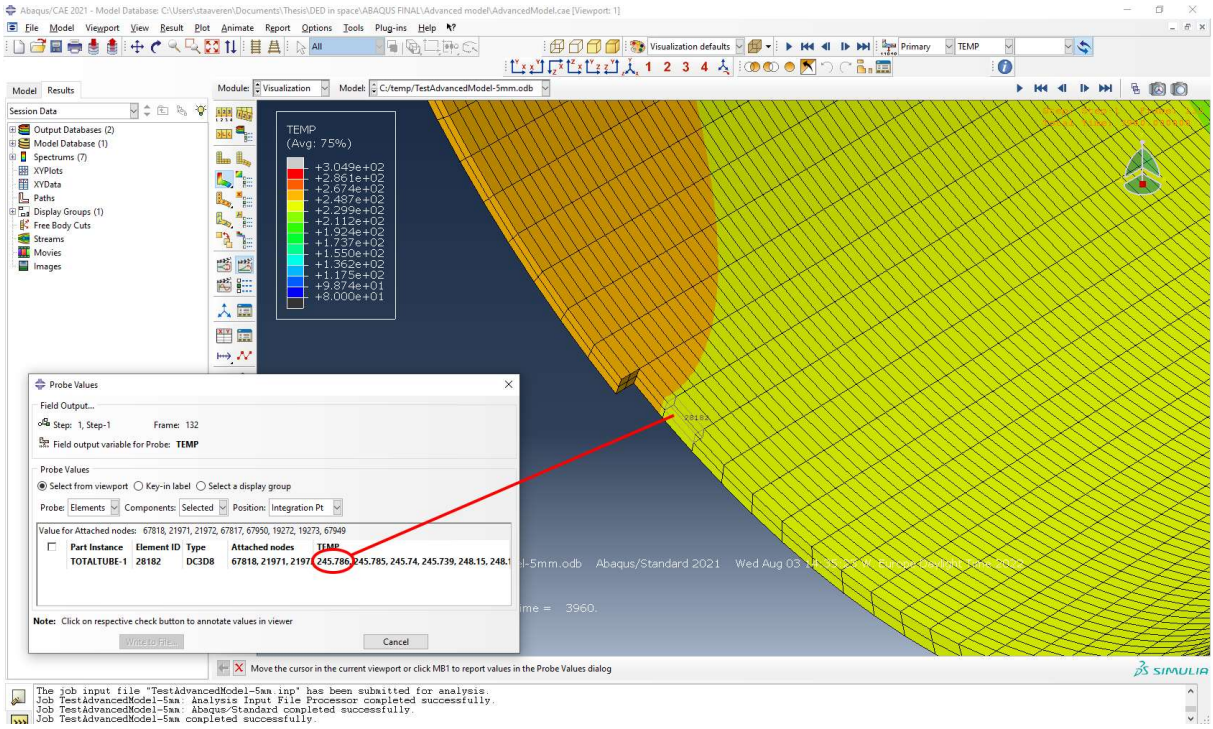

Figure 48: Interpass temperature of the advanced test simulation at 5 mm/s and 0 s idle time: 246 °C

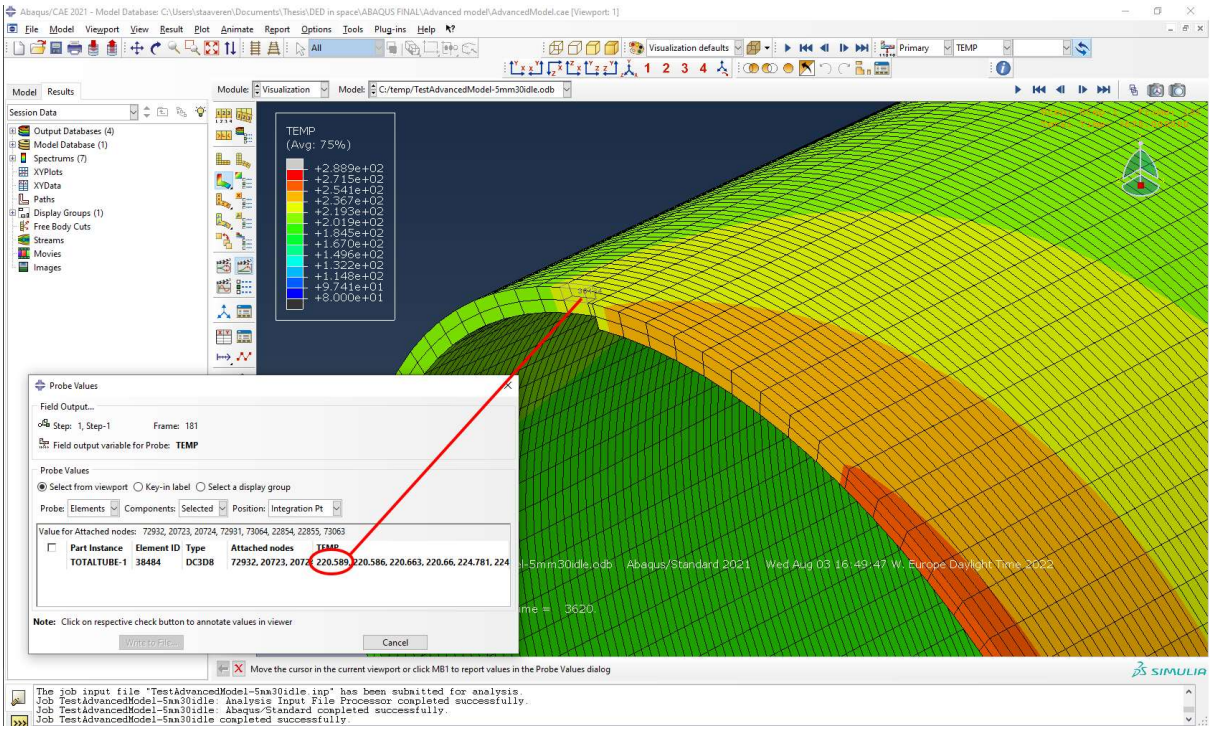

Figure 49: Interpass temperature of the advanced test simulation at 5 mm/s and 30 s idle time: 221 °C

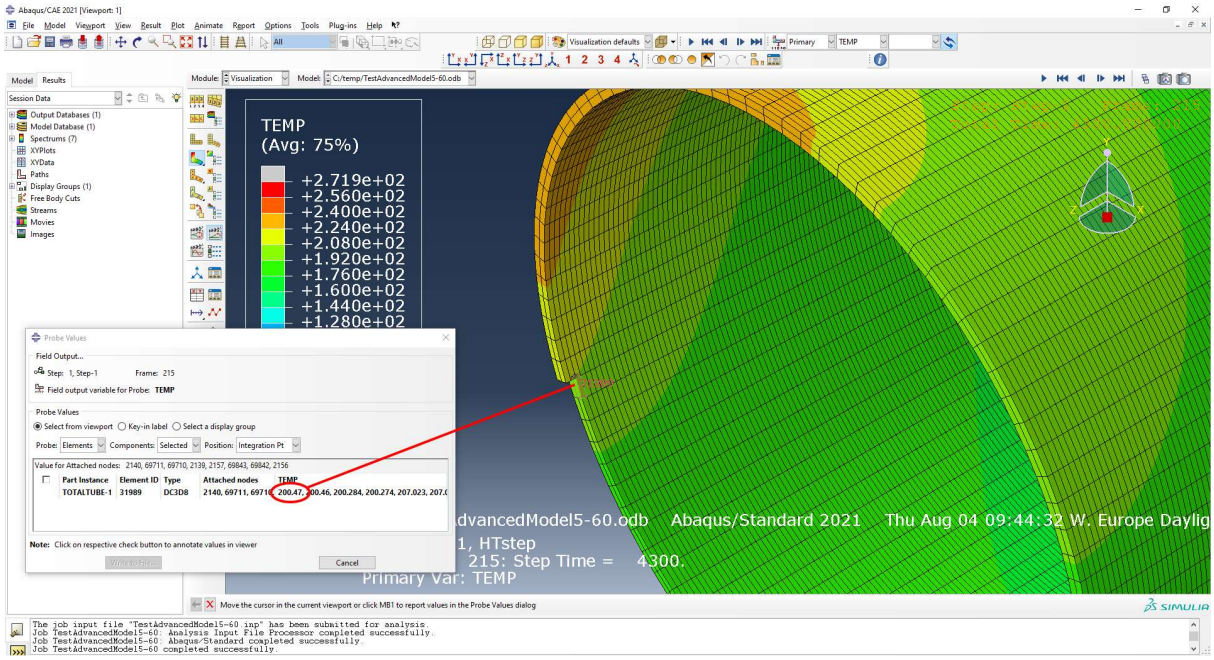

Figure 50: Interpass temperature of the advanced test simulation at 5 mm/s and 60 s idle time: 200 °C

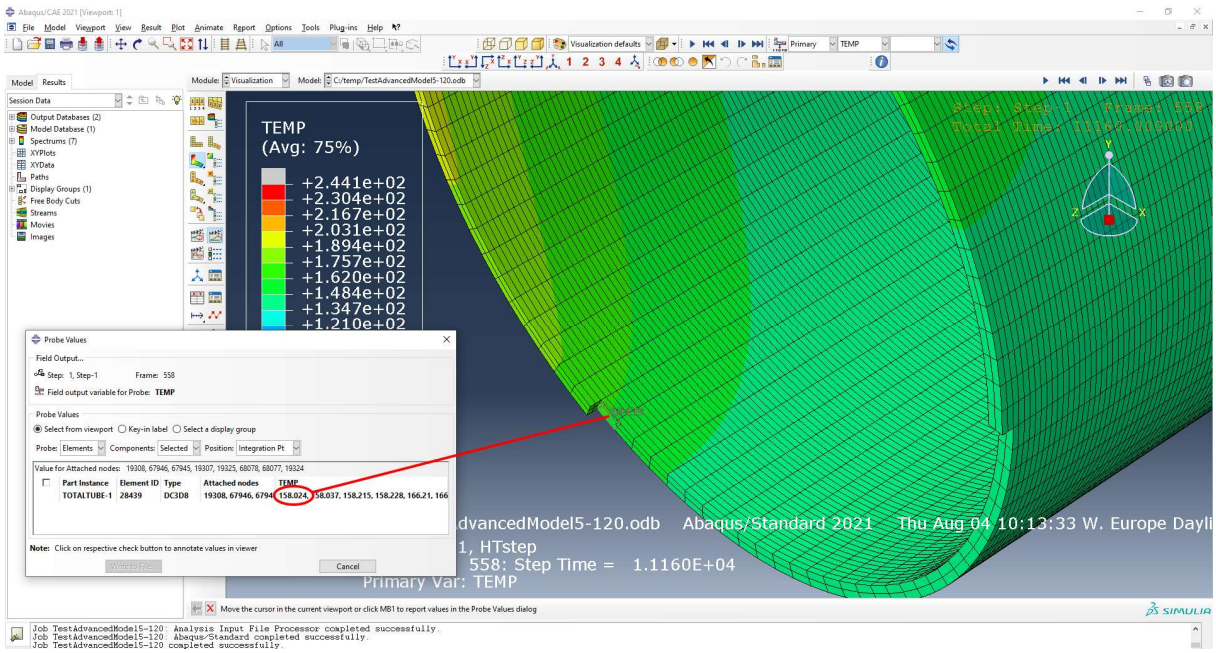

Figure 51: Interpass temperature of the advanced test simulation at 5 mm/s and 120 s idle time: 158 °C

Setting up the advanced model

Two cases are simulated in the full length simulation, for which the parameters are presented in Table 14. The first case will use the model 1 parameters. It demonstrated wire-based DED in space at full speed. The second case, model 2, has the goal to not exceed an interpass temperature of 150 ℃. To achieve this, the print speed is reduced to $5\ mm/s$ and an idle time between layers of $120\ s$ is added. Blank cells have the same value as model 1.

Table 14: Parameters used in the advanced model

Parameter	Value model 1	Value model 2	Unit
Material	Al 6005A T5		–
Base tube length	0.2		m
AM tube length	1		m
Outer tube diameter	0.05		m
Tube thickness	2		mm
AM layer height	1.5		mm
Radiation environment temperature	-270		℃
Emissivity	0.25		–
No. of mesh elements in Z-direction	1333		$1/m$
No. of mesh elements over diameter	100		–
No. of mesh elements over thickness	2		–
Step time	10		s
Solar irradiance	683		W/m^2
Earth irradiance	211.4		W/m^2
Initial temperature base tube	80		℃
Temperature deposition material	1726.85		℃
Print speed	10	5	mm/s
Initial idle time between layers	0	120	s
Interpass temperature goal	-	150	℃

Advanced model results

It took the advanced model 1 19.5 hours and the advanced model 2 70 hours to complete processing of the simulation. Visual results of the advanced model without adjusted parameters can be seen in Figure 55. Printing starts at $\tau = 0\ s$ and printing $1\ m$ of tube is finished at $\tau = 20535\ s$. In the beginning stage, about 1000 seconds or 33 layers, the base tube heats up until the part reaches a relatively steady state. The lower temperature of the base tube benefits the cooling process of the printed material initially, but the base tube has quickly heated up. In comparison to the basic model, where the base tube was a lower temperature, the cool-down effect by the base tube is in this simulation smaller.

It can be seen that the maximum temperatures that are experienced are slightly lower than in the basic model, but the difference is small. An important difference between the basic and advanced model is the addition of incoming flux from the Sun and Earth. The effect of solar radiation incoming from one side and Earth's radiator incoming from the opposite side appears to be small in the simulation results, but the effects are visible. Figure 52 demonstrates this. In this figure, the solar irradiance is directly from the top and the Earth's irradiance directly from the bottom, in the

pattern that was presented earlier in this section. In the basic model the temperature over the cross section of the tube was nearly constant, with the exception of the region close to the active material deposition. For the advanced model this is no longer the case, which can be seen by the curved lines of equal temperature. The effect is small though. Measured at multiple points on the object, the temperature difference between the hottest and coldest point in one layer is only about $3℃$.

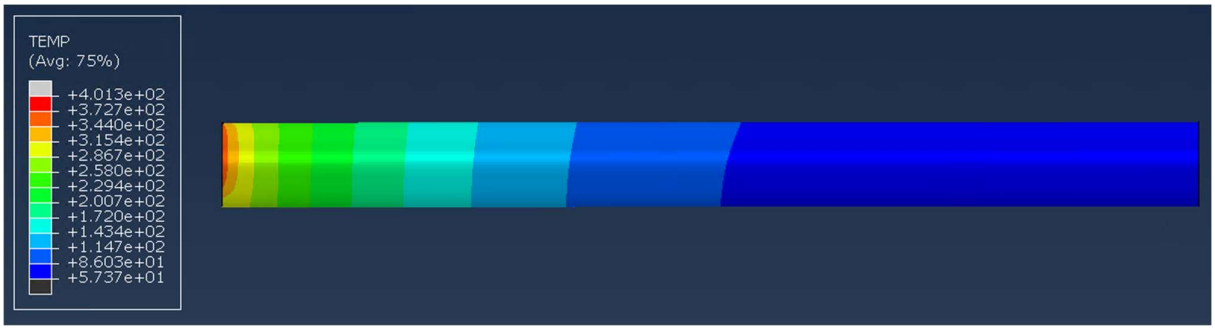

Figure 52: The effects of solar irradiation become visible in the advanced model, as the temperature profile is no longer symmetric over the object

The interpass temperature was measured over the duration of the printing process. The results are plotted in Figure 53. As was explained in 0, a slight inconsistency in the measurement is cause by the fact that it was not possible to measure at the exact same location due to the set time step. In the result it can be seen that the interpass temperature reaches a maximum at around $1000\ s$. After this point, the interpass temperature slowly reduces until it become nearly constant around $310℃$.

After the printing process was finished, the simulation was continued until $\tau = 21000\ s$ to look at the cool down behaviour of the tube. The visual results can be seen in Figure 54. Within 500 seconds the object has cooled down to a maximum temperature of $130℃$.

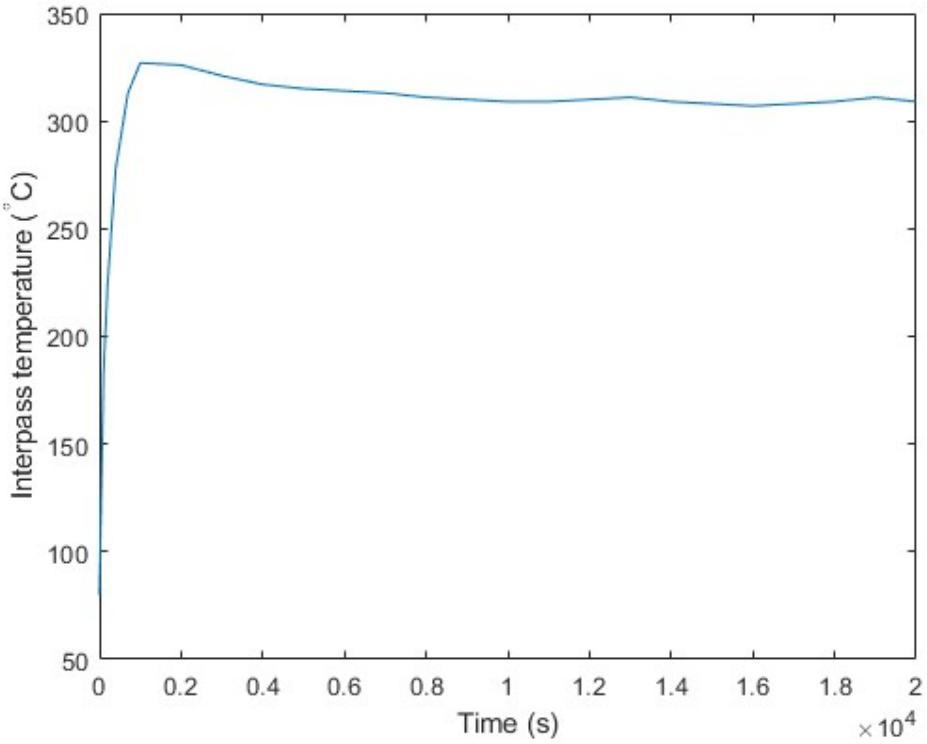

Figure 53: Interpass temperature over the duration of the printing process for the advanced model 1 without idle time

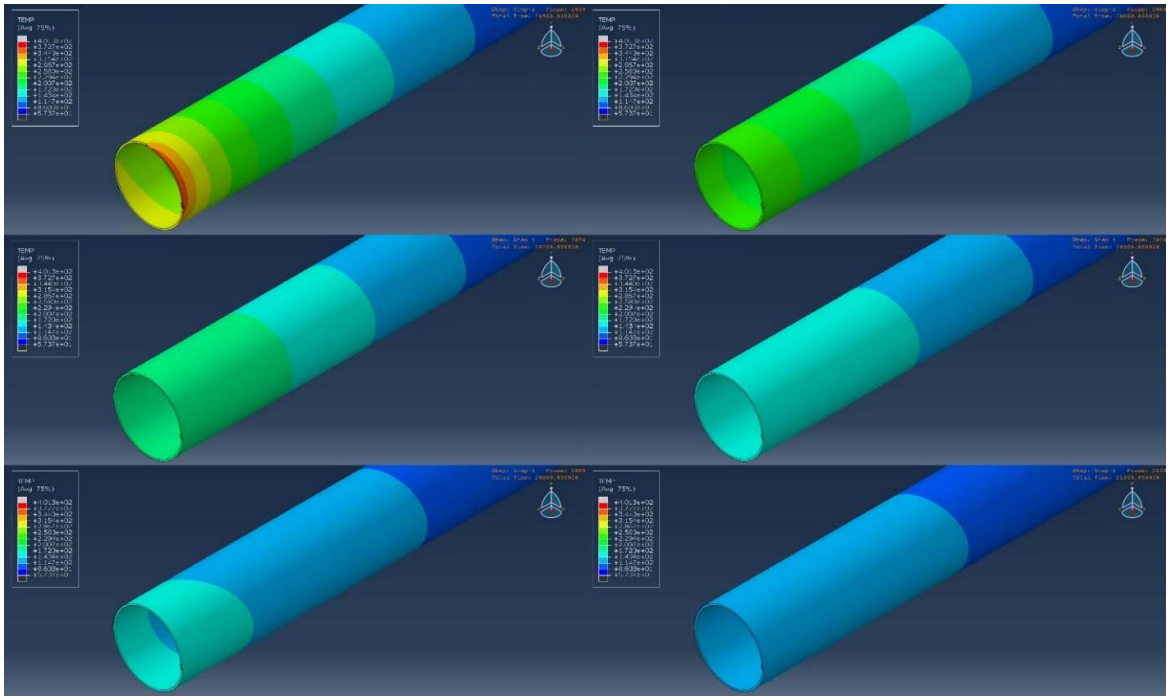

Figure 54: Cool down process of advanced model 1 after finishing the AM process

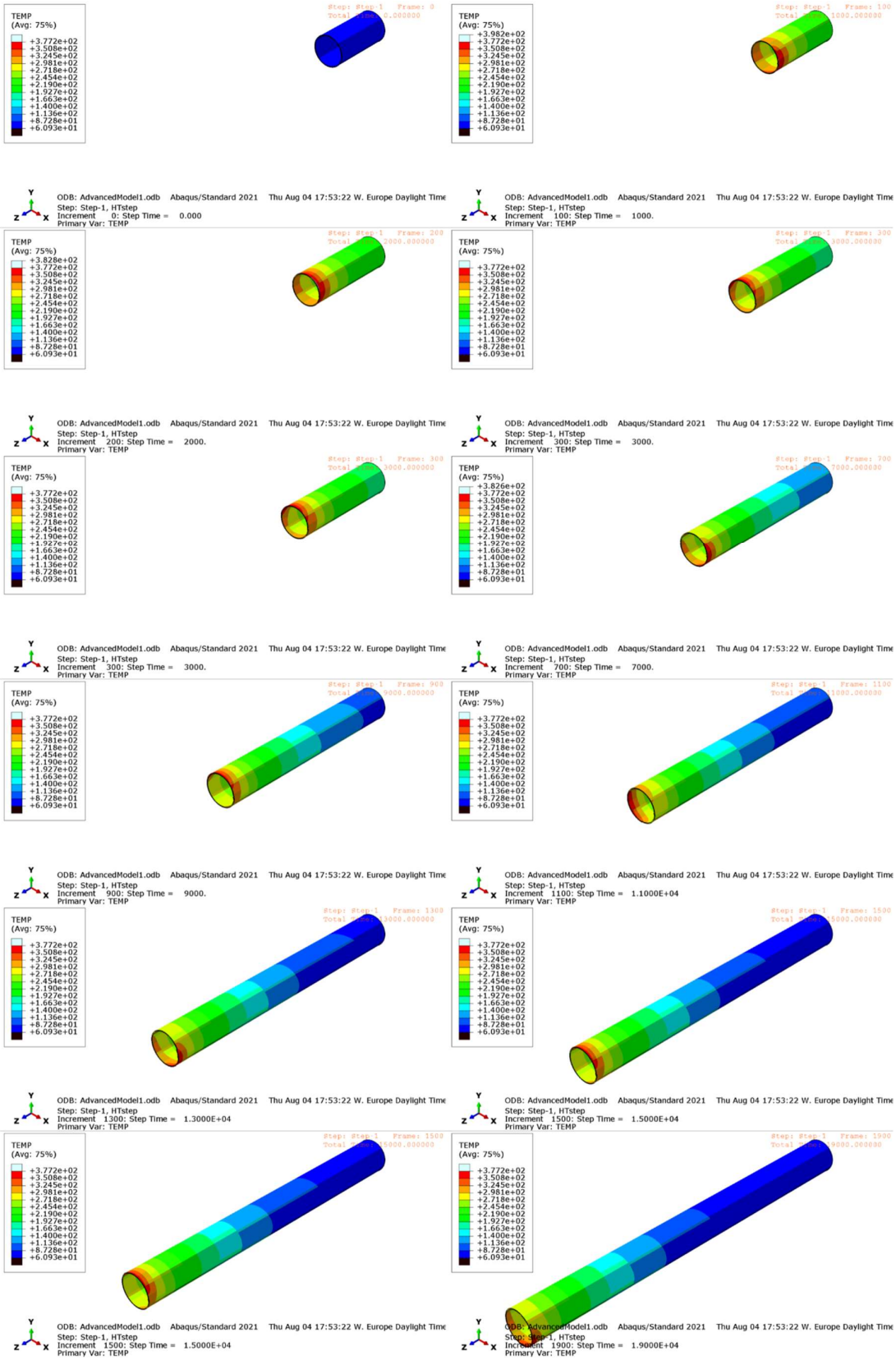

Figure 55: Various timesteps of the advanced thermal model 1 without idle time (see top right corner)

The same results are presented for the advanced model 2, where idle time is added and the deposition speed is lowered to achieve the interpass temperature goal. The visual results of the simulation can be seen in Figure 58. Also, the cool down behaviour of the object after the printing process was finished can be seen in Figure 57. The first frame occurs right at the moment where the printing process stops. It can be seen that model 2 cools down quicker than model 1, which is evidently cause by a lower initial temperature due to more time to dissipate heat during the printing process.

The interpass temperature for advanced model 2 is presented in Figure 56. It must be noted that it is even harder to obtain a consistent measurement location in model 2, due to the idle time. This causes the graph to be less smooth. Again, a peak is experienced at the start of the simulation. After about 20000 seconds the interpass temperature reaches a point where it constantly decreases by a minimal amount. From this point until the end of the simulation the interpass temperature averages about $138℃$. The interpass temperature is significantly lower than in model 1. Only in the first peak is the goal temperature of $150℃$ exceeded.

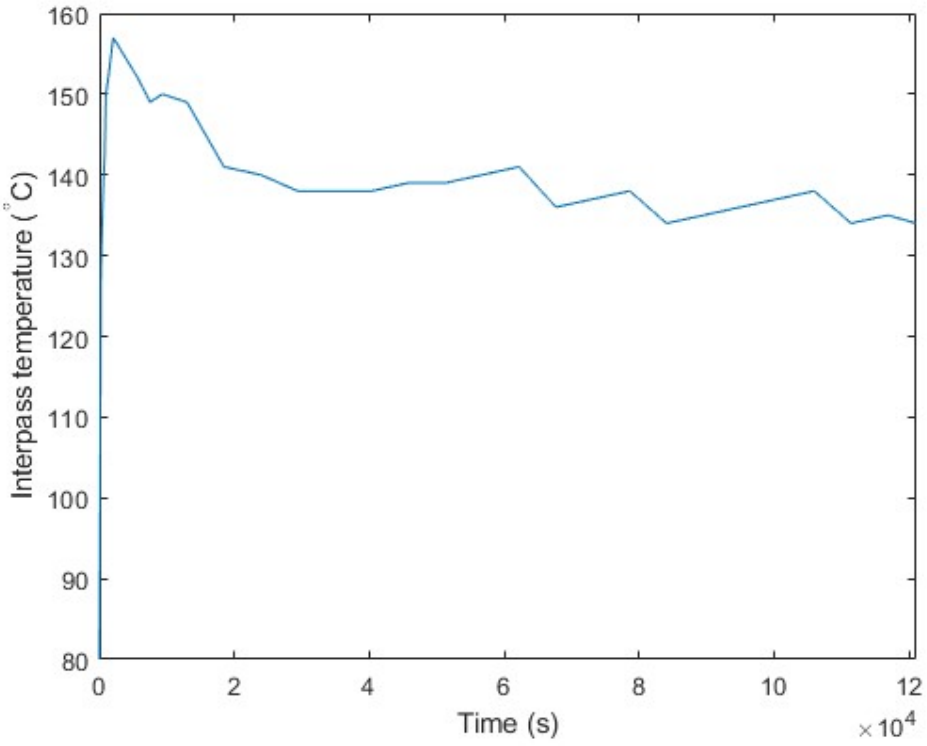

Figure 56: Interpass temperature over the duration of the printing process for the advanced model 2 with idle time

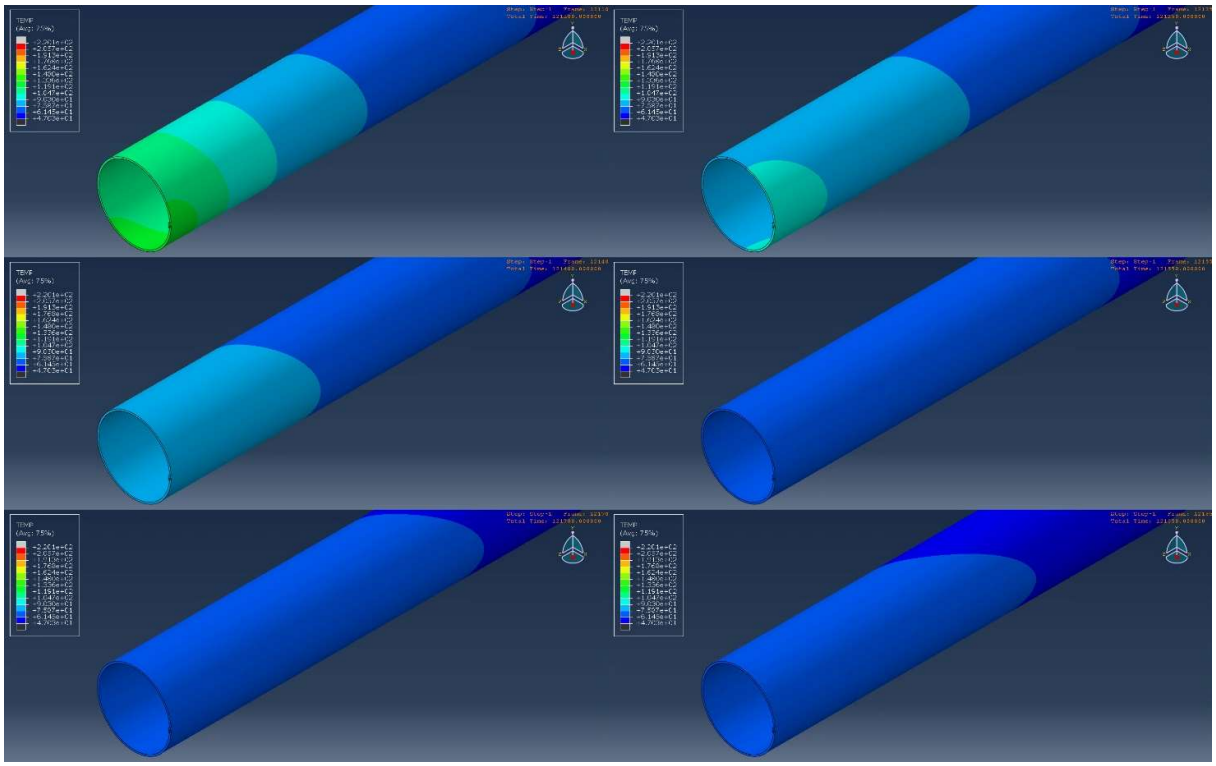

Figure 57: Cool down process of advanced model 2 after finishing the AM process

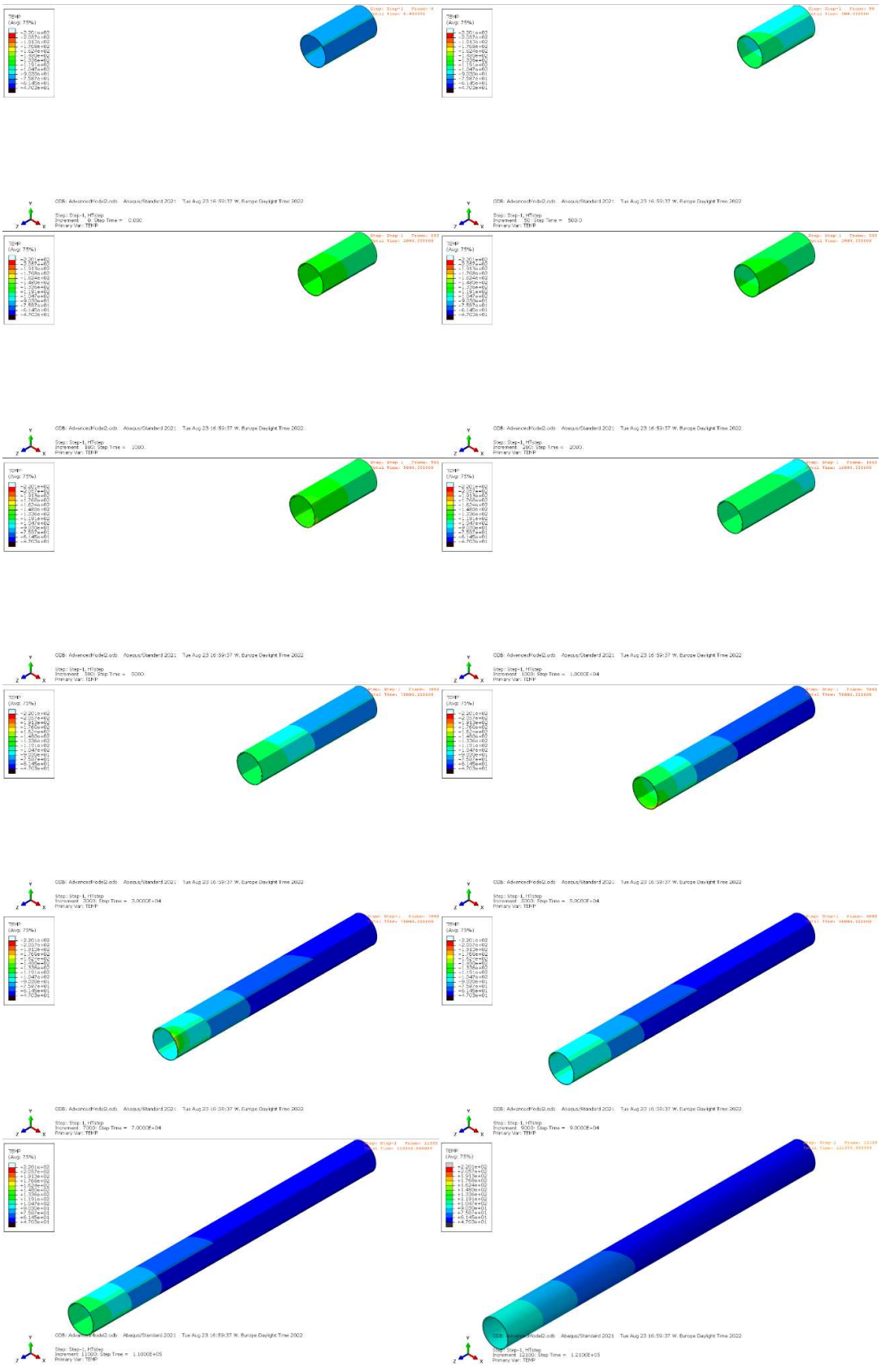

Figure 58: Various timesteps of the advanced thermal model 2 with idle time (see top right corner)

4.2.5 Model verification

To see if the simulation behaviour is accurate to the real world behaviour, some kind of validation is required. With the resources that are available it is difficult to validate the simulations by experiments of the exact same application. To do an experiment where wire-based DED is applied to manufacture a tube in a space environment, a serious setup is needed. Unfortunately, NLR is not in possession of a wire-based DED machine. But, even if a wire-based DED machine was available at NLR, it would not be feasible to place it in a thermal vacuum chamber. Finding a thermal vacuum chamber of sufficient size is difficult and the DED machine components would most likely not be suitable to operate in a vacuum.
For these reasons, another direction is chosen to do validation. The goal is to demonstrate that the method used to simulate the space environment is accurate. This method is applied to an experiment that has been performed in a paper and the simulation results are compared to the experimental results. The paper that is used for this is written by Nayak and Roy [93]. In their research they perform temperature measurements during electron beam welding of stainless steel 304, which is a similar process to WEAM. The process chosen in this thesis, WAAM, differs from this as the heat source is an arc instead of an electron beam. Nevertheless, it made more sense to use a research where an electron beam was used, because WEAM is always applied in a vacuum environment. This is a critical aspect of the simulated space environment and needs to be part of the validation. No research is available of WAAM in vacuum. Another difference is that this paper is about welding. The process is exactly the same as for AM, but it is just one layer. Therefore, validation of the AM aspect is limited, but focus of the validation lays on the environmental aspect.

In the experiment of Nayak and Roy, they applied a weld on a base block of $50\ mm$ x $30\ mm$ x $15\ mm$. Both the base and the weld were of the material AISI SS304. The weld was applied parallel to the longest side and in the centre of the block. The weld run from one edge of the base block all the way to the other edge of the block in a straight line. To measure the temperature profile, three K-type thermocouples were spot-welded on the base block on $2.8\ mm$, $3.4\ mm$ and $4.0\ mm$ out of the centreline of the weld, in the middle of the weld length. These measurement points are called TC1, TC2 and TC3, respectively. See Figure 59 for an overview of the setup.

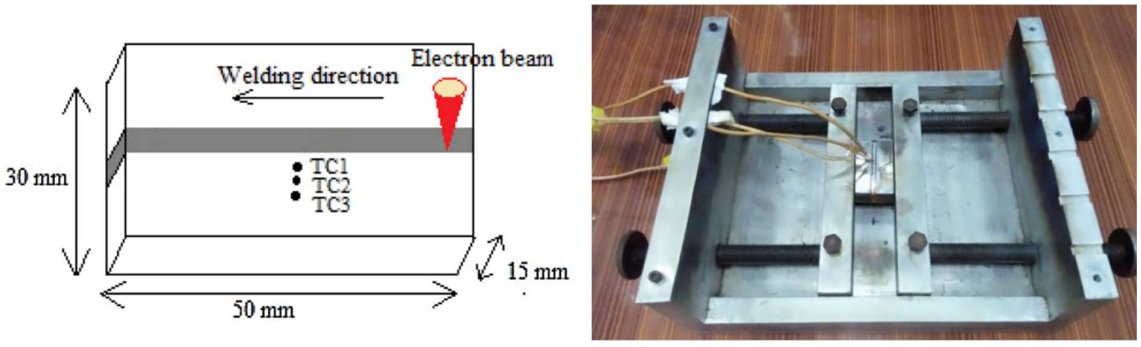

Figure 59: Overview of the setup of the experiment performed by Nayak and Roy

The experiment is simulated in Abaqus, the same way as the simulations have been performed previously. In their paper, results were published of the temperature profile of these measurement points during the welding process. These points were also marked in the validation model to obtain the same results from the simulation. One difference in the validation model is that a laser was added as a heating element to simulate the electron beam. This laser element works in Abaqus as a heat flux based on laser power, efficiencies and material properties. Therefore, it works similar to an electron beam in the model. It was found that depositing hot material, as was done in the previous models, was not

sufficiently accurate to match the experiment results. A limitation to using a laser in the Abaqus AM plugin is that a circle cannot be selected as the shape. Instead a square laser spot was used.

Data for simulation parameters are mostly taken from the paper. Extensive data on material properties are provided in the paper. Unfortunately, the temperature dependent data of multiple material properties, combined with the high laser power, made the simulation so complex that it became unfeasible to work with. The available processing power and time were reasons to make the decision to simplify the material properties in the model. An average of the material property in the approximate temperature range was taken instead of temperature dependent properties.

The mesh for the validation model was made to have a high element density in the region around the weld and a low element density for the rest of the part. How the model was meshed can be seen in Figure 60. The dense area has ten times more elements per unit of volume than the course area. This significantly reduces the computing time of the simulation. A refined mesh was also required in the welding region for the simulation to run without making the step size extremely small, which would increase the simulating time.

The parameters used in the validation model can be found in Table 15. Visual results of the validation model simulation can be seen in Figure 61 and Figure 62.

Table 15: Parameters used in the validation model

Parameter	**Value**	**Unit**
Material	AISI SS304	-
Density	7700	kg/m^3
Thermal conductivity	20	$W/(m*K)$
Specific heat capacity	800	$J/(kg*K)$
Specific latent heat of fusion	260000	J/kg
Solidus temperature	1424	℃
Liquidus temperature	1454	℃
Laser power	3000	W
Laser efficiency	0.9	-
Absorptivity	0.9	-
Laser spot size	0.2 x 0.2	mm
Base block length	50	mm
Base block width	30	mm
Base block thickness	15	mm
Weld width	1.6	mm
Weld height	0.5	mm
Radiation environment temperature	30	℃
Emissivity	0.20	-
Mesh element size in dense area	0.2	mm
Mesh element size in course area	2	mm
Initial material temperature	30	℃
Print speed	10	mm/s
Total simulation time	7	s
Step time	0.1	s
Start AM process after	1	s

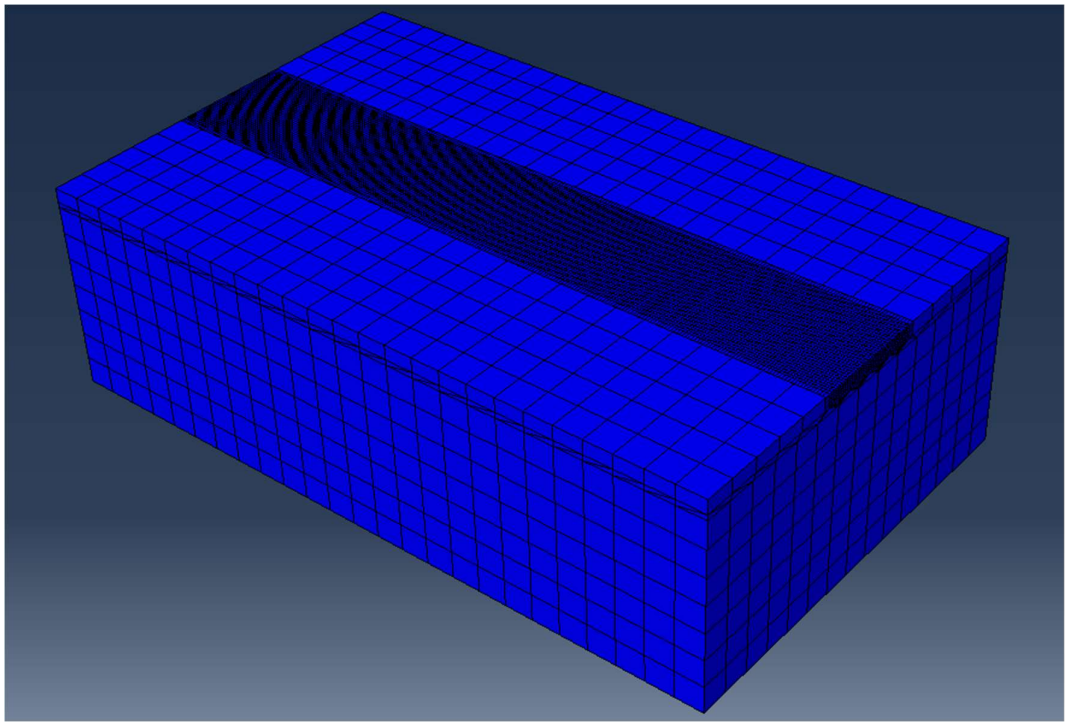

Figure 60: Mesh for the validation model

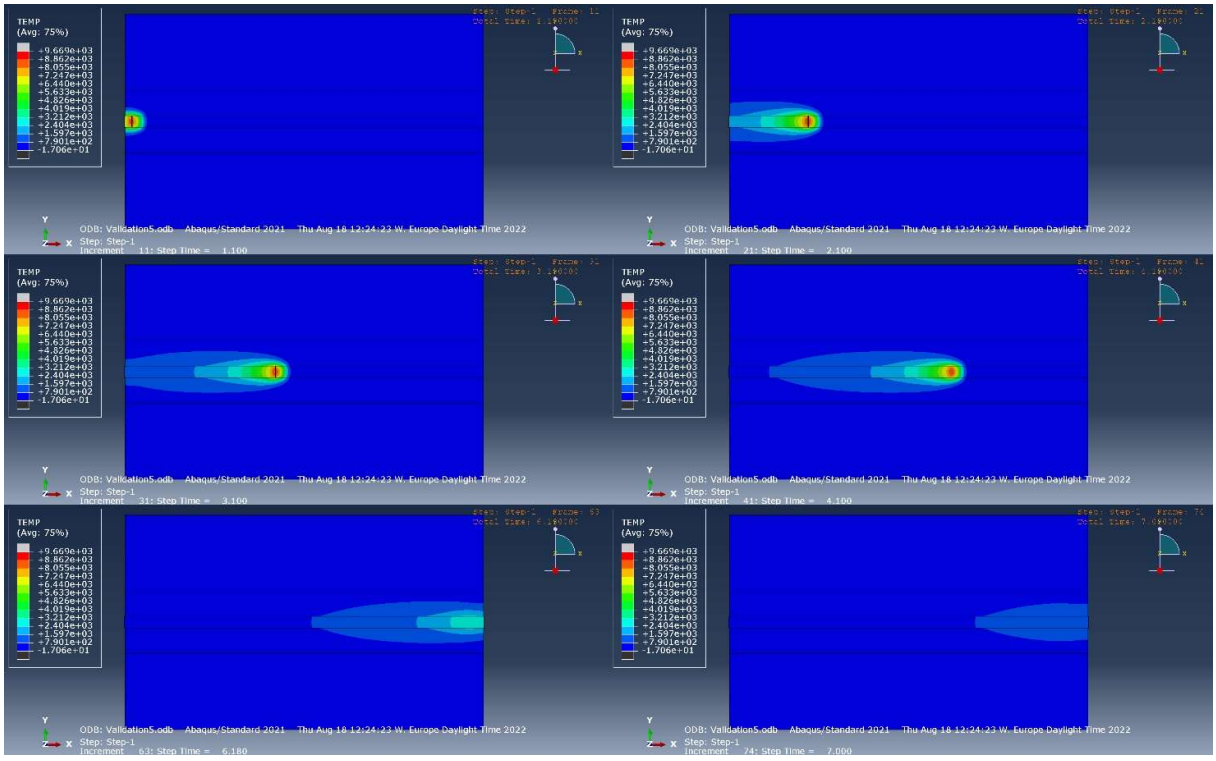

Figure 61: Time lapse of the validation model simulation, with the timestamp listed at the bottom of the frame

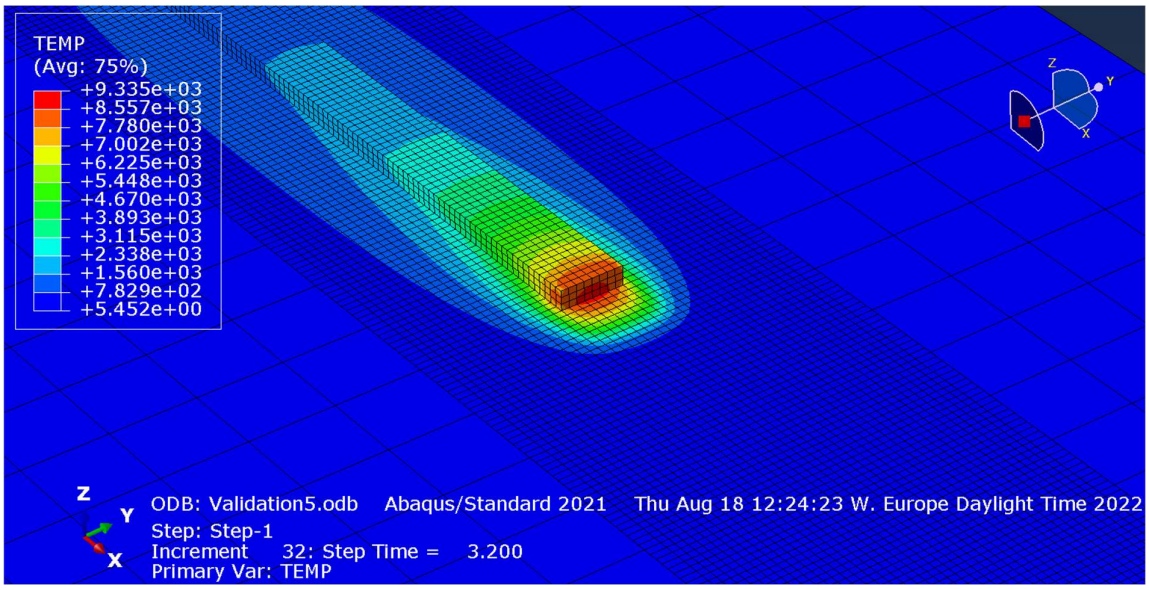

Figure 62: Close up of the weld pool during the validation model simulation

The temperature profiles that resulted from the validation model are compared to the results of the experiment from Nayak and Roy. The results from their experiment that are used as reference can be seen in Figure 63. In this graph, temperature is plotted over time for the three measurement points. For each measurement point, three method are presented that were used to determine the temperature profile. 'Corrected TCx' is the result from the experiment, which has been corrected for delays in the thermocouple. Additionally, two computational models have been applied to theoretically determine the temperature profile, which were compared to the experiment in the paper. The results from the validation model have been overlapped with the respective experiment results. These graphs can be seen in Figure 64, Figure 65 and Figure 66. The graphs have both the timescale of the experiment and the simulation included.

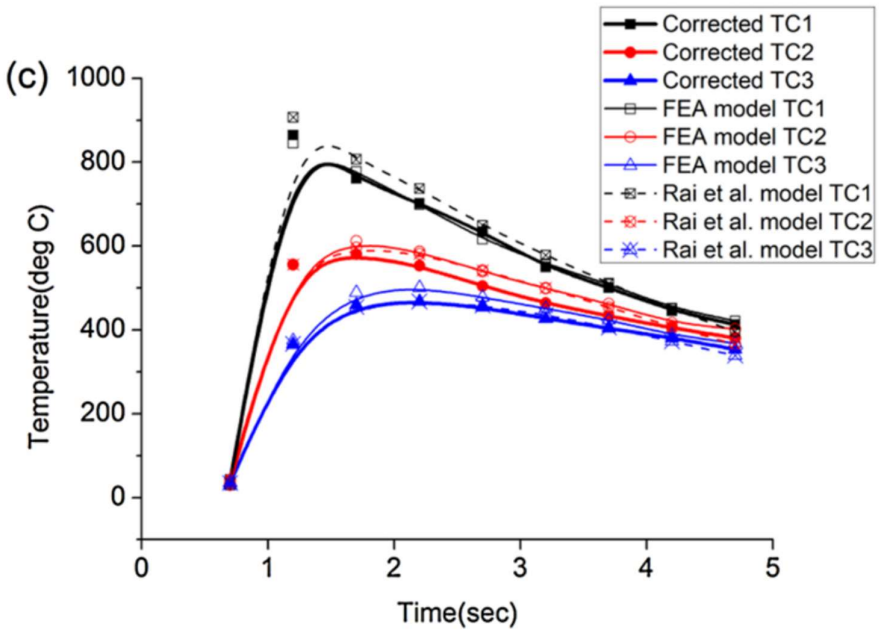

Figure 63: Results from Nayak and Roy containing the thermal profile from TC1, TC2 and TC3 for the experient (corrected) and two theoretical calculations

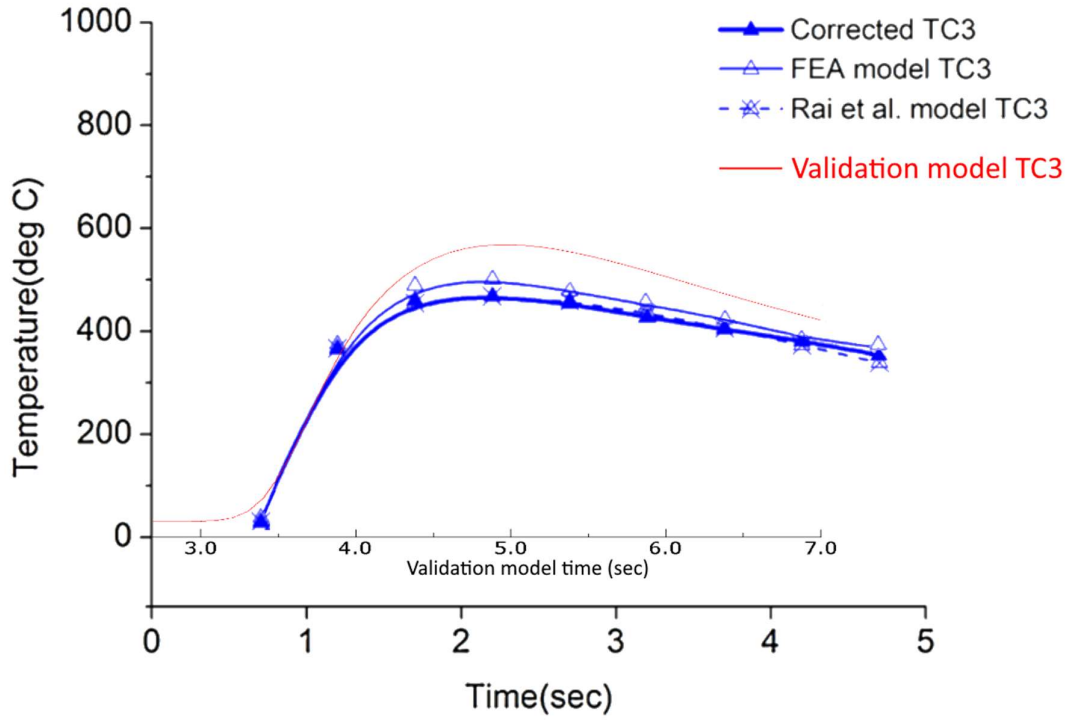

Figure 64: Comparison of TC3 between the results from Nayak and Roy, and validation model

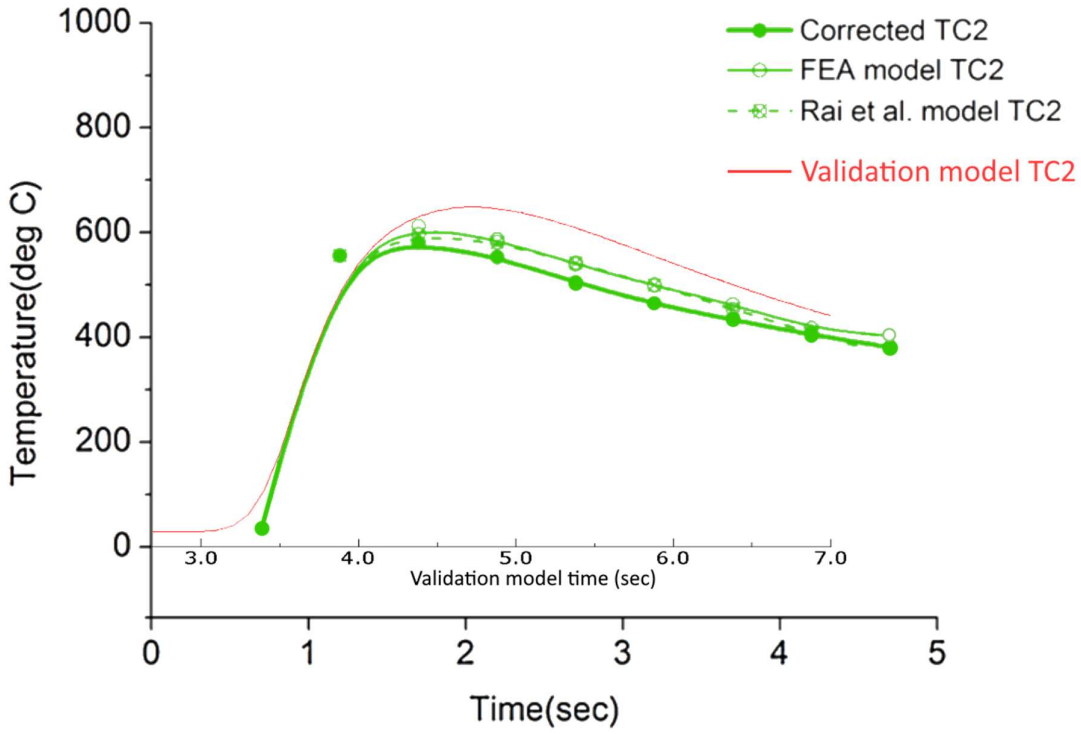

Figure 65: Comparison of TC2 between the results from Nayak and Roy, and validation model

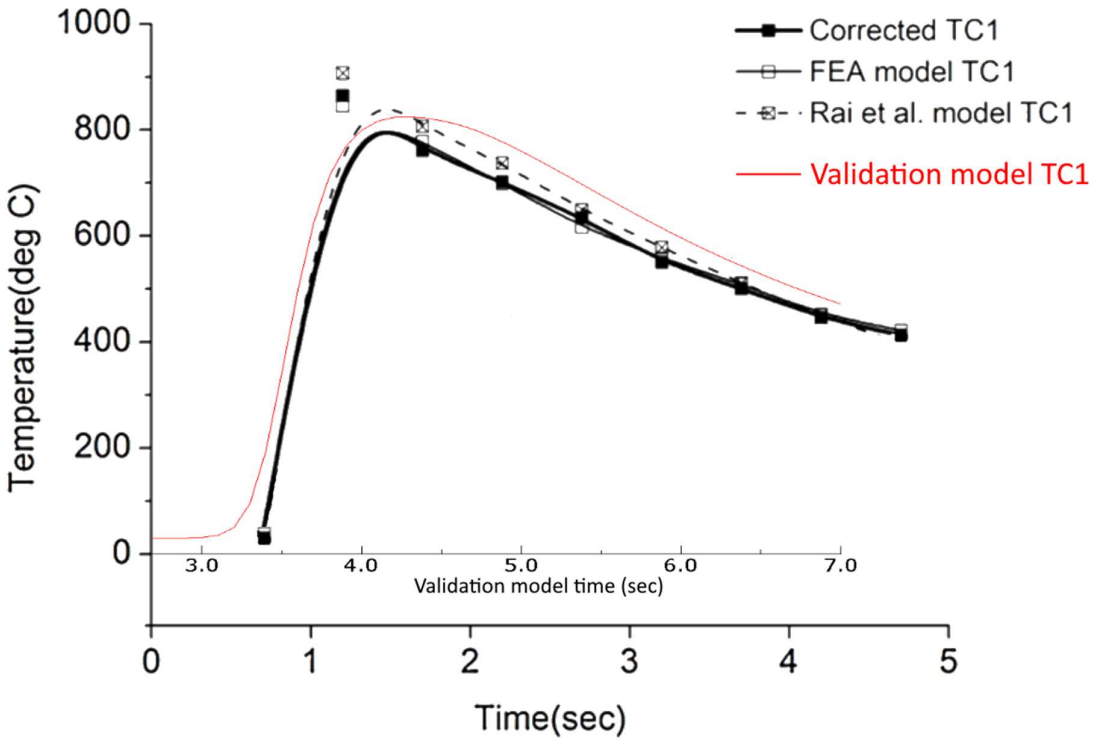

Figure 66: Comparison of TC1 between the results from Nayak and Roy, and validation model

In the results of the comparison between the experiment and the validation model simulation it can be seen that the thermal profiles are comparable, but improvements can be made. The validation model that was made is not as accurate as the models that were made by Nayak and Roy. The temperature profiles become slightly less accurate further away from the weld. Nevertheless, it can be concluded that the simulation method is accurate enough for course estimations of the temperature profile of additive manufacturing in space. That is sufficient for the purpose of this thesis research.

Some reasons for the discrepancies between the experiment and simulation are known. Certain technical limitations and lacking information in the reference paper caused the model to be less accurate than it could have been. In the paper it was not written what the dimensions of the weld were. For the electron beam, some information was given, but it did not become apparent from the paper what the beam diameter was on the surface of the part. So, these had to be estimated. Technically, compromises had to be made. The variable material properties made the simulation too complex. The laser spot had to be square instead of round. Additionally, the impact of metal evaporation was neglected, same as for the previous models. All of these discrepancies combined cause inaccuracy in the model.

4.2.6 Discussion

The results of the thermal modelling work have shown the thermal behaviour of additive manufacturing in a space environment for realistic parameters. Performing aluminium wire-based DED in space at deposition rates that are common for applications on Earth, the interpass temperature get extremely high. Idle time in between the deposition of layers allow the object to cool down. The idle time required to reach an interpass temperature of $150°C$ is not infeasible. But in this model, it resulted in a manufacturing rate that is nearly six times slower than the case where no interpass temperature goal was taken into account. This is highly significant for the economical aspect of the application. When the manufacturing rate get too low, it becomes simply undesirable to create a manufacturing platform, even though it is technically possible. Interpass temperature has negative effects on the microstructure of the material, thus material properties, as well as on the AM behaviour. There is a weigh-off between achieving the ideal interpass temperature and the manufacturing rate. In future research in this project an evaluation needs to be made how much deterioration in material properties is accepted at the benefit of production rate. An ideal interpass temperature for the application needs to be found.

During the process of creating this thermal model, factors were found that will improve the accuracy of the model. Due to technical limitations and the lack of available data and time, these improvements could not me made during this thesis project.
The most important improvement that needs to be made is the addition of the welding arc in the simulation. In the presented model, the effects of an arc were neglected and simplified to solely the deposition of hot material. The main reason for this was that an arc was not an available option in the Abaqus AM plugin. An arc is a relatively complex factor to simulate, compared to a laser or electron beam. In future work on thermal modelling, a good solution needs to be found for simulating the welding arc. It is expected that adding the effects of an arc would increase the material temperatures in the simulation. Besides adding heat to the deposited material, the arc also heats up the surrounding material to create a weld pool. It is expected that the results of the thermal model in this report are a lower bound of temperature that can be expected. Nevertheless, all work on parameter sensitivity still hold up. The results on manufacturing rate and absolute temperatures provide a course expectation for the thermal behaviour of GMAW WAAM in space.

It was found that the impact of the initial temperature of the base tube is small. In a relatively short period of time the base tube heats up and the process reaches a steady state. Still, the initial temperature of the base tube should be controlled, as it is a relevant parameter in the process. It is not uncommon for DED applications to heat the base material to a desirable temperature. This improves binding of the deposited material to the base, which is particularly important.

In the advanced model 2, the print speed was reduced compared to model 1. This was done to create more time for the object to dissipate heat. However, this change has more consequences. The print speed is a parameter that is connected to multiple other parameters, such as current. In the literature study on in-space manufacturing [1] it was found that generally, slower print speeds result in high power consumption. This is undesirable, since the printer's energy consumption is the biggest energy consumer on the spacecraft. Therefore, this change could mean that larger solar arrays are needed. Additionally, the combination of print speed and power input have an effect on the microstructure of the material, because it affects the material temperature. This can negatively impact the material properties. An alternative approach would be to keep the print speed high, but increase the idle time between layers. All of these effects need to be taken in account and an optimum needs to be found.

5 Conclusions

In this report, important aspects of applying wire-based directed energy deposition for in-space manufacturing of solar array structures have been researched. The main research question was: *How can metal wire-based directed energy deposition be applied to in-orbit manufacturing of solar array structures?* Efforts have been made to find the best options for different technical aspects in the pursuit of making this novel application a reality.
Wire-based DED is a relatively new and unique manufacturing method that has now been adopted by industry as an established manufacturing method. However, the Earth's environment is vastly different from the space environment. Through investigation of the impact of the space environment on the manufacturing method, critical factors have been identified that require consideration. It can be concluded that wire-based DED in space is possible. An initial concept system design has been proposed in this report.

The first research sub-question is: *What does the system architecture of the in-space manufacturing platform look like?* This sub-question consists of the following parts:

a. *Which functionalities and subsystems are required on the platform?*
b. *What are the power system requirements for the manufacturing platform?*
c. *What is the limiting factor in manufacturing rate for DED in space?*

This was answered by finding and investigating the functionalities and subsystems of such a platform. Various decisions were made for the application and subsystems. It was determined that the best DED method at this stage is GMAW WAAM. This is not the only right option for this application, arguments can be made to implement a laser or electron beam as the heat source. GMAW WAAM offers great simplicity and high energy efficiency. This comes at the cost of higher amounts of spattering. CMT is a technique that can be implemented to reduce spattering and heat input for GMAW WAAM.
Deployable flexible solar panels are the best type of solar array to combine with AM structures. The lowest level of mass and volume in stowed configuration can be achieved with this panel type.
In the concept design, a dedicated manufacturing platform with restocking capabilities for donating solar arrays was chosen as the use case. Two DED printers on robotic arms simultaneously print the support structure on each side of the solar panel. The spacecraft is equipped with a robotic assembly arm to be able to install the manufactured solar array on another spacecraft.

Energy consumption of the components for the manufacturing system has been investigated. A manufacturing spacecraft, such as the one proposed, will require a large amount of power. In a first estimation for the power budget, a total average spacecraft power generation of $3043\ W$ was calculated to be required. The spacecraft has the option to be launched with small solar arrays initially and to manufacture its own bigger solar array. Until this step is done, the spacecraft will be power limited and needs to pause the manufacturing process at times to recharge its batteries. When the spacecraft is equipped with a suitable power generation system, the manufacturing rate will be limited by heat dissipation, as was found through thermal simulations.

The second research question that was answered is: *What are material and design possibilities for the solar array structures?* This sub-question consists of the following parts:

a. *What environment will the solar array structure endure?*
b. *What is the optimal feedstock material?*
c. *What are the geometrical limitations of the manufacturing process?*

Attributes of the space environment, application and manufacturing method have been investigated to find out which materials are not suitable and which material properties are desirable. Through a structural approach to material selection, it was found that aluminium is the best feedstock material for the structure in this application, specifically aluminium 6005A T5.

Research on the geometrical accuracy of DED found that extremely bad performance for part accuracy and surface roughness is to be expected for this manufacturing method. Due to the way material is deposited layer by layer, a surface roughness around $1\ mm$ is expected. Depending on system specifics, part accuracy can be off by centimetres in the worst cases. Process monitoring can greatly improve part accuracy and will be required for application of DED in space.

The third research question is: *How will wire-based directed energy deposition handle the space environment?* This sub-question consists of the following parts:

a. *What are the influences of performing DED in space and how will this impact the manufacturing process?*
b. *What does the thermal behaviour of the additive manufacturing process look like in space?*

Microgravity, vacuum and thermal fluctuations are critical aspects of the space environment that have a big impact on the design and technology of this system. Microgravity causes the weld pool to behave differently than on Earth. The effects of surface tension are strongly enhanced. Vacuum has an effect on various material properties. Both high and low temperatures need to be accounted for in the AM machine design. A large focus in this project was put on the thermal behaviour of metal additive manufacturing in space. A thermal model was made to get an idea about the heat dissipation in space and to identify important process parameters.

In the simulation it was found that idle time between the deposition of layers is required to prevent the object from overheating. It is expected that this will cause the manufacturing rate to be in the order of six times slower than on Earth. Additionally, it was found that the effect of solar and Earth's irradiation on the AM part do not have a large impact on material temperature. It is expected that the difference in temperature between the hottest and coldest point on a cross section of the AM part will be no more than a couple of degrees Celsius due to the effects of irradiation.
There are improvements to be made on the model to make it more accurate. It is of the highest importance to achieve a great level of model accuracy to make additive manufacturing in space feasible. AM is known to be unreliable. This must be improved, because in contrast to AM on Earth, human interference is not an option. In addition to a great level of understanding of the process behaviour, efforts need to be made to combine this with process monitoring. Implementing adaptive process parameter based on process data will create the highest part quality.

The most important work that needs to be done to make wire-based DED in space possible, is to develop the process for a space environment. That means that the process and material behaviour need to be better understood. The effects of material properties and process parameters need to be known to the highest degree. This must be implemented in a model that is able to predict the not only the thermal behaviour, but also the mechanical behaviour. The importance of modelling cannot be overstated. The process must become highly predictable to achieve success in space.
Manufacturing solar arrays in space using DED is possible, but a lot of maturing and development of the technology is required before it can be realized.

6 Recommendations for future research

Given the fact that this thesis research is the first work in NLR's project on in-space manufacturing, it is obvious that there is still a considerable amount of research to be done. During this thesis research, numerous points interesting points for future research have been mentioned in the concerning sections of the report. Here, all of these points, as well as new recommendations are summarized. The points can be divided into three areas: required work, modelling improvements and additional research topics.

6.1 Required work

A lot of work needs to be done before 3D printing solar arrays in space becomes a reality. An important research area that must be explored to obtain more detailed information about cost, mass and capabilities is the structural geometry of the solar array structures. In this report, a tube was assumed, but through geometry optimization, it is likely that better performing structures can be achieved. This is particularly interesting for the design freedom that is enabled through additive manufacturing.

Once a suitable structure geometry has been found, relevant figures can be calculated. With the (structural) mass per square meter solar array known, estimations for cost, stowed volume, maximum achievable array size without restocking and more can be determined. Most importantly, the tipping point can be determined where in-space manufacturing of solar arrays is more advantageous than on-Earth produced deployable solar arrays. The manufacturing system adds mass to the spacecraft, but the ISM arrays are lighter than conventional arrays. That means that for a certain array size and larger, ISM arrays are more light-weight than conventional arrays. The same applies to volume. This number is of great importance, because this says something about the feasibility of this application.

In general, the behaviour of welding aluminium in space must be better understood. A few specific aspects came to light during this thesis research. Metal evaporation is relevant for welding on Earth, and even more so in space due to the vacuum. Reviewing the literature on the welting temperature of aluminium in vacuum yielded few results. Yet, this is important for predicting material behaviour. This can relatively simple be researched by melting aluminium in a vacuum chamber. Surface tension was identified as the most important fluid behaviour factor in microgravity. The fluid behaviour can be researched in models. This can be researched in experiments on Earth as well.
Additionally, a good understanding of performing DED in a microgravity environment needs to be achieved. Based on the fact that welding and another 3D printing method have been performed in space successfully, DED is most likely to function in space as well. Nevertheless, more specific research will have to show if adaptations to the equipment is required for space applications. Drop tests and parabolic flight test, as well as simulations can be used to learn more about this.
For dealing with thermal fluctuations in space, either a machine needs to be designed for that or heat shielding solutions need to be used. In a later stage of the project, this needs to be investigated.

In this report, various system design choices were made by exploring the advantageous and disadvantageous characteristics of the options, such as for use case, DED heat source and material selection. Such decisions for the top-level system design require iteration, especially in this early stage of the technology. These well-considered decisions provide a starting point for research, because without top-level decisions, it is impossible to go into details. Those decisions are made with the information available. But, as the project progresses, the best option may change based on

newly available information. In particular, the choice for the DED heat source, GMAW WAAM, needs to be further investigated and re-evaluated. The results of the trade-off for different options were close. If in practical tests the method is experienced negatively, another method can be tried. Spattering is the most concerning trait of GMAW WAAM that can cause problems.

6.2 Modelling improvements

Creating an accurate model is super important and many improvements can be made to the models shown in this report. Most importantly, the next model needs to be thermomechanical. The models in this report were solely thermal models, because temperature is the most critical aspect to this application's feasibility. However, understanding the mechanical behaviour is critical to making AM in space functional. Thermal and mechanical behaviour are strongly connected. Therefore, it must be a combined model. The mechanical properties must be modelled for a space environment, so effects of microgravity need to be accounted for.
A problem that may arise for a more complex thermomechanical model is computing time. Even for the thermal model in this report, computing time was a limiting factor in the rate of progress. Alternative solutions for faster computing need to be looked into, such as better computers, optimized models and smart 'test bench models' which are simplified models to speed up setup time.

The thermal side of the model can also use improvement. Effects of metal evaporation must be accounted for in the model, since this has significant impact [78]. Practical tests can be performed to find the exact emissivity for the chosen material. The orbit scenario can be improved upon: instead of a constant irradiation for the worst case, orbit movement can be simulated by making the angle of incidence and magnitude of each irradiance dynamic over time.

The interpass temperature is something that requires special attention. This parameter was found to be the limiting factor in the manufacturing rate of the system. The manufacturing process needs to pause between each layer to allow the material to cool down enough to not exceed the interpass temperature limit. Interpass temperature has an effect on the microstructure of the material, thus material properties. This effect needs to be better understood. With that knowledge, a trade-off can be made between manufacturing rate and print quality. This will result in an interpass temperature to design the system for and will provide better understanding in the ultimate capability of applying wire-based directed energy deposition in space for solar array structures.

6.3 Additional research topics

Besides the technical work that is required to make this application a reality, there is also research to be done in non-functional aspects of the system.
An interesting, not functionality related topic that can be further investigated is space debris. Space debris is a hot topic and ISM is a new possible way of creating space debris that has not been seen before. Spattering and non-binding particles created in the additive manufacturing process will drift into space. Through experiments data needs to be found on how many particles can be expected and of what size. Such an analysis can be used to decide is the AM process is harmful to the space environment. It would be interesting to compare these numbers to the particles that are created by propulsion systems in space. If the results would say that the number of particles created is indeed harmful, solutions need to be found to contain these particles. Based on the found solution, the feasibility of the system needs to be reconsidered, because of the possible mass and complexity that is added.

Related to space debris is legislation. The rules for space debris and allowable particle size have been briefly investigated in this report, but legislation is relevant in more ways. An in-space manufacturing spacecraft is an unprecedented type of mission. Therefore, it may be more difficult to get approval this type of spacecraft. More research needs to be done to find out if rules, legislation and advice exists for in-space manufacturing platforms. Possibly, a requirement can be made for the direction in which the solar array is produced. Considering that the length of the array can become large, maybe hundreds of metres, it may be undesirable to produce in the direction of the spacecraft's orbit. The direction of printing determines the irradiance, which influences the additive manufacturing process.

Lastly, a business plan can be developed based on this application. In this report a use case was decided upon, without going far in-depth on the space missions that will benefit from this. A non-technical research can be done to learn about what is needed by the solar-powered satellite market, such as expected number of spacecrafts that can use this technology, expected array sizes that are desired, potentially interested companies, competitors in the field, cost of production, and more topics of such nature.

7 References

[1] N. v. Staaveren, “Literature study: In-space manufacturing,” TU Delft - Unpublished, Delft, 2022.

[2] C. L. Mansfield, “Spread Your Wings, It's Time to Fly,” NASA, 26 7 2006. [Online]. Available: https://www.nasa.gov/mission_pages/station/behindscenes/truss_segment.html. [Accessed 13 5 2022].

[3] B. R. Spence, S. White, M. LaPointe, S. Kiefer, P. LaCorte, J. Banik, D. Chapman and J. Merrill, “International Space Station (ISS) Roll-Out Solar Array (ROSA) Spaceflight Experiment Mission and Results,” IEEE Xplore, Santa Barbara, California, 2018.

[4] E. C. Warmann, P. Espinet-Gonzalez, N. Vaidya, S. Loke, A. Naqavi, T. Vinogradova, M. Kelzenberg, C. Leclerc, E. Gdoutos, S. Pellegrino and H. A. Atwater, “An ultralight concentrator photovoltaic system for space solar power harvesting,” *Acta Astronautica,* vol. 170, pp. 443-451, 2020.

[5] L. Langnau, “How to develop a 3D printed, optimized industrial robot arm,” Make Parts Fast, 20 11 2019. [Online]. Available: https://www.makepartsfast.com/how-to-develop-a-3d-printed-optimized-industrial-robot-arm/. [Accessed 08 06 2022].

[6] “Convention on the international liability for damage caused by space objects,” 29 March 1972.

[7] M. Mejía-Kaiser, “Space Law and Hazardous Space Debris,” 30 01 2020. [Online]. Available: https://oxfordre.com/planetaryscience/view/10.1093/acrefore/9780190647926.001.0001/acrefore-9780190647926-e-70. [Accessed 07 06 2022].

[8] D. Ahn, “Directed Energy Deposition (DED) Process: State of the Art,” *International Journal of Precision Engineering and Manufacturing-Green Technology,* vol. 8, pp. 703-742, 2021.

[9] D. Svetlizky, M. Das, B. Zheng, A. L. Vyatskikh, S. Bose, A. Bandyopadhyay, J. M. Schoenung, E. J. Lavernia and N. Eliaz, “Directed energy deposition (DED) additive manufacturing: Physical characteristics, defects, challenges and applications,” *Materials Today,* vol. 49, pp. 271-295, 2021.

[10] C. Valdivieso, “The Complete Guide to Directed Energy Deposition (DED) in 3D Printing,” 3D Natives, 10 09 2019. [Online]. Available: https://www.3dnatives.com/en/directed-energy-deposition-ded-3d-printing-guide-100920194/. [Accessed 10 06 2022].

[11] Dassault Systèmes, “3D PRINTING - ADDITIVE,” [Online]. Available: https://make.3dexperience.3ds.com/processes/3D-printing. [Accessed 14 03 2022].

[12] ASTM International, “F3187-16: Standard Guide for Directed Energy Deposition of Metals,” West Conshohocken, PA, 2016.

[13] D. Ding, Z. Pan, D. Cuiuri and H. Li, “Wire-feed additive manufacturing of metal components: technologies, developments and future interests,” *The International Journal of Advanced Manufacturing Technology,* vol. 81, pp. 1-4, 2015.

[14] J. Weeks and D. Todd, “Vacuum Gas Tungsten Arc Welding,” Boeing, Huntsville, AL, 1996.

[15] H. Toya, K. Hieda and T. Saitou, “Preliminary Study on Arc Welding in Vacuum,” in *Symposium on Discharges and Electrical Insulation in Vacuum*, Matsue, 2006.

[16] J. M. Lafferty, “Vacuum Arcs,” in *Encyclopedia of Physical Science and Technology (Third Edition)*, Tarzana, CA, Elsevier Science Ltd., 2003, pp. 359-370.

[17] 3D Printing Media Network, “Wire Arc Additive Manufacturing (WAAM),” [Online]. Available: https://www.3dprintingmedia.network/additive-manufacturing/am-technologies/waam-wire-arc-additive-manufacturing/. [Accessed 10 06 2022].

[18] xBeam, “xBeam Technology,” [Online]. Available: https://xbeam3d.com/technology.html. [Accessed 10 06 2022].

[19] P. Hanaphy, “Hybrid Manufacturing Technologies launches innovative UK-backed ‘FastWireAM’ project,” 3D Printing Industry, 11 01 2021. [Online]. Available: https://3dprintingindustry.com/news/hybrid-manufacturing-technologies-launches-innovate-uk-backed-fastwiream-project-182120/. [Accessed 10 06 2022].

[20] N. Naden and T. Prater, “A Review of Welding in Space and Related Technologies,” NASA, Huntsville, AL, 2020.

[21] L. Xiaomeng, D. Quanlin, W. Pengfei and C. H. , “Review of Electron Beam Welding Technology in Space Environment,” *Optik - International Journal for Light and Electron Optics,* vol. 225, 2021.

[22] SBIR STTR, “Welding and Repair in Space,” 19 08 2019. [Online]. Available: https://www.sbir.gov/sbirsearch/detail/1671065. [Accessed 13 06 2022].

[23] D. Allen, “A Survey of Next Generation Solar Arrays,” in *35th Aerospace Sciences Meeting & Exhibit*, Reno, Nevada, 1997.

[24] R. P. Hoyt, J. I. Cushing, J. T. Slostad, G. Jimmerson, T. Moser, G. Kirkos, M. L. Jaster and N. R. Voronka, “SpiderFab: An Architecture for Self-Fabricating Space Systems,” in *AIAA SPACE 2013 Conference and Exposition*, San Diego, California, 2013.

[25] R. Hoyt, J. Cushing, G. Jimmerson, J. Slostad, R. Dyer and S. Alvarado, “SpiderFab™: Process for On-Orbit Construction of Kilometer-Scale Apertures,” Tethers Unlimited, Bothell, Washington, 2016.

[26] J. Gibb, “Lightweight Flexible Space Solar Arrays, Past, Present and Future,” Lockheed Martin Missiles and Space, Sunnyvale, California, 2018.

[27] J. Banik, S. Kiefer, M. LaPointe and P. LaCorte, “On-Orbit Validation of the Roll-Out Solar Array,” in *2018 IEEE Aerospace Conference*, Big Sky, Montana, 2018.

[28] National Geographic, “Orbital Objects,” [Online]. Available: https://www.nationalgeographic.com/science/article/orbital-objects. [Accessed 11 03 2022].

[29] NASA, “ISS P6 truss solar array - close-up,” 18 12 2006. [Online]. Available: http://spaceflight.nasa.gov/gallery/images/shuttle/sts-116/html/iss014e10053.html. [Accessed 11 03 2022].

[30] B. Spence, S. White, N. Wilder, T. Gregory, M. Douglas and R. Takeda, “Next Generation UltraFlex Solar Array for NASA’s New Millennium Program Space Technology 8,” in *2005 IEEE Aerospace Conference*, Goleta, California, 2005.

[31] R. Coppinger, “NASA successfully tests Orion solar array technology,” FlightGlobal, 15 10 2008. [Online]. Available: https://www.flightglobal.com/nasa-successfully-tests-orion-solar-array-technology/83421.article. [Accessed 11 03 2022].

[32] NASA, “SpaceX CRS-11 mission overview,” 01 06 2017. [Online]. Available: https://www.nasa.gov/sites/default/files/atoms/files/spacex_crs-11_mission_overview.pdf. [Accessed 23 05 2022].

[33] B. Zandbergen, “Reader AE1222-II: Aerospace Design & Systems Engineering Elements I, spacecraft design and sizing,” Delft University of Technology, Delft, 2018.

[34] A. Shrivastava, M. Krones and F. E. Pfefferkorn, “Comparison of energy consumption and environmental impact of friction stir welding and gas metal arc welding for aluminum,” *CIRP Journal of Manufacturing Science and Technology,* vol. 9, pp. 159-168, 2015.

[35] N. Raju, G. Balaganesan and G. S. Kumar, “Energy Consumption of Welding-Based Additively Manufactured Materials,” in *AIMTDR 2018: Advances in Additive Manufacturing and Joining*, 2019.

[36] M. Martin, “The Best MIG Welder, According to 3,500+ Customer Reviews,” Thomas Publishing Company, 04 2022. [Online]. Available: https://www.thomasnet.com/articles/machinery-tools-supplies/best-mig-welders/. [Accessed 24 08 2022].

[37] MD Robotics, “Datasheet: Mobile Servicing System,” Brampton, Ontario, 2002.

[38] ESA, “European Robotic Arm (ERA) - ESA-HSO-COU-007,” ESA, Paris.

[39] FANUC Europe Corporation, “Datasheet CR-4iA - MDS-03903-EN,” Echternach, 2020.

[40] ABB, “Datasheet YuMi IRB 14050,” Zürich, 2021.

[41] ABB, “Datasheet OmniCore™ C30 and C90XT Controllers,” Zürich, 2021.

[42] Elite Robots, “EC63 / 3KG 6-AXIS COLLABORATIVE ROBOT,” [Online]. Available: https://www.elite-robotics.com/en/products/ec63-robot. [Accessed 24 08 2022].

[43] SIASUN, “Collaborative robot,” [Online]. Available: https://www.siasunrobot.eu/public/uploads/20190226/0a7037f365f50744e4cdfc863a41a51f.pdf. [Accessed 24 08 2022].

[44] STÄUBLI, “POWER cobot TX2touch range,” 2021. [Online]. Available: https://www.staubli.com/content/dam/robotics/brochures/cobot/TX2touch-robot-range-product-leaflet.pdf. [Accessed 24 08 2022].

[45] AUBO, “AUBO-i3: Collaborative Lightweight Robot,” [Online]. Available: https://www.leadrobotics.dk/_files/ugd/d6a7bf_d8e4844e248b42e28be065941d0c53b4.pdf. [Accessed 24 08 2022].

[46] C. P. Blankenship and R. J. Hayduk, “Large Space Structures — Structural Concepts and Materials,” *SAE Transactions,* vol. 96, pp. 1810-1838, 1987.

[47] J. Dever, B. Banks, K. d. Groh and S. Miller, “Degradation of spacecraft materials,” *Handbook of Environmental Degradation of Materials,* pp. 465-501, 2005.

[48] M. M. Finckenor and K. K. d. Groh, “A Researchers Guide to: Space Environmental Effects,” in *ISS Researcher's Guide Series*, Washington, D.C., NASA ISS Program Science Office, 2020, pp. 14-15.

[49] D. Lichodziejewski, G. Veal, R. Helms, R. Freeland and M. Kruer, “Inflatable rigidizable solar array for small satellites,” in *44th AIAA/ASME/ASCE/AHS/ASC Structures, Structural Dynamics, and Materials Conference*, Norfolk, Virginia, 2003.

[50] M. Ashby, Materials Selection in Mechanical Design, fifth ed., Elsevier Science & Technology, 2016.

[51] “GRANTA EduPack,” Ansys, Cambridge, 2021 R2.

[52] C. Moosbrugger, Engineering Properties of Magnesium Alloys, Novelty, Ohio: ASM International, 2017.

[53] N. Mo, Q. Tan, M. Bermingham, Y. Huang, H. Dieringa, N. Hort and M.-X. Zhang, “Current development of creep-resistant magnesium cast alloys: A review,” *Materials & Design,* vol. 155, pp. 422-442, 2018.

[54] J. Davis, “Aluminum and aluminum alloys,” in *Alloying: Understanding the Basics*, Novelty, Ohio, ASM International, 2001, pp. 351-416.

[55] Materion, “Beryllium metal,” [Online]. Available: https://materion.com/products/beryllium-products/beryllium-metal. [Accessed 05 07 2022].

[56] J. Emsley, Nature's Building Blocks, Oxford: Oxford University Press, 2001.

[57] Engineering ToolBox, “Emissivity Coefficients common Products,” 2003. [Online]. Available: https://www.engineeringtoolbox.com/emissivity-coefficients-d_447.html. [Accessed 05 07 2022].

[58] A. Langebeck, A. Bohlen, R. Rentsch and F. Vollertsen, “Mechanical Properties of High Strength Aluminum Alloy EN AW-7075 Additively Manufactured by Directed Energy Deposition,” *Metals,* 2020.

[59] TWI Ltd, “Aluminium alloys,” [Online]. Available: https://www.twi-global.com/technical-knowledge/job-knowledge/weldability-of-materials-aluminium-alloys-021. [Accessed 06 07 2022].

[60] A. Haselhuhn, M. Buhr, B. Wijnen, P. Sanders and J. Pearce, “Structure-property relationships of common aluminum weld alloys utilized as feedstock for GMAW-based 3-D metal printing,” *Materials Science and Engineering: A,* vol. 673, pp. 511-523, 2016.

[61] K. Vimal, M. N. Srinivas and S. Rajak, “Wire arc additive manufacturing of aluminium alloys: A review,” *Materials Today: Proceedings,* vol. 41, no. 5, pp. 1139-1145, 2020.

[62] RAMLAB, [Online]. Available: https://www.ramlab.com/resources/ded-101/. [Accessed 09 06 2022].

[63] P. Singh and D. Dutta, “Multi-Direction Layered Deposition – An Overview of Process Planning Methodologies,” in *Proceedings of the Solid Freeform Fabrication Symposium*, 2003.

[64] Made In Space, “Additive Manufacturing Facility (AMF) User Guide,” Jacksonville, Florida, 2016.

[65] T. Prater, N. Werkheiser and F. Ledbetter, “Summary Report on Phase I and Phase II Results From the 3D Printing in Zero-G Technology Demonstration Mission, Volume II,” NASA, Huntsville, Alabama, 2018.

[66] Redwire, “Vulcan Advanced Hybrid Manufacturing (VULCAN),” REDWIRE, [Online]. Available: https://redwirespace.com/products/vulcan/. [Accessed 25 08 2022].

[67] J. Molina, R. Voytovych, E. Louis and N. Eustathopoulos, “The surface tension of liquid aluminium in high vacuum: The role of surface condition,” *International Journal of Adhesion & Adhesives,* vol. 27, pp. 394-401, 2007.

[68] Redwire, “Archinaut,” [Online]. Available: https://redwirespace.com/products/archinaut/. [Accessed 28 12 2021].

[69] Dassault Systèmes, *SIMULIA Abaqus/CAE,* Johnston, RI, 2021.

[70] Dassault Systèmes, “ABAQUS UNIFIED FEA: complete solutions for realistic simulation,” [Online]. Available: https://www.3ds.com/products-services/simulia/products/abaqus/. [Accessed 29 05 2022].

[71] Simulia, “PRINT TO PERFORM: simulation for additive manufacturing,” Dassault Systèmes, [Online]. Available: https://www.3ds.com/products-services/simulia/trends/digital-additive-manufacturing/. [Accessed 14 09 2022].

[72] The Mathworks, Inc., “MATLAB R2022a,” Natick, Massachusetts, 2022.

[73] Simulia, “Parameter table type reference,” Dassault Systèmes , [Online]. Available: https://help.3ds.com/2020/english/DSSIMULIA_Established/SIMACAEANLRefMap/simaanl-m-AMSpecialPurposeParameterTableTypeReferences-sb.htm?contextscope=all&id=4402022b9b08490fbdae244ed1f1e466. [Accessed 14 09 2022].

[74] C. Obbink-Huizer, “Use Abaqus to simulate additive manufacturing – printing a hip implant,” Simuleon, 04 02 2020. [Online]. Available: https://info.simuleon.com/blog/using-abaqus-to-simulate-additive-manufacturing-printing-an-optimized-hip-implant. [Accessed 14 09 2022].

[75] T. Mukherjee and T. DebRoy, “Printability of 316 stainless steel,” *Science and Technology of Welding and Joining,* vol. 24, no. 5, pp. 412-419, 2019.

[76] MatWeb, “Aluminum 7075-T6; 7075-T651,” [Online]. Available: https://www.matweb.com/search/DataSheet.aspx?MatGUID=9852e9cdc3d4466ea9f111f3f0025c7d&ckck=1. [Accessed 29 05 2022].

[77] A. Liu, X. Tang and F. Lu, “Arc profile characteristics of Al alloy in double-pulsed GMAW,” *The International Journal of Advanced Manufacturing Technology,* vol. 65, pp. 1-7, 2012.

[78] A. B. Murphy, “Influence of droplets in gas–metal arc welding: new modelling approach, and application to welding of aluminium,” *Science and Technology of Welding and Joining,* vol. 18, no. 1, pp. 32-37, 2013.

[79] Thyssenkrupp, “Aluminium Alloy 5754 H22 H24 H26 Material Data Sheet,” 07 2016. [Online]. Available: https://ucpcdn.thyssenkrupp.com/_legacy/UCPthyssenkruppBAMXUK/assets.files/material-data-sheets/aluminium/5754-h22-h24-h26.pdf. [Accessed 14 09 2022].

[80] Thyssenkrupp, “Aluminium Alloy 6005A - T6 Extrusion Material Data Sheet,” 07 2016. [Online]. Available: https://ucpcdn.thyssenkrupp.com/_legacy/UCPthyssenkruppBAMXUK/assets.files/material-data-sheets/aluminium/6005a-t6-extrusion.pdf. [Accessed 14 09 2022].

[81] Apac, “Material Specifications 6005A T5 Aluminium Alloy,” [Online]. Available: https://apacinfrastructure.com.au/material-specifications-6005a-t5-aluminium-alloy. [Accessed 07 07 2022].

[82] M. Leitner, A. S. Thomas Leitner, K. Aziz and G. Pottlacher, “Thermophysical Properties of Liquid Aluminum,” *Metallurgical and Materials Transactions A,* vol. 48, pp. 3036-3045, 2017.

[83] National Institute of Standards and Technology, “Aluminum,” [Online]. Available: https://webbook.nist.gov/cgi/cbook.cgi?ID=C7429905&Units=SI&Mask=2&Type=JANAFL&Plot=on. [Accessed 01 08 2022].

[84] K. Matsuda and K. Tamura, “Structure and Electronic State in a Fluid Alkali Metal: Synchrotron Radiation Studies,” *Zeitschrift für Physikalische Chemie,* vol. 235, pp. 25-36, 2021.

[85] C. Fröhlich and J. Lean, “Solar irradiance variability and climate,” *Astronomical Notes,* vol. 323, no. 3-4, pp. 203-212, 2002.

[86] Engineering ToolBox, “Absorbed Solar Radiation,” 2009. [Online]. Available: https://www.engineeringtoolbox.com/solar-radiation-absorbed-materials-d_1568.html. [Accessed 12 07 2022].

[87] J. Meseguer, I. Pérez-Grande and A. Sanz-Andrés, Spacecraft Thermal Control, Cambridge: Woodhead publishing, 2012.

[88] J. Li, S. Yan and R. Cai, “Thermal analysis of composite solar array subjected to space heat flux,” *Aerospace Science and Technology,* vol. 27, pp. 84-94, 2013.

[89] H. Geng, J. Li, J. Xiong and X. Lin, “Optimisation of interpass temperature and heat input for wire and arc additive manufacturing 5A06 aluminium alloy,” *Science and Technology of Welding and Joining,* vol. 22, no. 6, pp. 472-483, 2016.

[90] K. Derekar, J. Lawrence, G. Melton, A. Addison, X. Zhang and L. Xu, “Influence of Interpass Temperature on Wire Arc Additive Manufacturing (WAAM) of Aluminium Alloy Components,” *MATEC Web of Conferences,* vol. 269, 2019.

[91] J. D. Spencer, P. M. Dickens and C. M. Wykes, “Rapid prototyping of metal parts by three-dimensional welding,” *Proceedings of the Institution of Mechanical Engineers, Part B: Journal of Engineering Manufacture,* vol. 212, no. 3, pp. 175-182, 1998.

[92] N. Kozamernik, D. Bračun and D. Klobčar, “WAAM system with interpass temperature control and forced cooling for near-net-shape printing of small metal components,” *The International Journal of Advanced Manufacturing Technology,* vol. 110, pp. 1955-1968, 2020.

[93] L. J. Nayak and G. G. Roy, “Thermocouple temperature measurement during high speed electron beam welding of SS 304,” *Optik,* vol. 201, no. 163538, 2020.

Appendix A – Abaqus script Advanced Model 1

```
*Heading
** Job name: AdvancedModel1 Model name: Model-1
** Generated by: Abaqus/CAE 2021
*Preprint, echo=NO, model=NO, history=NO, contact=NO
**
** PARTS
-removed geometry section-
*End Part
**
** ASSEMBLY
-removed geometry section-
*ELEMENT PROGRESSIVE ACTIVATION,NAME="__AM-Model-1_Material Source -1_EPA__",ELSET=TotalTube-
1.PrintTube,FOLLOW=No
*End Assembly
**
** MATERIALS
**
*Material, name="Aluminium 6005A T5"
*Conductivity
  122.15, -172.
 165.606, -84.6
 189.264,  3.18
 206.696,   91.
 219.148,  179.
 226.619,  267.
 229.109,  354.
 225.374,  442.
 217.903,  530.
 214.7    ,  582.
 207.7    ,  609.
 132.8    ,  647.
 122.7    ,  672.
 118.7    ,  722.
 120.7    ,  822.
 129.8    ,  1184.
 137.6    ,  1770.2
*Density
2705.,
*Latent Heat
388500.,607.,654.
*Specific Heat
  257.4, -204.
   544., -147.
```

```
 705.8, -90.9
 815., -34.4
 892.,  22.
 944.6,  78.4
 984.6,  135.
1004.1,  191.
1033.4,  248.
1052.9,  304.
1072.3,  361.
1091.8,  417.
1121.1,  473.
1150.3,  530.
1180. ,  654.
1180.0,  1800.
**
** PHYSICAL CONSTANTS
**
*Physical Constants, absolute zero=-273.15, stefan boltzmann=5.67e-08
**
**-------------------------------------------------------------
**--------Table Types Defined in the Abaqus AM-Interface------
**-------------------------------------------------------------
*PROPERTY TABLE TYPE, NAME = "ABQ_AM.AbsorptionCoeff" , PROPERTIES = 1
"AbsorptionCoeff", Unitless
*PROPERTY TABLE TYPE, NAME = "ABQ_AM.EnclosureAmbientTemp" , PROPERTIES = 1
"VATTemperature",
*PARAMETER TABLE TYPE, NAME = "ABQ_AM.MovingHeatSource" , PARAMETERS = 2
STRING,,"Event Series","Laser Event Series",
STRING,,Concentrated|Uniform|Goldak,"Energy Distribution",
*PARAMETER TABLE TYPE, NAME="ABQ_AM_MaterialDeposition_Advanced", PARAMETERS=6
STRING, "Partial", "Activation Type", , "Full|Partial",
FLOAT, 0, "Min Volume Fraction Threshold for Partial Activation", , ,
FLOAT, 1, "Max Volume Fraction Threshold for Partial Activation", , ,
FLOAT, 0, "Max Volume Fraction Threshold for Full Activation", , ,
STRING, "Yes", "Update Orientation", Dimensionless, ,
INTEGER, "0", "Element Subdivision Order", Dimensionless, ,
*PARAMETER TABLE TYPE, NAME = "ABQ_AM.MovingHeatSource.Uniform" , PARAMETERS = 9
INTEGER,,,"SubDivX",
INTEGER,,,"SubDivY",
INTEGER,,,"SubDivZ",
FLOAT,,,"offset1",
FLOAT,,,"offset2",
FLOAT,,,"offset3",
FLOAT,,,"BoxLength1",
FLOAT,,,"BoxLength2",
FLOAT,,,"BoxLength3",
```

```
*PARAMETER TABLE TYPE, NAME = "ABQ_AM.MovingHeatSource.Goldak" , PARAMETERS = 10
INTEGER,,,"SubDivX",
INTEGER,,,"SubDivY",
INTEGER,,,"SubDivZ",
FLOAT,,,"a",
FLOAT,,,"b",
FLOAT,,,"cf",
FLOAT,,,"cr",
FLOAT,,,"ff",
FLOAT,,,"fr",
FLOAT,,,"BoxSizeFactor",
*PARAMETER TABLE TYPE, NAME = "ABQ_AM.MovingHeatSource.Advanced" , PARAMETERS = 7
STRING,False,True|False,"Conserve Total Energy",
STRING,False,True|False,"Control increment size",
STRING,Relative,Absolute|Relative,"Offset type",
FLOAT,0.0,,"LaserVectorX",
FLOAT,0.0,,"LaserVectorY",
FLOAT,-1.0,,"LaserVectorZ",
FLOAT,1.0,,"Field factor",
*PARAMETER TABLE TYPE, NAME = "ABQ_AM.MaterialDeposition.Bead" , PARAMETERS = 5
STRING,Z,X|Y|Z,"Stack Direction",
FLOAT,,,"Bead Height",
FLOAT,,,"Bead Width",
FLOAT,,,"Activation Offset",
STRING,,Below|Above,"Deposition Position",
*PARAMETER TABLE TYPE, NAME = "ABQ_AM.MaterialDeposition" , PARAMETERS = 2
STRING,,"Event Series","Material Event Series",
STRING,,Roller|Bead,"Deposition Process",
*Event Series Type, FIELDS = 1, NAME = "ABQ_AM.MaterialDeposition"
"On and off", Unitless
*Event Series Type, FIELDS = 1, NAME = "ABQ_AM.PowerMagnitude"
"Power", ML2T03
**------------------------------------------------------------
**-------Event Series defined in the Abaqus AM-Interface------
**------------------------------------------------------------
*EVENT SERIES, NAME = "MaterialPath" , TIME =TOTAL TIME,
        TYPE = "ABQ_AM.MaterialDeposition",
        INPUT = "C:/Users/staaveren/Documents/MATLAB/MaterialPathAdvancedModel1.inp"
**------------------------------------------------------------
**-----Table Collections defined in the Abaqus AM-Interface---
**------------------------------------------------------------
*TABLE COLLECTION, NAME = "ABQ_AM_Table Collection-Material"
*PARAMETER TABLE, TYPE = "ABQ_AM.MaterialDeposition.Bead"
"Z", 0.0025, 0.002, 0, "Below"
*PARAMETER TABLE, TYPE = "ABQ_AM.MaterialDeposition"
"MaterialPath", "Bead"
```

```
*PARAMETER TABLE, TYPE = "ABQ_AM.MaterialDeposition.Advanced"
"Full", 0.0, 1.0, 0.0, "Yes", 0
**
**
** PREDEFINED FIELDS
**
** Name: InitialDepositionTemp   Type: Temperature
*Initial Conditions, type=TEMPERATURE
TotalTube-1.PrintTube, 1726.85
** Name: InitialBaseTemp   Type: Temperature
*Initial Conditions, type=TEMPERATURE
TotalTube-1.BaseTube, 80.
** ----------------------------------------------------------------
**
** STEP: Step-1
**
*Step, name=Step-1, nlgeom=NO, inc=10000
HTstep
*Heat Transfer, end=PERIOD, deltmx=2000.
10., 21000., 10., 10.,
**
*ACTIVATE ELEMENTS , ACTIVATION = "__AM-Model-1_Material Source -1_EPA__"
"ABQ_AM_Table Collection-Material"
*RADIATE
TotalTube, RFS , -270 , 0.25
**
** LOADS
**
** Name: EarthFlux   Type: Surface heat flux Using Field: AnalyticalField-2
*Dflux, op=NEW
-removed geometry section-
**
** OUTPUT REQUESTS
*Restart, write, frequency=0
** FIELD OUTPUT: F-Output-1
*Output, field
*Node Output
NT,
*Element Output, directions=YES
HFL, IVOL, TEMP
*Contact Output
HFLA,
*Radiation Output
RADFL,
*Output, history, frequency=0
*End Step
```

Appendix B – Material path Matlab script

```
close all
clear all
clc

%Variables
n_layernodes = 100;
h = 1;
d = 0.1;
t = 0.002;
h_layer = 0.0015;
v_printhead = 10; %mm/s
h_base = 0.2;
T_idle = 0;

%Calculations

n_layers = round(h/h_layer);
n_totalnodes = n_layernodes*n_layers;
r = d/2 - t/2;
T_layer = 2*pi*r/(v_printhead/1000);
T_step = T_layer/n_layernodes;
R_step = 2*pi/n_layernodes;
T_total = n_layers*(T_layer+T_idle);
h = n_layers*h_layer;

%Start parameters
R = 0;
T = 0;
m = 0;
z = h_base + h_layer;
a = zeros(n_totalnodes,5);

for n = [1:n_totalnodes+n_layers*round(T_idle/T_step)]
    if R > 2*pi
        m = n + round(T_idle/T_step);
        z = z + h_layer;
        R = 0;
    end

    if n < m
        x = r*cos(R);
        y = r*sin(R);

        a(n,:) = [T,x,y,z,1];
        T = T + T_step;
    else
        x = r*cos(R);
        y = r*sin(R);

        a(n,:) = [T,x,y,z,1];
        T = T + T_step;
        R = R + R_step;
    end

end
```

```
h
T_total

figure
plot3(a(:,2),a(:,3),a(:,4),"o:")

writematrix(a,'MaterialPathAdvancedModel1.txt','Delimiter',',')
```

Appendix C – Temperature dependent material properties Matlab script

```
close all
clear all
clc

SH = [530 1180;
    473 1150;
    417 1120;
    361 1100;
    304 1080;
    248 1060;
    191 1030;
    135 1010;
    78.4 969;
    22 915;
    -34.4 836;
    -90.9 724;
    -147 558;
    -204 264;
    -260 2.41];
TC = [530 175;
    442 181;
    354 184;
    267 182;
    179 176;
    91 166;
    3.18 152;
    -84.6 133;
    -172 98.1;
    -260 18.8];


SH22 = 915
TC22 = (166-152)/(91-3.18)*(22-3.18)+152

SH22_6005 = 892;
TC22_6005 = 193;
fTC = TC22_6005/TC22
fSH = SH22_6005/SH22

SH6005 = [SH(:,1) SH(:,2)*fSH]
TC6005 = [TC(:,1) TC(:,2)*fTC]

figure
hold on
plot(SH(:,1),SH(:,2),'b')
plot(SH6005(:,1),SH6005(:,2),'b--')
plot(TC(:,1),TC(:,2),'r')
plot(TC6005(:,1),TC6005(:,2),'r--')
legend({'SH6061','SH6005','TC6061','TC6005'},'Location','northwest')
xlabel('Temperature (°C)')
ylabel('Specific heat capacity (J/(kg*K)) & Thermal conductivity (W/(m*K))')

SH6005_total = [1800 1180;
```

```
                654 1180;
                SH6005];
TC_liquid =    flip([%720-273.15 200;
                885-273.15 190;
                912-273.15 183;
                950-273.15 108;
                975-273.15 98;
                1025-273.15 94;
                1125-273.15 96;
                1487-273.15 105;
                1800 112.8]);
TC_liquid_adj = [TC_liquid(:,1)-29.82 TC_liquid(:,2)+24.75];

TC6005_total = [TC_liquid_adj;
                TC6005];

ymelt = [0:1:1200];
Tmelt = (654+607)/2 * ones(length(ymelt));


figure
hold on
plot(SH6005_total(:,1),SH6005_total(:,2),'b')
plot(TC6005_total(:,1),TC6005_total(:,2),'r')
plot(Tmelt,ymelt,'--g')
legend({'Specific heat','Thermal conductivity','Melting temperature
(630.5°C)'},'Location','east')
xlabel('Temperature (°C)')
ylabel('Specific heat capacity (J/(kg*K)) & Thermal conductivity (W/(m*K))')
```